Study of a Small Electric Race Car with Regenerative Braking using Hardware-In-the-Loop Emulation

By

Tommaso Transi

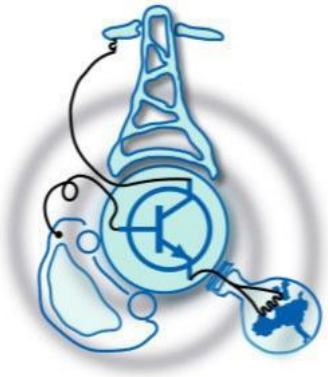

Submitted to the Department of Electrical Engineering, Electronics, Computers and Systems

In partial fulfilment of the requirements for the degree of
Erasmus Mundus Master Course in Sustainable Transportation and Electrical Power Systems
at the
UNIVERSIDAD DE OVIEDO
September 2018

Author…….

Tommaso Transi

Certified by…….

Professor Paulo Pereirinha

Polytechnic Institute of Coimbra (ISEC-IPC), Coimbra, Portugal

Thesis Supervisor

Professor Alain Bouscayrol

University of Lille, Lille, France

Thesis Supervisor

Study of a Small Electric Race Car with Regenerative Braking using Hardware-In-the-Loop Emulation

By

Tommaso Transi

Abstract

The objective of this work is to study the behaviour of an electric Formula Student car, from the Coimbra Institute of Engineering - Polytechnic of Coimbra (ISEC-IPC, *Instituto Superior de Engenharia de Coimbra - Instituto Politécnico de Coimbra*), Coimbra, Portugal, through a Hardware-In-the-Loop simulation, using Energetic Macroscopic Representation (EMR) graphical formalism. EMR, used to easily define a control design and tuning of the system, has been studied during a one month stay at the University of Lille, Lille, France. The corresponding EMR models were developed for software, Full Power Hardware-In-the-Loop (HIL) and Reduced Power HIL simulations. To obtain the driving cycle that the car should follow on the race track, OptimumLap© software was used. Software simulation is used to verify the validity of the model. Reduced Power Hardware-In-the-Loop simulation is implemented and verified using the experimental test bench in ISEC's laboratory. Finally, results from software simulation and from Reduced Power HIL simulation are compared to demonstrate the validity of the two simulations.

Keywords: Electric Vehicle, EV, Energetic Macroscopic Representation, EMR, Hardware-In-the-Loop simulation, HIL, Reduced Power HIL, Formula SAE Electric, OptimumLap, SPMSM, regenerative braking.

First Thesis Supervisor: Paulo G. Pereirinha

Title: Professor Coordenador

Second Thesis Supervisor: Alain Bouscayrol

Title: Full Professor

Acknowledgments

First of all, I would like to thank Prof. Pereirinha and Prof. Bouscayrol for the big opportunity that they gave me, with this work of thesis: it was an exciting experience to work with them and with their research groups.

Secondly, my gratitude goes to my family that allows me to complete this master course, against all the odds of these two years, and with the serenity that I needed.

To my friends, my girlfriend and whoever was next to me for a long or short time during this path: thank you. Without your help and your constant support maybe, this achievement would have not been reached.

"Perfer et Obdura:

Dolor Hic tibi Proderit Olim"

Contents

Table of Figures

LIST OF TABLES

List of Abbreviations and Symbols

Abbreviations

CAN	*Controller Area Network*
COG	*Causal Ordering Graph*
ECU	*Electronic Control Unit*
EMI	*Electro Magnetic Interferences*
EMR	*Energetic Macroscopic Representation*
EV	*Electric Vehicle*
FSAE	*Formula SAE*
GHG	*Green House Gases*
HIL	*Hardware-In-the-Loop*
ICEV	*Internal Combustion Engine Vehicle*
IPMM	*Interior Permanent Magnet Machine*
IS	*Interface System*
MCS	*Maximal Control Structure*
NEDC	*New European Driving Cycle*
OCV	*Open Circuit Voltage*
PA	*Power Adaptation*
PI-IP	*Proportional Integral. Integral Proportional*
SAE	*Society of Automotive Engineers*
SoC	*State of Charge*
SPMSM	*Surface Permanent Magnet Synchronous Machine*
SRM	*Switched Reluctance Machine*

Symbols

Symbol	*Unit*	*Property*
f	Nm/(rad/s), N	Friction coefficient or friction
g	m/s^2	Gravitational acceleration
i	A	Current
J	kg m^2	Moment of inertia
e	V	Back emf
c_x	-	Aerodynamic Drag Coefficient
u	V	Voltage
L	H	Inductance
k	-	Coefficient of the subscript value
T	Nm	Torque
v	m/s	Velocity
η	%	Efficiency
ω	rad/sec	Rotational speed
M	kg	Mass
m		Modulation ratio
R	Ω	Resistance
k_d	-	Distribution Factor
k_w	-	Weighting Factor
k_{br}	-	Braking Factor

Subscripts

Subscript	*Property*
batt	battery
dcm	DC machine
ch	chopper
eq	equivalent
meas	measured
ref	reference
red	reduced
br	braking
wh	wheel
m	machine
arm	armature
nom	nominal
diff	differential
ve	vehicle
res	resultant

1. Introduction

1.1. Electric mobility

Nowadays transportation sector represents almost a quarter of Europe's Green House Gases (GHG) and also the main cause for air pollution. Trying to invert this trend, European Commission has stated that the pace at which the shift towards low-emission mobility occurs, has to be increased. The transport field nowadays still depends for about 94% from fossil fuels; the introduction of electric mobility, renewable energy sources and new technologies will lead to a significative reduction of this percentage. In this scenario, is crucial the development of more efficient hybrid/electric vehicles [1].

Electric vehicles (EVs) market is still penalised by some technology barriers such as battery capacity, charging facilities, charging time and also by economic aspects such as their higher cost respect to conventional internal combustion engine vehicles (ICEVs); from some studies in 2024 is expected that the cost of EVs will be competitive compared to ICEVs and in 2029 most segments will reach parity in term of costs, due to the fall of battery prices [2] [3].

The possibility to use the regenerative braking is also an advantage; this allows to improve the efficiency of the system, recovering part of the energy instead of dissipating it through the mechanical brakes. This will give back a range improvement of about 15 to 32 percent accordingly to some consumers experiences [4]. This strongly depends on the driving profile (urban, highway etc.) and the percentage of electric braking that is used, over the total braking force required; if the electric braking will be equal to 100% of the total braking a big improvement of the overall effectiveness can be achieved, and on the other hand if only a little part of the braking force will be recovered, the effect on the State of Charge (SoC) will be negligible. The situation in which the 100% of braking force is converted into electric energy (not counting the inevitable efficiency losses of the components) is not always achievable, because it strongly depends from the quantity of force and the time in which this has to be stored: these values can be higher than the ones that the electrical part of the system can withstand, and for this will be necessary the help of the mechanical braking system. Traffic conditions also play an important role in the strategy to decide the ratio between mechanical and regenerative braking power.

Research and Development departments in the major automotive companies are investing mainly in electrified powertrain-solution, helped also by some expertise derived by their involvement in ABB FIA Formula E Championship, one of the most followed Formula series after Formula 1.

In 2013, also the Society of Automotive Engineers (SAE) decided to focus its interest on e-mobility introducing next to the already existing Formula SAE, the Formula SAE Electric, a competition series based on all electric vehicles completely designed, manufactured and driven by undergraduate or graduate students from universities worldwide [5]. This Formula series is an interesting opportunity for students who want to have a direct contact with a real race-car and its production process from the scratch, stepping-in for the first time in the "e-motorsport" world.

1.2. Vehicle simulation

The software simulation part is fundamental in a system design process and is beneficial to deeply understand what will happen in real scenarios, with different environment conditions or in high-stress conditions such as a car race. After the software simulation, another preliminary step before the production of the first prototype can be inserted: Hardware-In-the-Loop Simulation (HIL). HIL Simulation consists in to replace idealised or simplified device models from the general simulation system, with actual devices such as real batteries, mechanical couplings or traction motors [6].

HIL has been used initially in aerospace and automotive field in order to test ECU (Electronics Control Units) [7], but nowadays the automotive field is the one that leads the investments, that are supposed to reach

USD 826.7 million by 2020 [8]. The main idea of HIL simulation is to replace some parts of the modelled power system in software simulation with actual components. Indeed, this is useful to get results closer to real conditions on one hand, and on the other hand to insert in the simulation some devices difficult to represent through a software-based model. The big advantage is given also by the possibility to test products without endangering lives or simply without destroying expensive components or equipment. The production times are shortened and this is another reason why companies are deeply investing in it. Another step before inserting in the simulation loop the actual hardware (full power simulation), is to use a low-power test bench to validate results in a reduced scale system [6].

This work of thesis is based on the simulation of the actual Formula SAE Electric car from ISEC, that is currently stopped from 2010, but it still works; the idea is to create a starting point to later give the possibility to some students to take back the car, update it and bring it back to the race track. The work will be divided in different steps:

- Modelling of the small race car using Energetic Macroscopic Representation (EMR)
- Creation of a Matlab-SimuLink©-based simulation
- Implementation of a reduced-power HIL simulation
- Comparison between results coming from software simulation and reduced power HIL simulation.

2. Energetic Macroscopic Representation

EMR is an extension of the Causal Ordering Graph (COG), a graphical formalism that was developed in '90s to describe and structure in an easy way the control for electromechanical systems [9]. From this, EMR inherits the concept of physical causality. The physical causality states that an output value of a function must be an integral function of the input value and not a derivative one. Following this rule there will be no discontinuities in output variables [9]. Another important notion that is present in EMR is the notion of interaction: this states that any action of a subsystem on another one, induces a reaction; the product of action and reaction represents the instantaneous power exchanged by two elements[1].

Another important characteristic of both COG and EMR, is the type of description of the physical system that they depict. In general, two types of description exist: the structural description and the functional description. The structural description gives more importance to the topological description of the systems, i.e. in the case of an electrical circuit, it describes exactly the components and their location, reproducing the circuit as it can be seen. The functional description instead is not interested in such a representation of the actual system but is focused into represent the functionality of each part of the system. It can also be said that in the functional description the priority is for the function (or equation) that represents the behaviour of the various subsystems and not for the structure (or topology) of the system. Both EMR and COG are functional descriptions. As example it can be used a simple resistance and (1) that describes its behaviour (Figure 1).

$$u_r = i_r R \tag{1}$$

[1] Some reactions of subsystems are neglected, in order to get an easier study. An example can be the interaction between a sensor and the physical system: this exchanges an infinitesimal power amount with it, so it is safe to neglect its reaction.

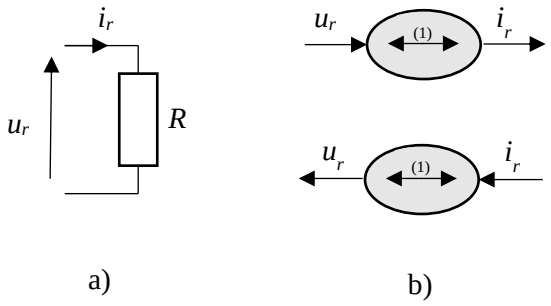

Figure 1, Representations of a resistance: a) Structural, b) COG (functional).

In this example it can be noticed that the COG pictogram has a double-sided arrow. This means that the input and output can be also inverted, accordingly with changes into (1) to get i_r as output and u_r as input (called *rigid processor* [9]). That is not the case of an inductor, expressed by (2) and Figure 2.

$$L\frac{di_L}{dt} = u_L \quad or \quad i_L = \frac{1}{L}\int u_L\, dt \tag{2}$$

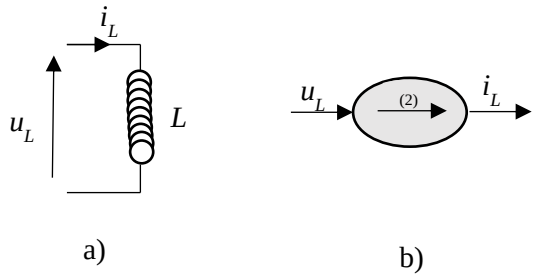

Figure 2,Representation of an inductor: a) Structural, b) COG (functional)

Here is clear that (2) has to be expressed using natural causality (or integral causality) principle when COG is used; that is why the arrow in b) now has only one direction (called *causal processor* [9]). Here the input and the output are fixed, whatever quantity comes from a previous or next block.

This last characteristic can create some conflict problems when the assembling-blocks procedure is started in order to represent an entire system that is composed by various blocks; the solution of this problem will be later explained.

Finally, one big advantage of the functional description such as COG or EMR is the easiness with which the structure of control can be designed, by simply inverting the blocks used to describe the plant. The inversion of a rigid processor consists only in the direct inversion of the initial equation. The inversion of a causal processor

instead, implies the use of a controller that will insert a delay into input-output relation (indirect inversion). The input in this case will be the difference between the reference value of the signal and the measured value, that will feed the controller, to later get as output the reference value of the desired signal.

2.1. EMR Description

The EMR concept comes from the same basis of COG, as is more focused into the macroscopic vision of subsystems by considering the energetic exchanges between them. In EMR, the causality concept is expressed through the use of accumulation elements.

EMR is done through the use of four different kinds of basic elements, and their relative inversion elements:

- Source Elements

Are represented by green ovals and represent the system environment. They generate or receive energy and for this they have one ingoing arrow and an outgoing one.

Figure 3, Source Elements

- Accumulation Elements

Are represented by orange-barred rectangles. They accumulate an internal energy (with or without losses) and their outputs are integral functions of the input (to fulfill the natural causality principle). The delay effect of the causality principle is expressed through the oblique bar inside the rectangle. They have two outgoing vectors and two ingoing ones. Their inversion elements are light blue-barred parallelograms including a closed loop.

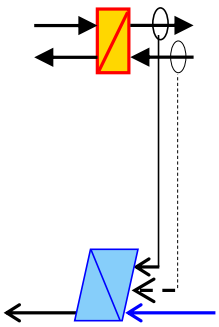

Figure 4, Accumulation Elements

The inversion element, as it can be seen in Figure 4, has as inputs not only the solid blue arrow, but also two other arrows: they represent measured variables from the direct path that are used inside the inversion element to implement the controller.

- Conversion Elements

They are represented by orange squares (if mono domain conversion) or circles (if multi domain conversion). These elements are used to represent an energy conversion (with or without losses) without storage and for this reason they do not have fixed outputs and inputs before connection with other blocks. They have one outgoing and one ingoing vector on the upper side, and the same formation on the downside; they could present also another ingoing vector that can be used to insert inside the block a signal input vector or to modulate the energy conversion (red arrow in top left element in Figure 5). Their inversion elements are light blue parallelograms (both mono-physical and multi-physical conversion), which consists in direct inversion (no closed loop)

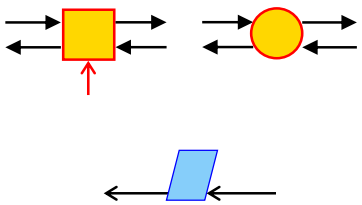

Figure 5, Conversion Elements

- Coupling Elements

They are described by orange overlapped circles (multi-physical conversion) or squares (mono-physical inversion). They are used to distribute the energy following certain criteria, without storage (with or without losses). Their inversion elements are light blue overlapped parallelograms (both mono-physical and multi-physical inversion).

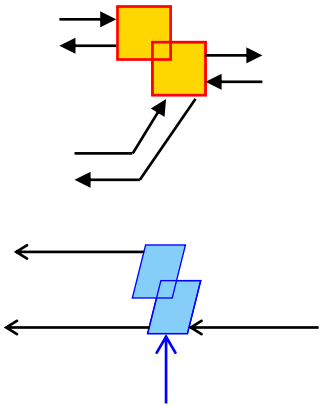

Figure 6, Coupling Elements

In Figure 6, it can be noticed a blue arrow going into the inversion element: this is the input for the criteria used to manage the coupling between the elements; it can be for example a ratio factor for the input value that rules how to split it in the two output values.

2.2. Rules of Association

In EMR two rules of association are used to solve conflicts within the framework of a real systemic approach: the rule of merging and the rule of permutation. With these two rules, an association of real subsystems can be transformed into an association of virtual subsystems without any conflict. Conflicts can occur in situation where two elements that have to be connected between them, want to impose at the same time two different values for the same state variable: this is physically impossible and for this reason conflict has to be solved to go on with EMR. The two rules are the following:

- Rule of Permutation

This rule allows to permute two close elements, finding the parameters of the new virtual subsystem. The same parameters will be present on the top and bottom right side of the subsystem and also on the left side: what it will change will be the parameters between the two elements.

The easiest example is the one of a transformer, with an impedance "*L, r*" at the primary and a transformation ratio "*m*" between primary and secondary; the impedance is represented with an accumulation element, and the passage between primary-side values to secondary-side values, is related to a conversion element (mono-physical). The permutation between these two blocks is the same thing that passing the impedance from primary to secondary side. To do this the only thing that has to be done is to divide the impedance value by the transformation ratio squared (m^2). The graphical representation is described in Figure 7:

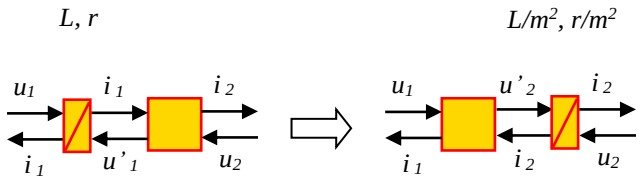

Figure 7, Example of Permutation

- Rule of Merging

This rule is used in cases in which two close blocks are trying to impose the same state variable. With this rule the two elements can be merged in a single virtual one.

As example can be used the behaviour of two capacitors in parallel, with different values of capacitance and internal resistances: is necessary to merge the two accumulation elements that represent them into only one. This can be done creating an equivalent one that behaves as a capacitor with capacitance value equal to the sum of the two initial capacitances, and internal resistances equal to the parallel between the initial internal resistances. In Figure 8 the process is graphically explained.

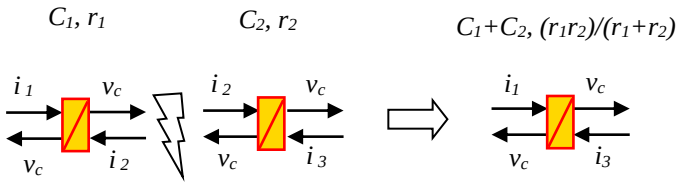

Figure 8, Example of Merging

3. Hardware-In-the-Loop simulation

Once that EMR of the vehicle is well defined, HIL simulation can be implemented simply substituting or adapting some elements of the original representation, in order to allow the co-simulation between a software such as Matlab® and its simulation program Simulink©, and others that allows real-time simulation and control of actual devices (i.e. dSPACE® ControlDesk). To do so, HIL simulation can to be divided into three steps:

- Signal HIL simulation
- Reduced Power HIL simulation
- Full Power HIL simulation

In next three paragraphs, the three steps will be explained and analysed.

3.1. Signal HIL simulation

First of all, a Signal HIL has to be performed, to check if the ECU and its control algorithm is well developed. The simulation of the entire power system is taken in real-time environment and an external ECU will be the platform to run and test the control algorithm (Figure 9). Connection between the two parts is done through an Interface System (IS) that only manages signal variables. It is crucial to well define the simulation time and the sampling periods to get some valuable results: the most important rule is that the sampling period of the emulated part (the power system model) has to be lower than the sampling period of the tested ECU. This allow to let the tested ECU see the measurements as taken from an analogic system. Also, the synchronization of the two sampling periods is recommended to avoid any undesirable effect.

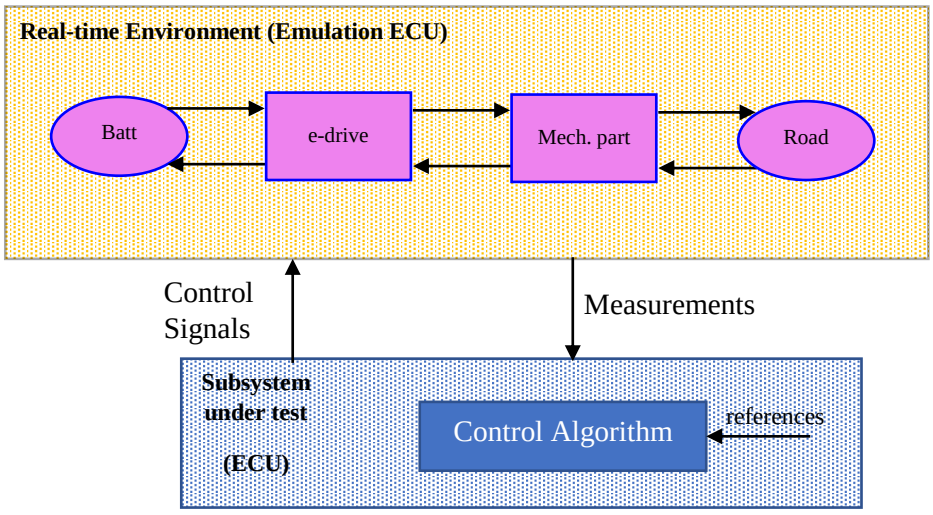

Figure 9, Implementation of Signal HIL simulation

3.2. Full Power HIL simulation

In this type of HIL simulation, the power parts are divided in two different ones: the one that has to be tested using actual components and the one that has to be simulated through some devices able to reproduce the desired conditions. Indeed, the simulated part is connected to the first one through an emulation device that has to be controlled by a dedicated emulation control block, elaborated in the emulation ECU (Figure 10). The addition of this controller sets another constraint from the point of view of the time response values: the closed loop controller of the emulation device has to be faster than the one of related virtual subsystem. Furthermore, the emulation

device has to be more powerful in respect to the related virtual subsystem, to let the virtual subsystem work through all the power range, without any problems. Reduced-Power HIL Simulation can be adopted as an intermediary step before developing a full-scale HIL simulation, as is explained next.

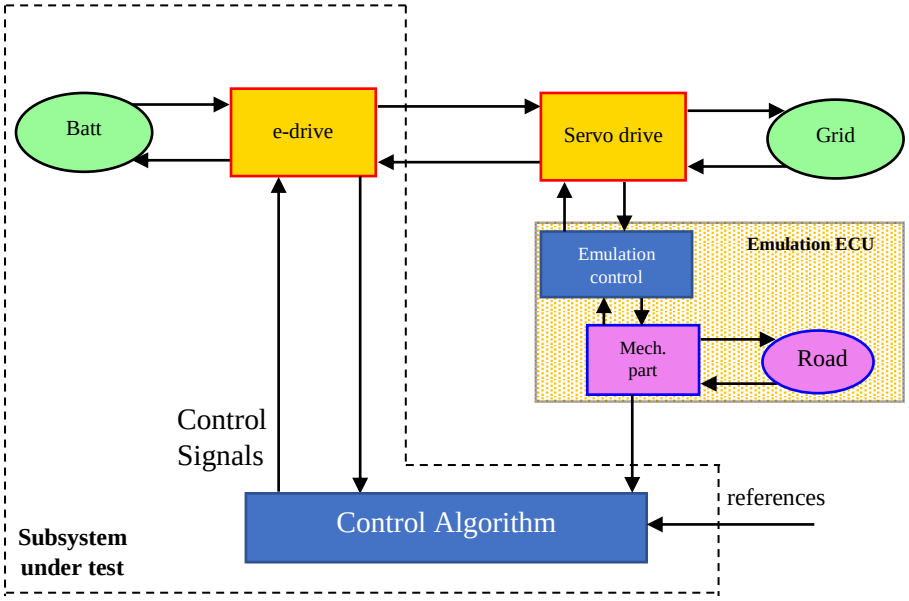

Figure 10, Implementation of Power HIL simulation

3.3. Reduced Power HIL simulation

In case the available test bench does not have enough power with for the subsystem to be emulated, a Reduced Power HIL simulation can be used as intermediary solution: the only difference from a structural and computational point of view from the Full Power HIL simulation is given by the addition of some Power Adaptation blocks (PA) (Figure 11) [10]. These blocks are inserted between the emulation control and the subsystem model (in this case the mechanical model) and between the control of the subsystem model (mechanical part) and the control of the tested subsystem (e-drive). This reduced-power HIL simulation is just an intermediary step before a full power HIL simulation or a replacement of it in the case of a big power range application, such as wind generators or other MW machines.

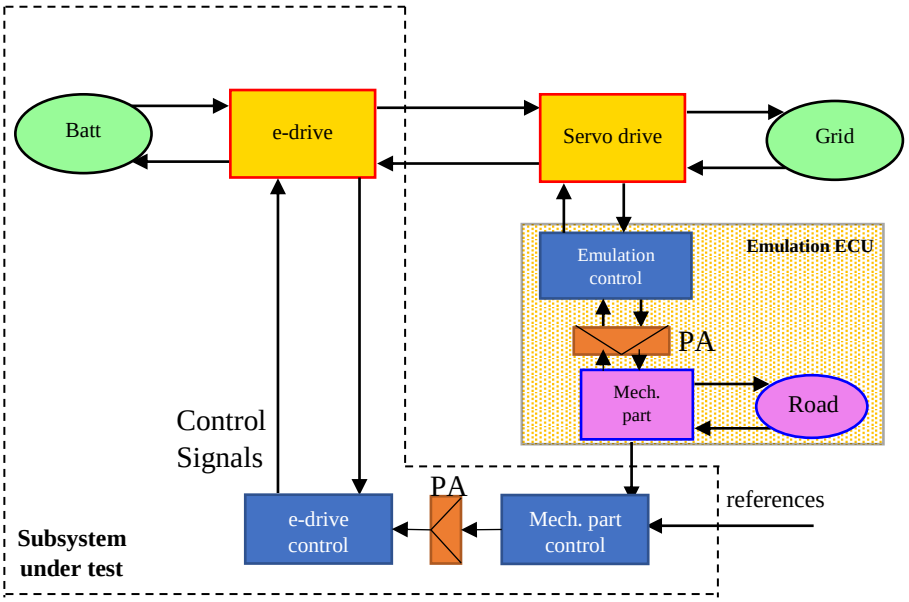

Figure 11, Implementation of Reduced Power HIL simulation

4. Modelling the ISEC Formula SAE electric car

4.1. The car and the track

The car that is going to be modelled is a small race-car that was initially supposed to compete in Formula SAE Electric competition. The developing of the car started in 2010, when the ISEC's team started to look for some motors that could be suitable for the application. Some students worked on the Simulink model of the car, to get some initial parameters to start building it [11]. After two years the car was built but it has never been used to compete in Formula SAE, due to some unexpected hardware problems and subsequent lack of students involved in the project. Nonetheless, the car has been used for some demonstration activities [12] such as IEEE Vehicle Power and Propulsion Conference (VPPC) 2014 [13], ISEC open-day and also other exhibitions.

Nowadays, the team involved in the ICE-version of the car, is considering to go back to the project, trying to put it back on the track, starting from an older project initially for the ICE version from 2014, with the aim to give a new body to the car [14]. Since in the cited report are presented various possibilities for the body design, the body option 4 is chosen, and all the relative aerodynamic parameters are selected.

The mechanical and aerodynamic specifications of the actual car are reported in Table 1.

Table 1, Mechanical and aerodynamic parameters for ISEC Car

Weight (included pilot)	**375 kg**
Width	**1.355 m**
Drag Coefficient (C_x)	**0.29**
Downforce Coefficient (C_z)	**1.2**
Front Area	**0.84 m^2**
Tire radius	**0.245 m**
Rolling Resistance	**0.030**

Table 2, Powertrain specifications for ISEC car

Total Nominal Torque	**95.4 Nm**
Total Nominal Power	**34.05 kW**
Gear Ratio	**constantly variable transmission**
Reduction ratio	**3.57**
Traction mode	**Rear Wheel Drive**

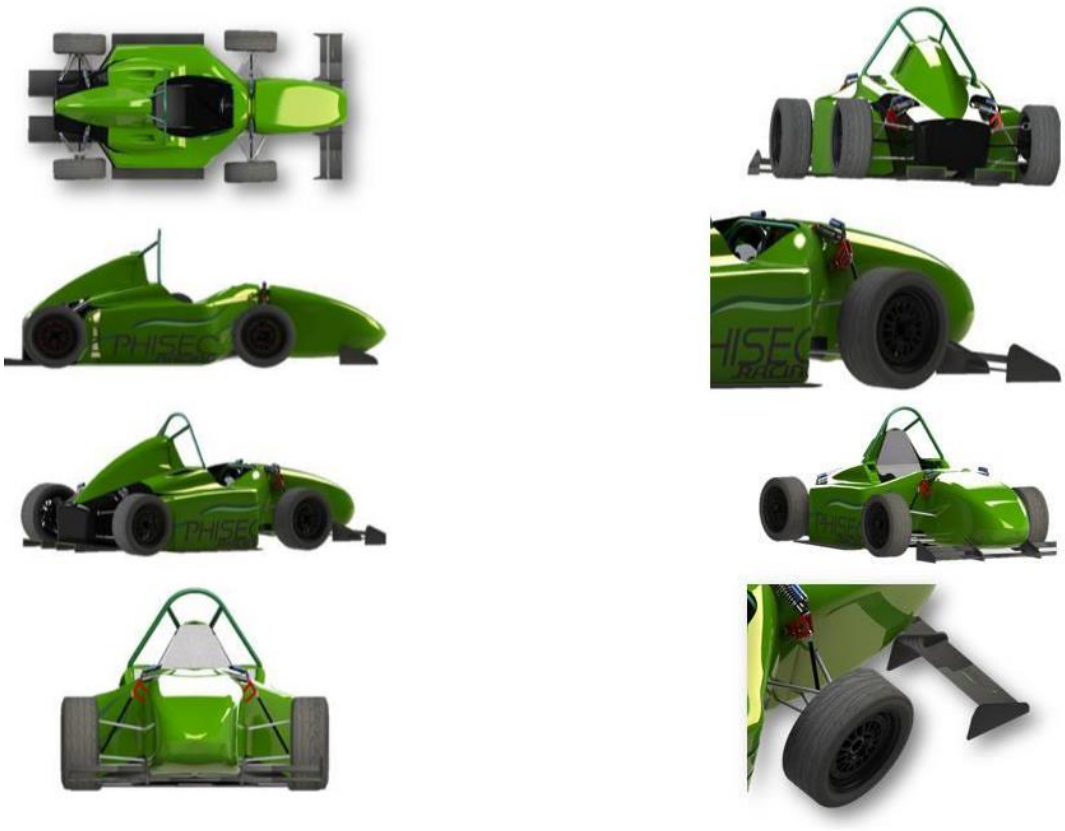

Figure 12, Rendering of the body option 4 [14]

Other problems with the car are related to the charging facilities that are now out of service, but the team is working to find a solution. For this reason, it was not possible to see the car in action and also to get actual readings of results such as acceleration 0-100 km/h, braking performance and handling of the vehicle; for this reason, the simulation will be based on results from a simulation software, that is able to evaluate these values only inserting the known parameters from the vehicle.

This work of thesis has the target to simulate the behaviour of the car on a Formula SAE actual circuit, to see how the car will react from the point of view of the performance but also the stress level at which batteries, inverters and electrical machines are subjected during one circuit lap.

To do so, the circuit used for FSAE 2012 competition in Nebraska is selected. Through a simulation software called OptimumLap© from OptimumG© the vehicle can be easily represented using some parameters already presented in Table 1 and the powertrain specifications presented in Table 2.

The software creates a track map, where the speed of the vehicle is presented for each part of the circuit (Figure 13).

Figure 13, Nebraska FSAE 2012 Endurance Track with speed values

Is important to note that the values that are used for torque and power of the powertrain is the result of the coupling of two Surface Permanent Magnet Synchronous Machines (SPMSM), model PMS 156 L from Perm Motor G.m.b.H., part of Heinzmann Group. The machines have the characteristics reported in Appendix A (Electrical Machines Datasheets).

An important assumption is done in order to properly use OptimumLap© configuration panel for the car: this software allows to insert only one set of values for the torque, losing the possibility to insert also the peak torque or the pulsed-operation torque values that are proper for the two motors. This obliges to insert the values for the continuous mode operation (S1) losing the matching with the actual values achievable from the car through a proper control strategy of the powertrain. For this reason, data presented in OptimumLap© Report as “Time for 0 to 100km/h” are very high. Nonetheless the max speed value can be taken as a feasible value for a car with such a weight and power range.

4.2. EMR of the car

The following paragraph is focused on the development of the EMR for the vehicle. To do so, a simplified model of the vehicle is used (Figure 14).

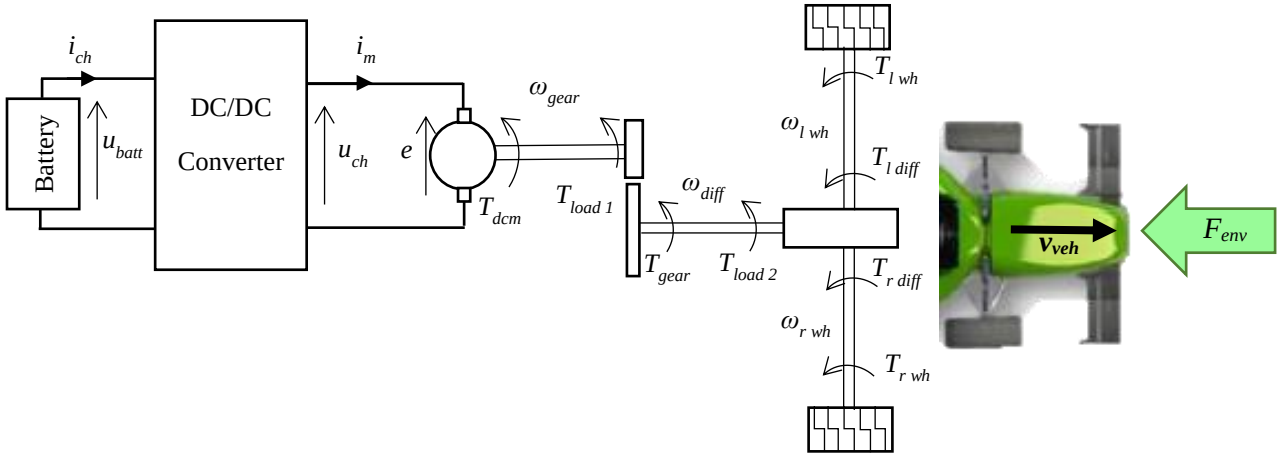

Figure 14, Simplified model of the vehicle

As the motor and its converter will be latter grouped in only one block as explained further on, it is considered at this point a DC/DC converter and a DC machine. Starting from this model, the analysis of all the parts can be done starting from the equations that rule their behaviour.

4.2.1. Battery

The battery in first approach was considered as a constant voltage source, but in the final simulation it was inserted a model that represents the behaviour of an actual battery, with only resistive losses and the monitoring of SoC [15]. This allows to see the residual SoC at the end of the driving cycle and verifying if the power delivered is enough for desired purposes. Table 3 represents the values for a single cell of the Li-Ion battery used. The battery cells used have a $LiFePO_4$ technology from the Chinese company Thunder Sky® Battery Ltd; the name of these cells is TS-LFP90AHA. The vehicle uses 30 cells in series.

Table 3, TS-LFP90AHA Battery Pack Characteristics

Nominal Cell Voltage	3.2-3.3 V
Max Cell Voltage	4.25 V
Min Cell Voltage	2.5 V
Nominal Cell Capacity	90 Ah
Pack Equivalent Resistance (R_s)	200 mOhm
Number of cells in Series	30
Number of cells in Parallel	1
Weight of each cell	3 kg

The equations that give the basis to create the battery source element are:

$$u_{batt} = OCV - R_s i_{batt} \tag{3}$$

$$SoC(t) = \left(SoC_{t_0} - \frac{\int_{t_0}^{t} i_{batt} dt}{3600 C_{batt}} \right) \tag{4}$$

where *OCV* is the open circuit voltage depending on *SoC* and i_{batt} is the current going out from the battery. C_{batt} is the capacity of the battery and SoC_{t_0} is the initial *SoC*. The model that is inserted in the source element is depicted in Figure 15:

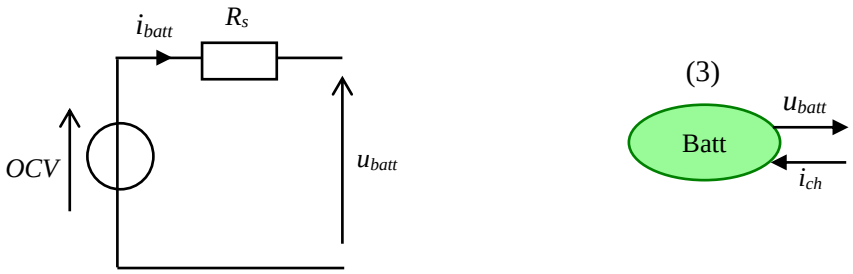

a) b)

Figure 15, Battery model: a) Structural representation, b) EMR (Functional representation)

4.2.2. Chopper

The DC-DC converter (chopper) is modelled using an average model. i_{ch} and u_{ch} can be varied through the use of the modulation factor m_{ch} [16]. The model is given by (5).

$$\begin{cases} i_{ch} = \eta_c^k m_{ch} i_m \\ u_{ch} = m_{ch} u_{batt} \end{cases} \quad \text{where } k = \begin{cases} 1, & P(t) < 0 \\ -1, & P(t) \geq 0 \end{cases} \tag{5}$$

in which i_m is the current imposed by the machine, η_c is the efficiency of the converter, u_{ch} is the voltage imposed by the chopper, and *P(t)* is the instantaneous power of the converter. In Figure 16 both the structural and functional representations are presented:

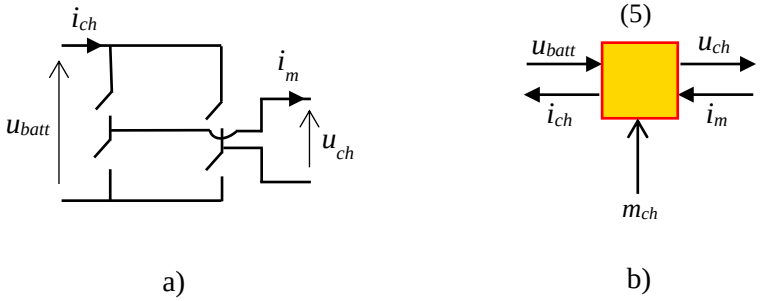

a) b)

Figure 16, Chopper conversion element: a) Structural representation, b) EMR (functional representation)

4.2.3. Electrical machine

The machine can be modelled as three parts. The first part is the electrical part, the second one is related to the electromechanical conversion and the third one is a mechanical part. As already said, this machine is a Surface Permanent Magnet Synchronous Machine (SPMSM) but in the simulation it can be treated as a DC machine. Regarding the electrical part, the armature has as characteristic values an equivalent inductor, L_{arm}, and an equivalent series resistor, R_{arm},

$$(u_{ch} - e) = L_{arm}\frac{di_m}{dt} + R_{arm}i_m \tag{6}$$

where *e* is the back-emf of the machine presented in Figure 17. To create the conversion element will be used the Laplace domain, getting (7).

$$I_m(s) = \left(\frac{k_{current}}{\tau_{current}s+1}\right)\left(V_{ch}(s) - E(s)\right) \quad \text{where} \begin{cases} \tau_{current} = \frac{L_{arm}}{R_{arm}} \\ k_{current} = \frac{1}{R_{arm}} \end{cases} \tag{7}$$

As already explained, the second part represents the electromechanical conversion, that is defined by the following equations:

$$\begin{cases} T_{dcm} = k_T i_m \eta_m^h \\ e = k_T \omega_{gear} \end{cases} \text{where} \quad h = \begin{cases} -1, & T_{dcm}\omega_{gear} < 0 \quad (Generator\ mode) \\ 1, & T_{dcm}\omega_{gear} \geq 0 \quad (Motor\ mode) \end{cases} \tag{8}$$

in which k_T is the torque coefficient and η_m is the efficiency of the motor.

The third part of the machine model represents the relation between the two torques T_{dcm} and $T_{load\,1}$, and the friction coefficient of the rotor f_1, the inertia of the rotor J_1 and the speed at the rotor-side of the gearbox ω_{gear} (cf. Figure 14) as it is showed in (9):

$$(T_{dcm} - T_{load\,1}) = J_1 \frac{d\omega_{gear}}{dt} + f_1 \omega_{gear} \tag{9}$$

The two representations are shown in Figure 17.

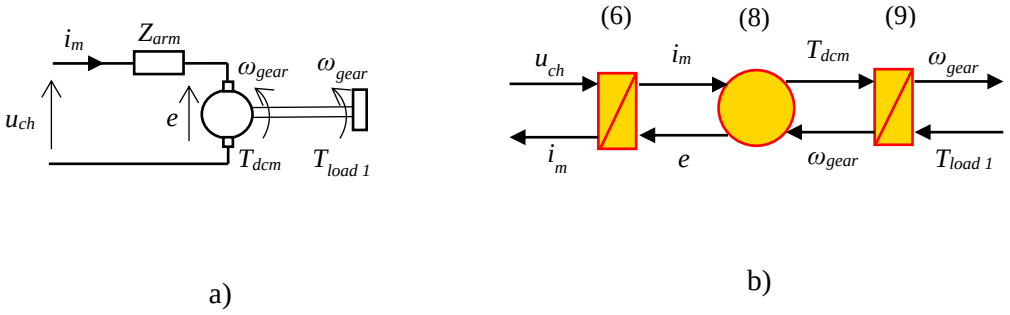

a) b)

Figure 17, Electrical machine representation: a) structural representation, b) EMR (functional representation)

The values used in simulation are reported in Table 4.

Table 4, Electrical machine parameters used in simulation

$\boldsymbol{R_{arm}}$	0.35 Ohm
$\boldsymbol{L_{arm}}$	6.5 mH
$\boldsymbol{u_{arm\,nom}}$	96 V
$\boldsymbol{i_{arm\,nom}}$	89.5 A
$\boldsymbol{\omega_{nom}}$	3000 rpm

4.2.4. Gearbox

The gearbox is connected to the motor's rotor from one side and to the differential on the other side; the equations that present its behaviour are the ones listed below:

$$\begin{cases} \omega_{diff} = \frac{\omega_{gear}}{k_{gear}} \\ T_{load\,1} = \frac{T_{gear}}{k_{gear}} \end{cases} \tag{10}$$

$$(T_{gear} - T_{load\,2}) = J_2 \frac{d\omega_{diff}}{dt} + f_2 \omega_{diff} \tag{11}$$

J_2 is the inertia moment of the masses rotating at ω_{diff} speed, f_2 is the gearbox friction coefficient, representing the mechanical losses in it.

Their representations are shown in Figure 18.

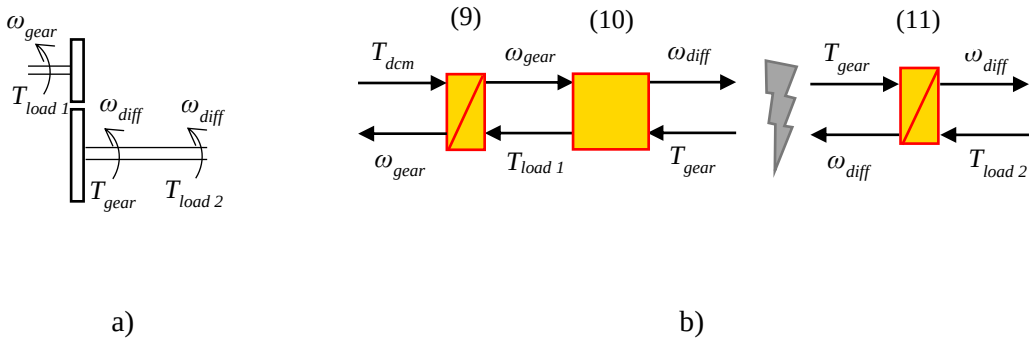

a) b)

Figure 18, Gearbox representation: a) structural representation, b) EMR (functional representation)

As it can be seen in b), there is a conflict of association in this part, due to the fact that two elements are trying to impose at the same time, different values for the same variable ω_{diff}. this will be solved later on, after having collected all the possible conflicts in the system.

4.2.5. Differential

The differential is connected on one side to the gearbox and on the other one to the wheels. The differential is used to allow having two different rotational speeds ($\omega_{l\,wh}$ and $\omega_{r\,wh}$) on the two wheels present on the same axle. This can be useful in situations such as slippy roads, where one of the two wheels loose friction, starting to slip; the differential allows to reduce the speed of that wheel, until it will gain more grip. The torque will be the same ($T_{l\,diff}$ and $T_{r\,diff}$), but the speed will change.

As a first approximation in this modelling will be used only one equivalent wheel, based on the assumption that the speed is the same for both wheels ω_{wh}.

$$\begin{cases} \omega_{wh} = \dfrac{\omega_{diff}}{k_{diff}} \\ T_{load\,2} = \dfrac{T_{diff}}{k_{diff}} \end{cases} \tag{12}$$

$$(T_{diff} - T_{wh}) = J_3 \frac{d\omega_{wh}}{dt} + f_3 \omega_{wh} \tag{13}$$

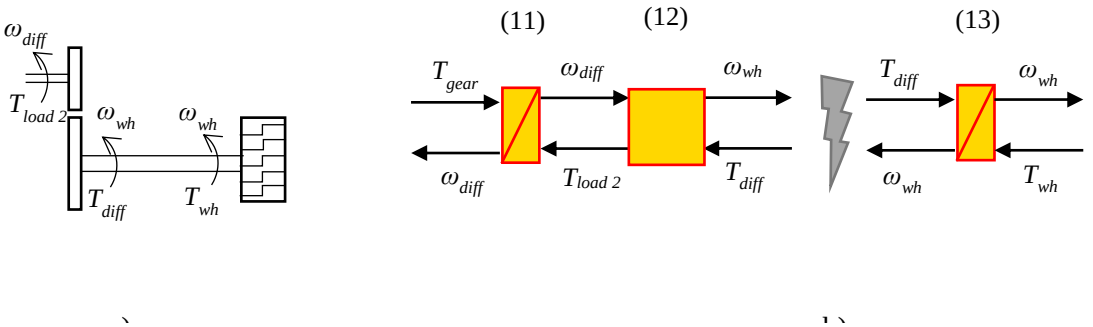

Figure 19, Differential and wheel representations: a) structural representation, b) EMR (functional representation)

As before, there is a conflict of association in these blocks, regarding ω_{wh} that will be later solved.

4.2.6. Chassis and wheels

The connection between the rotational variables to the translational variables is needed to connect the wheels to the chassis. This is given by the following equations.

$$\begin{cases} v_{ve} = \omega_{diff} R_{wh} \\ T_{wh} = F_{wh} R_{wh} \end{cases} \tag{14}$$

$$(F_{wh} - F_{res}) = M_{tot} \frac{dv_{ve}}{dt} \tag{15}$$

in which R_{wh} is the radius of the wheel, M_{tot} is the total mass of the vehicle and v_{ve} is the vehicle velocity, F_{res} is the resistive force opposed to the force produced by the car, that has to be overcome to let the car move.

This is the representation of this part, with again a conflict that has to be solved.

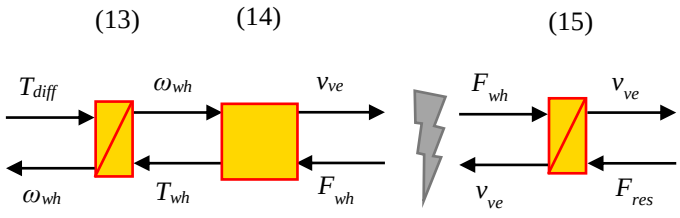

Figure 20, EMR of the Chassis

4.2.7. Road

The road can be seen as an energy source and is the third in the system after the battery and the mechanical brake, so it will be presented as an energy source element, ruled by the following equations:

$$F_{res} = f_{road} M_{tot} g + \frac{\rho C_x A (v_{ev} + v_{wind})^2}{2} + M_{tot} g \alpha \quad (16)$$

where, f_{road} is the coefficient of rolling resistance between asphalt and tires, g is the gravitational constant, ρ is the air density, C_x is the drag coefficient, A is the vehicle frontal area, v_{wind} is the wind velocity (considered 0 in this situation), and α is the road slope rate (that is 0 in this situation).

The representation is the one presented in Figure 21.

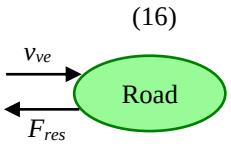

Figure 21, EMR of the Road

4.2.8. Solving conflicts of association

As it has been noticed, there are three different parts in which conflicts occur. To solve these, the two rules already explained in 2.2 will be applied.

- Conflict 1

This is the conflict that occurs in the gearbox EMR, expressed in 4.2.4 and visible in Figure 18:

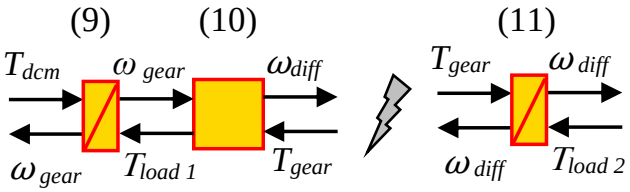

Figure 22, Conflict between rotor equation and gearbox equation

To solve this, first is used the rule of permutation, changing the order between the first two elements from the left, and later on the rule of merging between the two accumulation blocks (Figure 23). With the rule of permutation, only the order of the elements and the inner state variables between the two elements are changed.

First of all, a graphical solution of the conflict will be presented in Figure 23, and only after will be presented the equations describing the resulting elements.

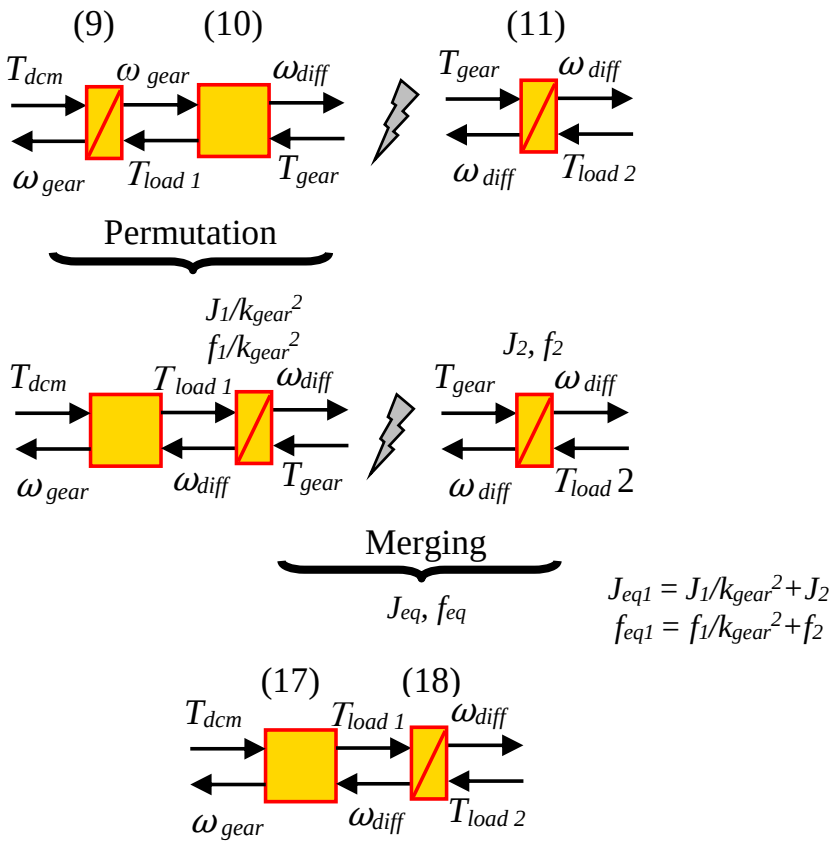

Figure 23, Solution to Conflict 1

Rearranging (10), a new equation can be defined that rules the conversion block in Figure 23:

$$\begin{cases} \omega_{gear} = \omega_{diff}\, k_{gear} \\ T_{load\ 1} = T_{dcm}\, k_{gear} \end{cases} \quad (17)^2$$

The rule of merging, creates from two accumulation elements, only an equivalent one with the following equation developed inside:

$$(T_{load\ 1} - T_{load\ 2}) = J_{eq1}\frac{d\omega_{diff}}{dt} + f_{eq1}\omega_{diff} \quad (18)$$

J_{eq1} and f_{eq1} are expressed inside Figure 23.

[2] $T_{load\ 1} = T_{gear}$ in the final model (Figure 29).

- Conflict 2

This conflict arises between the gearbox and the differential, as it is explained in 4.2.5. The procedure that has to be followed is exactly the same than before.

The final equations, founded through the same procedure used to solve the first conflict, are:

$$\begin{cases} \omega_{diff} = \omega_{wh}\, k_{diff} \\ T_{load\,2} = T_{load\,1}\, k_{diff} \end{cases} \quad (19)^3$$

$$(T_{load\,2} - T_{wh}) = J_{eq2}\frac{d\omega_{wh}}{dt} + f_{eq2}\omega_{wh} \quad (20)$$

J_{eq2} and f_{eq2} are expressed inside Figure 24.

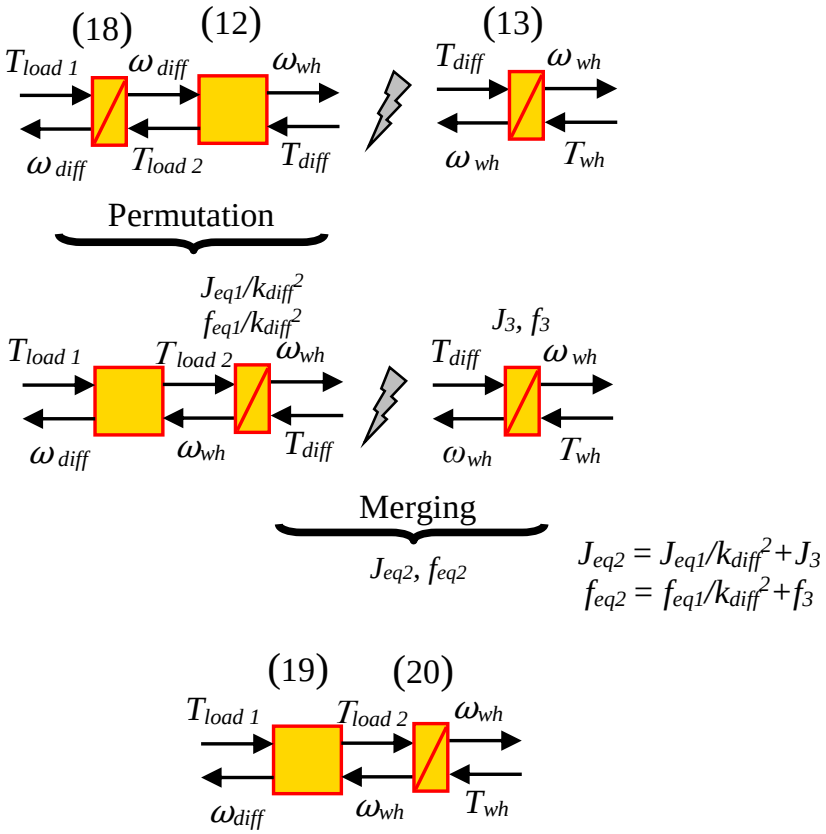

Figure 24, Resolution of Conflict 2

[3] $T_{load\,2} = T_{l\,diff} = T_{r\,diff}$ in the final model (Figure 29)

- Conflict 3

The third conflict occurs between the wheel and the chassis (4.2.6). The equations here are different from before because is necessary to insert also the switching from angular speed to linear velocity, indeed passing from torques to forces. The initial equations for the elements are (14) and (15) as already explained, and the connection to the rest of the system is done through the new equation (20). Using before the rule of permutation and after the rule of merging the results are the following equations:

$$\begin{cases} F_{tr} = \dfrac{T_{load\ 2}}{R_{wh}} \\ \omega_{wh} = \dfrac{v_{ve}}{R_{wh}} \end{cases} \tag{21}$$

$$(F_{tr} - F_{res}) = M_{eq3}\frac{dv_{ve}}{dt} + f_{eq3}v_{ve} \tag{22}$$

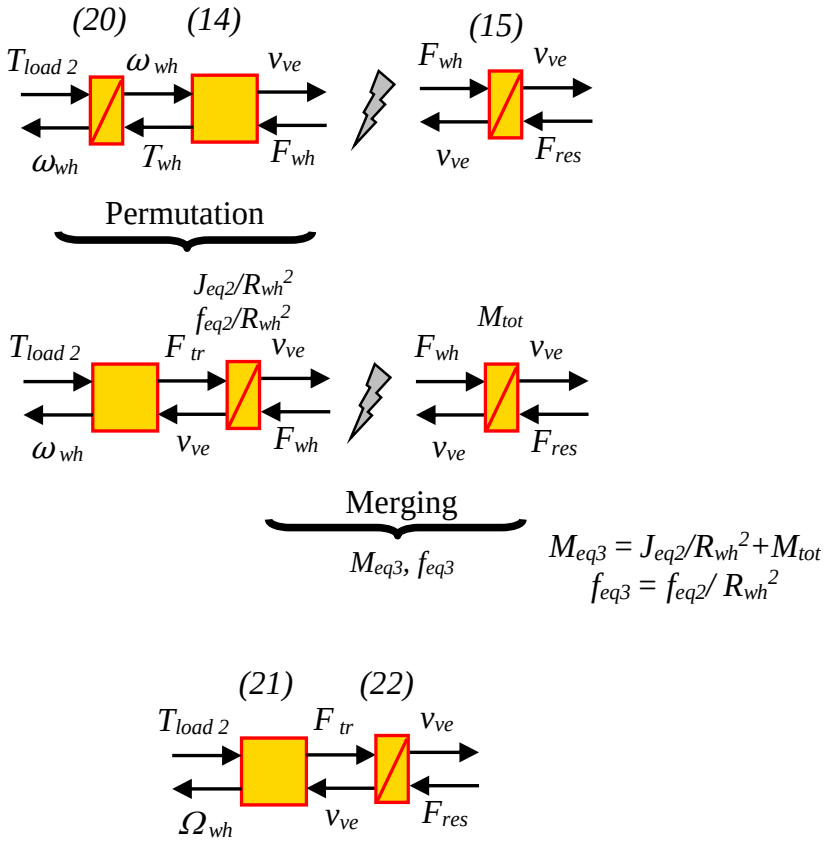

Figure 25, Resolution of Conflict 3

The values utilised in this part of the simulation are reported in Table 5.

Table 5, Parameters for gearbox, differential and wheels

J_1 **(for each motor)**	$0.00586\,\frac{kg}{m^2}$
J_2	$0.001\,\frac{kg}{m^2}$
J_3	$2.5\,\frac{kg}{m^2}$
f_1=f_2=f_3	0.001
k_{gear}	3.571
k_{diff}	1
R_{wh}	$0.245m$
M_{tot}	$375\ kg$
f_{road}	0.01
Gearbox and Differential Efficiency	97%

4.2.9. Coupling between F_{tr} and F_{br}

An important element that has to be inserted to develop the complete EMR, is the coupling element that allows to connect F_{tr} the force coming from the traction part of the system, and F_{br} the force coming from the mechanical brake, following the equation here reported:

$$F_{tot} = F_{tr} + F_{br} \tag{23}$$

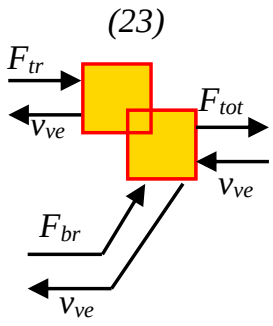

Figure 26, Coupling element inside the Chassis part

4.2.10. Other couplings

To insert also the two-wheels model other two coupling elements are needed, to split and then add again the forces from each wheel. The equations needed are the (24) and (25) listed below.

$$T_{l\ diff} = T_{r\ diff} = \frac{T_{gear}}{2} \tag{24}$$

$$F_{tr} = F_{l\ ve} + F_{r\ ve} \tag{25}$$

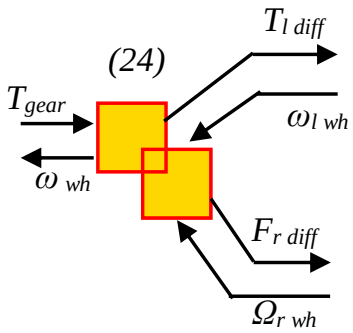

Figure 27,EMR of the Differential

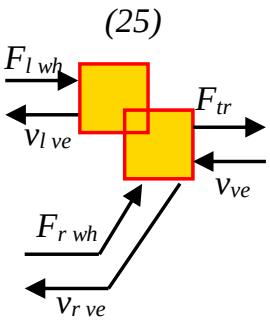

Figure 28, Partial EMR of the chassis

4.2.11. Complete EMR

The final result, assembling all the elements described is depicted in Figure 29.

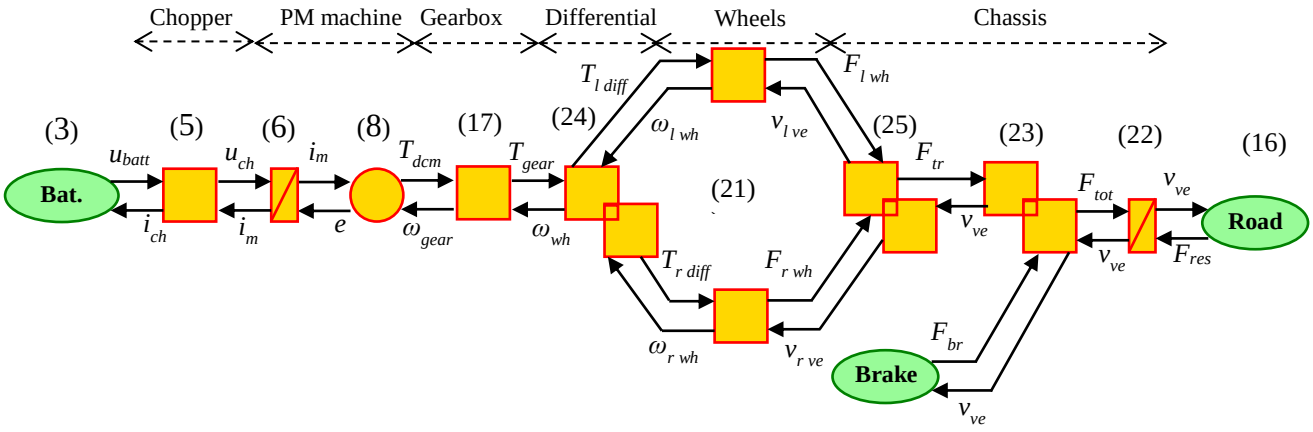

Figure 29, Complete EMR of the vehicle

4.3. Inversion-based Control of the Electric Vehicle

Once that the EMR is well defined, the next step is to define the tuning path, that explains which is the sequence that has to be respected to control the final variable v_{ve}, starting from the variables that can be controlled through a feedback loop, m_{ch} and $F_{br\ ref}$.

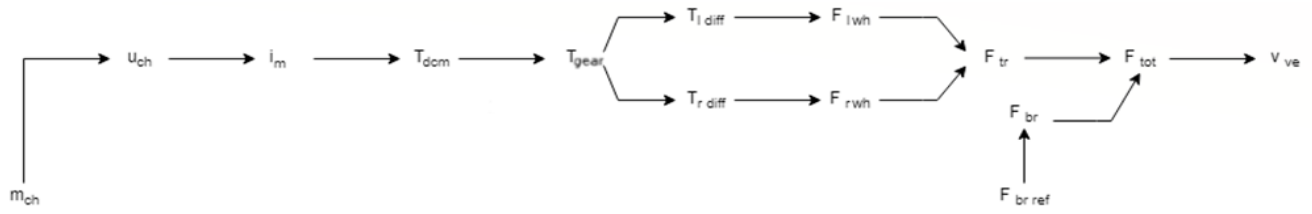

Figure 30, Tuning path for traction

Starting the inversion (cf. blue elements in Figure 31) element by element, coming backwards the first encountered is the chassis, in which is intrinsically present the causality principle. For this reason, is not possible to simply invert initial relations. To keep valid this principle, is mandatory to insert a closed loop controller in the inversion element presented in Figure 31. The equation will be:

$$F_{tot\ ref} = C_v\left(v_{ve_{ref}} - v_{ve_{meas}}\right) + F_{res_{meas}} \tag{26}$$

The controller C_v will be a PI, IP or another type, but this will be decided later on, basing this decision on simulation that will show which is the most suitable one for the application.

After this, the coupling element has to be inverted: if in the direct path (green and yellow blocks) the conversion rule is easy because it only adds the traction force and the braking force as is explained in (23), here a distribution input (k_{br}) has to be inserted that rules which percentage of the total force will be sent as a mechanical braking force ($F_{br\ ref}$), and how many will be sent back to the electrical part ($F_{tr\ ref}$), allowing the regenerative, or electrical braking. The equation for this inversion element is the following:

$$\begin{cases} F_{br_{ref}} = k_{br} F_{tot\ ref} \\ F_{tr_{ref}} = (1 - k_{br}) F_{tot_{ref}} \end{cases} \tag{27}$$

The next element is the coupling element ruled by equation (25): also here is needed another distribution input k_d that allows to choose the ratio between the forces injected in the two wheels. This element is ruled by the following equation.

$$\begin{cases} F_{r\ wh\ ref} = k_d F_{tr\ ref} \\ F_{l\ wh\ ref} = (1 - k_d) F_{tr\ ref} \end{cases} \tag{28}$$

After it, the next inversion elements are the conversion elements for the two wheels: here it is only needed to invert the second equation in (14), to pass from force to torque values:

$$T_{l\ diff\ ref} = R_{wh} F_{l\ wh\ ref} \tag{29}$$

The differential inversion element presents another coefficient to modulate the tuning path: the weighting input k_w allows to decide which is the wheel-related torque reference ($T_{l\ diff\ ref}$ or $T_{r\ diff\ ref}$) that has to "weight" more in the total amount of torque required to the motor. This further coefficient introduces the possibility for the strategy block to decide the proper value of $k_{w,}$ maybe analysing the slip of the two wheels and the general condition of the road and the driving mode; the strategy will be discussed in another section. The equation implemented in this element is:

$$T_{gear\ ref} = k_w T_{r\ diff\ ref} + (1 - k_w) T_{l\ diff\ ref} \tag{30}$$

The two following elements are simply conversion elements, so the only thing to do is to invert (17) and (8):

$$T_{dcm\ ref} = \frac{T_{gear\ ref}}{k_{gear}} \tag{31}$$

$$i_{m\,ref} = \frac{T_{dcm\,ref}}{k_t} \tag{32}$$

The electric conversion element, when is inverted, founds the same problem of the chassis element, because of its nature of accumulation element; the solution also here is to use a controller (PI, IP or other) to keep the integral causality safe. The equation here implemented is this:

$$u_{ch\,ref} = C_i\left(i_{m\,ref} - i_{m\,meas}\right) + e_{meas} \tag{33}$$

Last block that has to be inverted is the one related to the chopper, in which the equation is:

$$m_{ch\,ref} = \frac{u_{ch\,ref}}{u_{batt\,meas}} \tag{34}$$

Finally, Figure 31 shows the complete Maximal Control Structure (MCS) for the vehicle in the lower part. Nevertheless, depending on the objectives, this can be simplified, as will be in section 4.6.

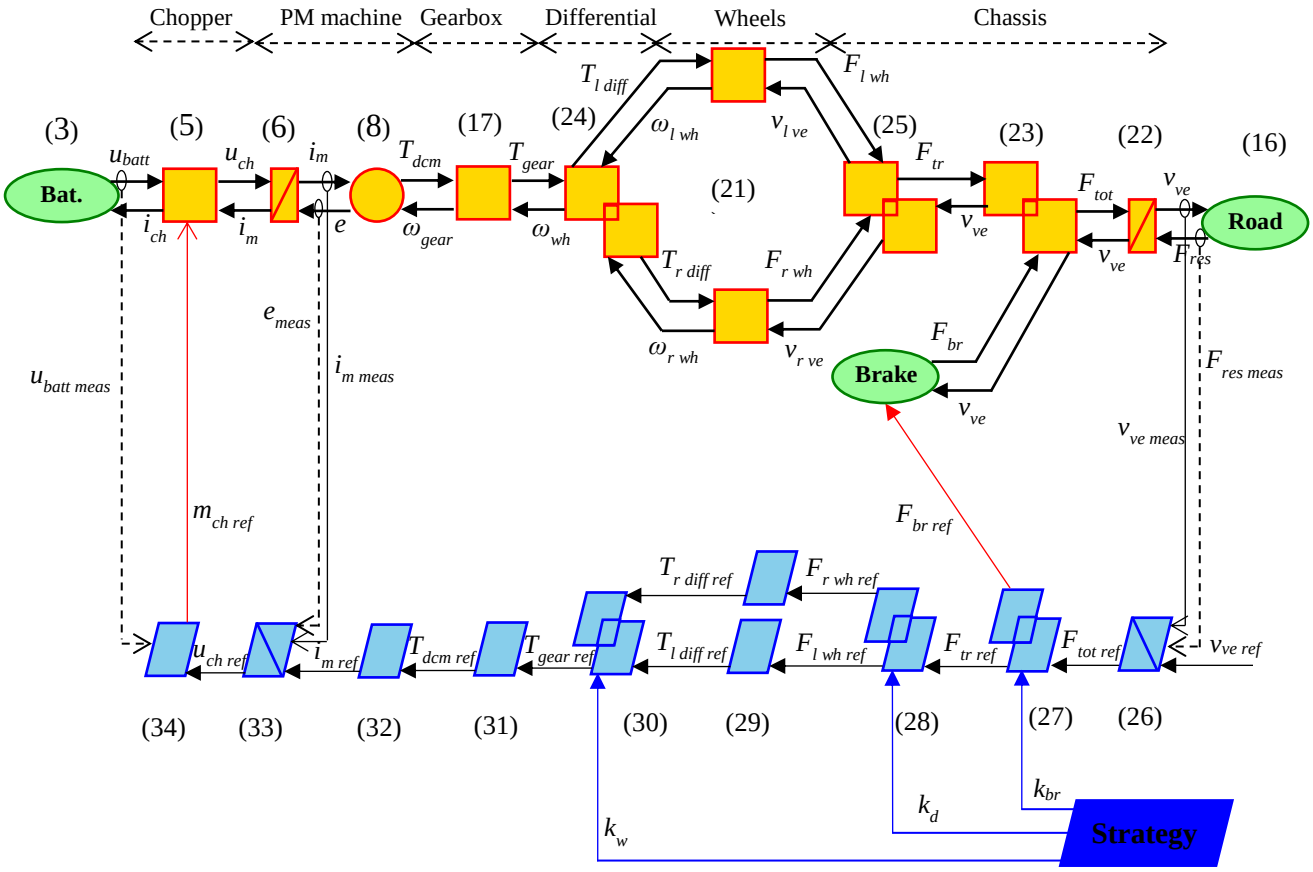

Figure 31, Complete EMR with the Maximal Control Structure

4.4. Controllers Tuning

In this chapter the tuning of the two controllers present in the tuning path are done: the velocity controller and the current controller.

The first general rule that has to be respected is that a minimal ratio of 10 between the inner loop and the outer loop-time constant is always present, i.e. the velocity controller time constant has to be at least 10 times bigger than the current controller time constant. It means that the outer loop will see the inner loop as ideal, because of its fast dynamic.

4.4.1. Velocity controller

The velocity controller has as inputs the speed reference, the actual velocity directly measured $v_{ve\,meas}$ and the resistive force directly measured from the system $F_{res\,meas}$. In this case, due to the nature of the reference signal, a proportional (P) controller would not be able to reach a zero steady-state error, so a proportional-integral (PI) controller seems to be the best option, for its characteristics. A feed-forward action ($F_{res\,meas}$) can be added, to improve the overall response of the controller [17]. The only contraindication that could occur in case of using a PI controller is an overshoot during the transients. This is due to the fact that this controller acts over the error signal, without separating the integral and the proportional part of the control: this has some effects on the transfer function that presents a zero as it is visible in (35), that could create some unexpected overshoots.

$$G(s) = \frac{(1 + s\tau)\omega_n^2}{s^2 + 2\xi\omega_n s + \omega_n^2} \tag{35}$$

The IP controller instead, separates the integral and the proportional effects (Figure 32), giving as final result a transfer function that does not present zeros, as it can be seen in (36).

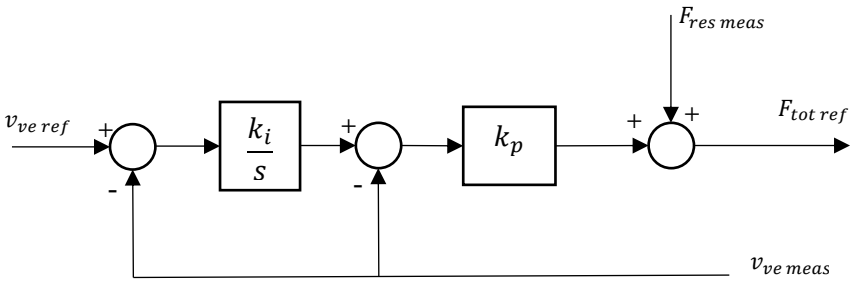

Figure 32, IP controller block diagram

$$G(s) = \frac{\omega_n^2}{s^2 + 2\xi\omega_n s + \omega_n^2} \tag{36}$$

Once that the IP controller is selected, the tuning can be done. Through some mathematical development, the final equations used to get k_p and k_i are the following:

$$\begin{cases} k_p = \dfrac{2\xi\omega_n\tau_v - 1}{K_v} \\ k_i = \dfrac{\omega_n^2\tau_v}{K_v k_p} \end{cases} \tag{37}$$

in which from previous equations:

$$\begin{cases} K_v = \dfrac{R_{wh}^2}{f_{eq2}} \\ \tau_v = \left(\dfrac{J_{eq2}}{R_{wh}^2} + M_{tot}\right)\left(\dfrac{R_{wh}^2}{f_{eq2}}\right) \end{cases} \tag{38}$$

These values represent the plant and are implemented in the chassis transfer function, showed below:

$$G(s) = \frac{K_v}{\tau_v s + 1} \tag{39}$$

The parameters ξ (damping factor), ω_n (natural frequency), t (time) and t_r (time response) depends from the choice. In this case these values are selected:

$$\omega_n t = 4.744$$

$$\xi = 1$$

$$t_r = 1\ second$$

With these values zero overshoot are expected, that is the desired result.

In Figure 33 is reported the comparison between an IP controller and a PI controller with the values previously indicated for a velocity step of 10 *m/s*. It is clear that the IP solution is the best, due to the absence of overshoots, as expected from previous discussion.

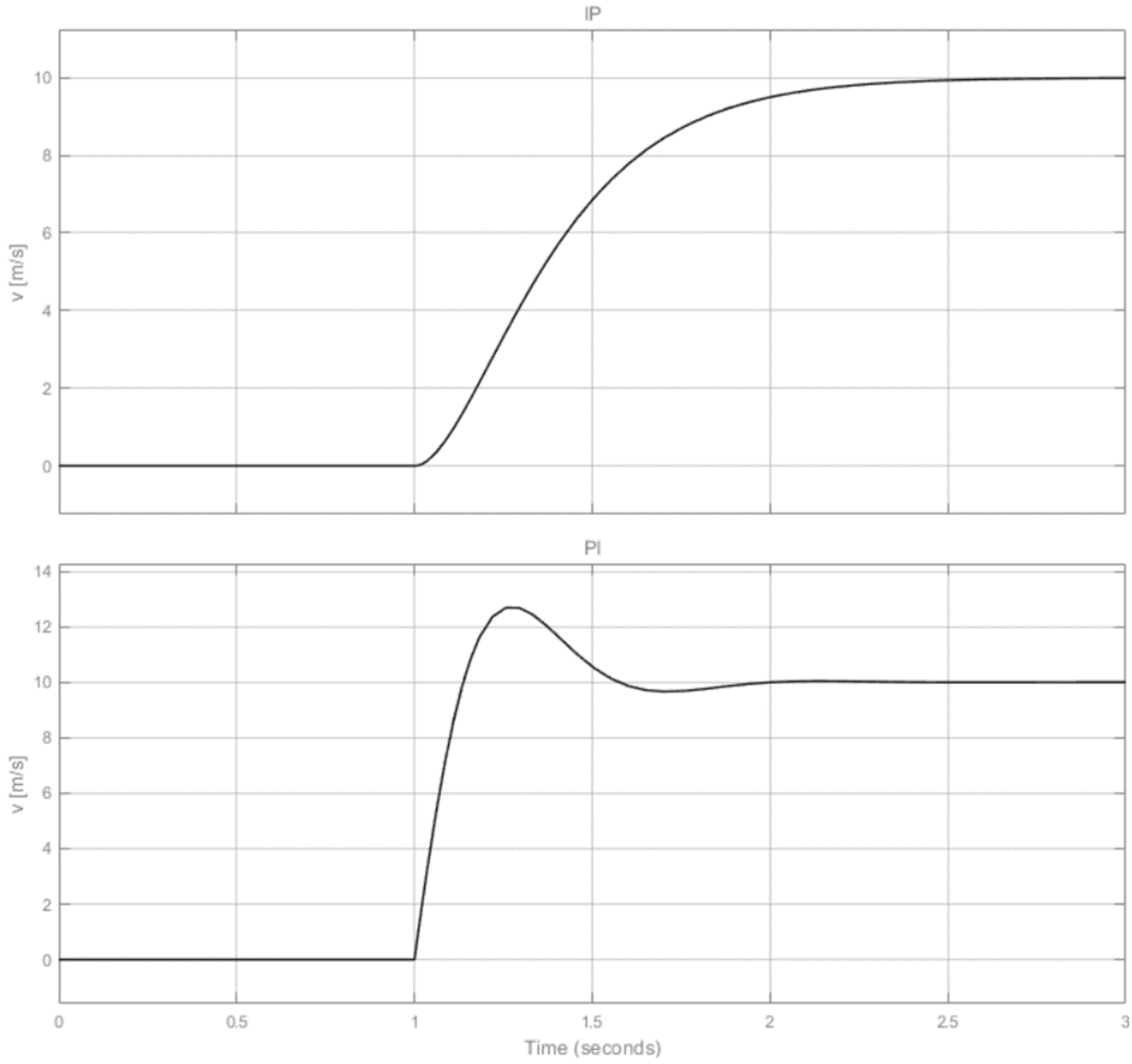

Figure 33, IP (top) and PI (bottom) Controllers comparison

4.4.2. Current Controller

The current controller follows exactly the previous reasoning, with the corresponding changes in the desired time response (lowered to 0.01 seconds) and other values such as:

$$\begin{cases} k_p = \frac{2\xi\omega_n\tau_c - 1}{K_i} \\ k_i = \frac{\omega_n^2\tau_c}{K_i k_p} \end{cases} \tag{40}$$

$$\begin{cases} k_i = \frac{1}{R_{arm}} \\ \\ \tau_c = \frac{L_{arm}}{R_{arm}} \end{cases} \tag{41}$$

4.5. Strategy

The strategy block is important to define all the parameters such as k_{br}, k_d and k_w that will affect the control part. In this simulation will be used constant values defined by experience and further works on this topic [18], instead of a dynamic and adjustable logic dependent from the actual scenario. About the k_d and k_w values, will be used for both 0.5, assuming that the differential is not transmitting a different speed to the two wheels and that the "importance-weight" of the two wheels is the same. For k_{br}, will be used at first a value of 0.4, that is usually the ratio between electrical and mechanical braking in normal conditions. To summarize, these are the values utilised to check if the model works properly:

$$k_{br} = 0.4$$

$$k_d = 0.5$$

$$k_w = 0.5$$

Is important to insert in the strategy block, a part that allows to define when the vehicle is decelerating; this is fundamental because in other case a braking force will be always applied to it, even during accelerations. This scenario corresponds to a driver that pushes the pedal of the brake even during accelerations. The identification of conditions in which the car is decelerating or accelerating can be done using this equation:

$$k_{br} = \begin{cases} k_{br}, & (F_{tot_{ref}} - F_{res_{meas}}) < 0 \\ 0, & (F_{tot_{ref}} - F_{res_{meas}}) \geq 0 \end{cases} \tag{42}$$

4.6. Quasi-static model

Some simplifications can be done: the final aim of the work is not the detailed simulation of the converter and the inverter, but only the external behaviour such as the torque response is considered. For this reason, the chopper and the PM machine can be merged and the current controller can be assumed to be instantaneous, and so (5), (6) and (8) with related inversion parts (32), (33), (34) can be omitted from Figure 31. The motor is torque-controlled and its relation with the battery and the rest of the system can be expressed through the following set of equations [19]:

$$\begin{cases} T_{dcm} = T_{dcm\,ref} \\ i_{ch} = \frac{\eta_c^k T_{dcm} \omega_{gear}}{u_{batt}} \quad where \quad k = \begin{cases} 1, & P(t) < 0 \\ -1, & P(t) \geq 0 \end{cases} \end{cases} \tag{43}$$

where η_c^k expresses the global efficiency of the converter and PM machine.

With this, the complete EMR and control scheme can be updated, as reported in Figure 34.

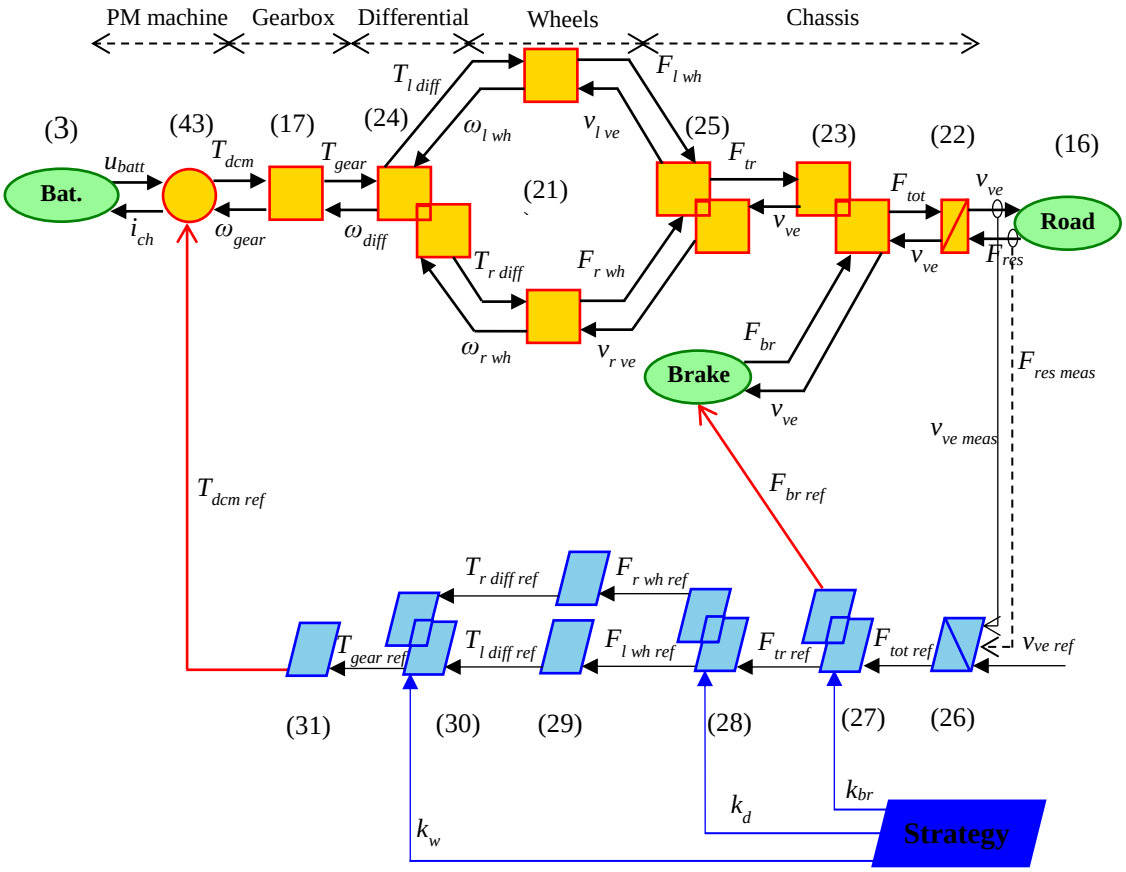

Figure 34, Complete EMR control scheme, for quasi-static model

This model is called quasi-static because of the omitted dynamic of the converter (static) but the presence of the dynamic of the mechanical parts, expressed through (22).

4.7. EMR for HIL simulation

The first step to get the EMR of HIL simulation is to update Figure 34 following the scheme already presented in Figure 10 for the Full Power HIL and Figure 11 for Reduced Power HIL simulation.

4.7.1. EMR for full power HIL simulation

In this situation, the e-drive block represents the block of the traction motor, described through (43). The interaction between the traction motor and the servo motor, is described with an accumulation element that is ruled through the following equation:

$$T_{dcm} - T_{servo} = (J_{dcm} + J_{servo})\frac{d\omega_{gear}}{dt} + (f_{dcm} + f_{servo})\omega_{gear} \tag{44}$$

in which the values that present the subscript *servo* are specific from the servo motor. This imposes the load to the traction machine, corresponding to the forces opposing the vehicle movement. As already described before, the transfer function has the following description:

$$G(s) = \frac{K_s}{\tau_s s + 1} \tag{45}$$

Regarding it, the servo motor is modelled using the following equation:

$$\begin{gathered} T_{servo} = T_{servo\,ref} \\ i_{servo} = \frac{\eta_{grid}^{k} T_{servo}\omega_{gear}}{u_{grid}} \quad where \quad k = \begin{cases} 1, & P(t) < 0 \\ -1, & P(t) \geq 0 \end{cases} \end{gathered} \tag{46}$$

The "Grid" source element presented in Figure 10 is ruled by:

$$u_{grid} = constant \tag{47}$$

to impose the voltage input to the servo motor, as the constant value given by the grid.

The last step is to create an inversion element that acts as control for the servo motor ("Emulation control" blue block in Figure 10); to do so, is used the same procedure to design all the other controllers. Starting from (44) the control block will have the following structure:

$$T_{servo-ref} = -C_s\left(\omega_{gear-ref} - \omega_{gear-red-meas}\right) + T_{dcm-red-meas} \tag{48}[4]$$

The controller C_S will be an IP controller, for the reasons already discussed in 4.4.1. The tuning is equivalent to the one already done for the velocity controller:

$$\begin{cases} k_p = \dfrac{2\xi\omega_n\tau_s - 1}{K_s} \\ k_i = \dfrac{\omega_n^2\tau_s}{K_s k_p} \end{cases} \tag{49}$$

[4] Is important to note the presence of the "minus" sign for the controller, due to the inverted reference for the servo motor compared to the traction one. This is the only difference between this inversion and the one expressed in (26).

where:

$$\begin{cases} K_s = \dfrac{1}{f_{dcm} + f_{servo}} \\ \tau_s = (J_{dcm} + J_{servo})\left(\dfrac{1}{f_{dcm} + f_{servo}}\right) \end{cases} \tag{50}$$

To respect the necessary ratio between time constants of the velocity controller (virtual subsystem control) and the speed controller of the servo motor (emulation ECU, in section 3.2) these parameters are used:

$$\omega_n t = 4.744$$

$$\xi = 1$$

$$t_r = 0.1\ second$$

The final structure for the controller will be:

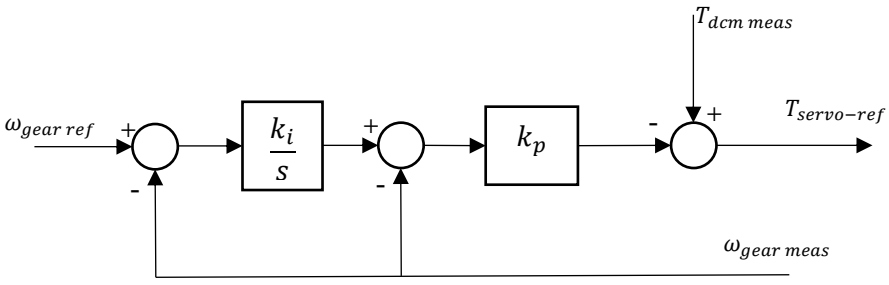

Figure 35, IP speed controller structure

The complete EMR for the Power HIL simulation is reported in Figure 37[5] and required parameters for the correct implementation are showed in Table 6.

[5] Please note that in this figure, in (17), ω_{gear} becomes $\omega_{gear\ ref}$.

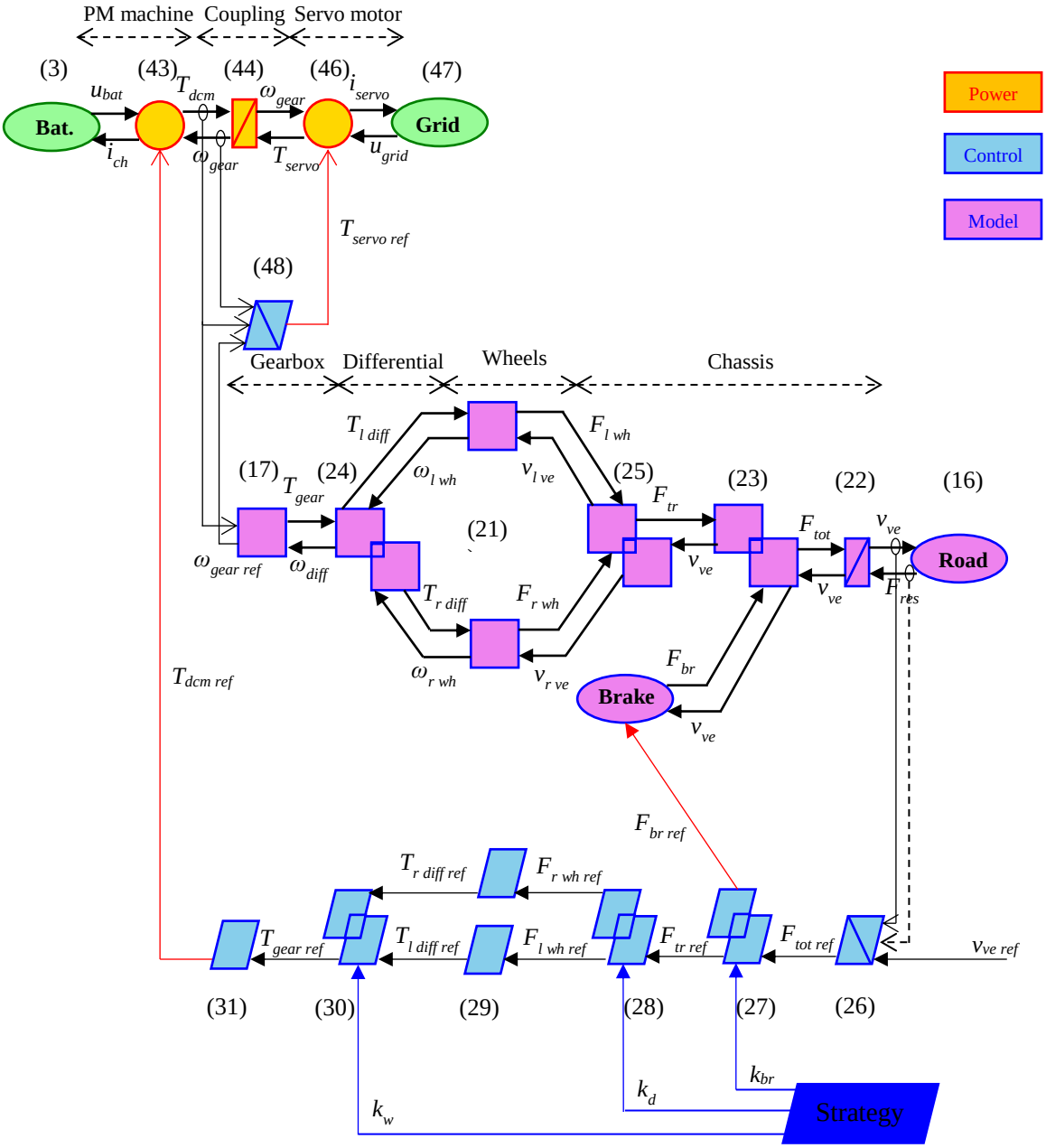

Figure 36, Complete EMR for full power HIL simulation

Table 6, Parameters for HIL simulation

J_{dcm}	$0.00263 \frac{kg}{m^2}$
J_{servo}	$0.001151 \frac{kg}{m^2}$
u_{grid}	$400\ V$

4.7.2. EMR for reduced power HIL simulation

Complete EMR for Reduced-Power HIL simulation, as already explained, differs from the full power only for the presence of two Power Adaptation blocks. The two adaptation blocks are represented through the following equations:

$$\begin{cases} T_{dcm} = k_T T_{dcm\,red} \\ \omega_{gear\,ref\,red} = \dfrac{\omega_{gear}}{k_\omega} \end{cases} \tag{51}$$

$$T_{dcm\,ref\,red} = \frac{T_{dcm\,ref}}{k_T} \tag{52}$$

As mentioned in [10], the two reduction factors k_T and k_ω have to be evaluated using a procedure that ensures some safe margins between the values of the emulation device and the related full-power subsystem (mechanical part in this case). This procedure is divided into some steps:

- First of all, the speed reduction factor (k_ω) is evaluated, dividing the maximal speed achievable by the full-scale subsystem by the maximal speed achievable by the reduced scale one; a safety margin of 5% is taken, to avoid any possible problem:

$$k_\omega = \frac{\omega_{max\,full\,power}}{0.95\ \omega_{max\,red\,power}} \tag{53}$$

- The power reduction factor (k_P) is evaluated through the ratio between the maximal power of the full scale and the maximal power for the reduced scale. For the same reason than before, a 5% margin has been kept:

$$k_P = \frac{P_{max\,full\,power}}{0.95\ P_{max\,red\,power}} \tag{54}$$

- The torque reduction factor (k_T) is directly derived by the ratio between the power reduction factor and the speed reduction ratio. Its value can be considered valid only if it respects the following relation:

$$k_T > \frac{T_{max\,full\,power}}{0.95\ T_{max\,red\,power}} \tag{55}$$

If not, the value of k_T is given by this equation:

$$k_T = \frac{T_{max\ full\ power}}{0.95\ T_{max\ red\ power}} \tag{56}$$

- And k_P has to be redefined in this way:

$$k_P = k_T k_\omega \tag{57}$$

All the process is briefly reported in Figure 38.

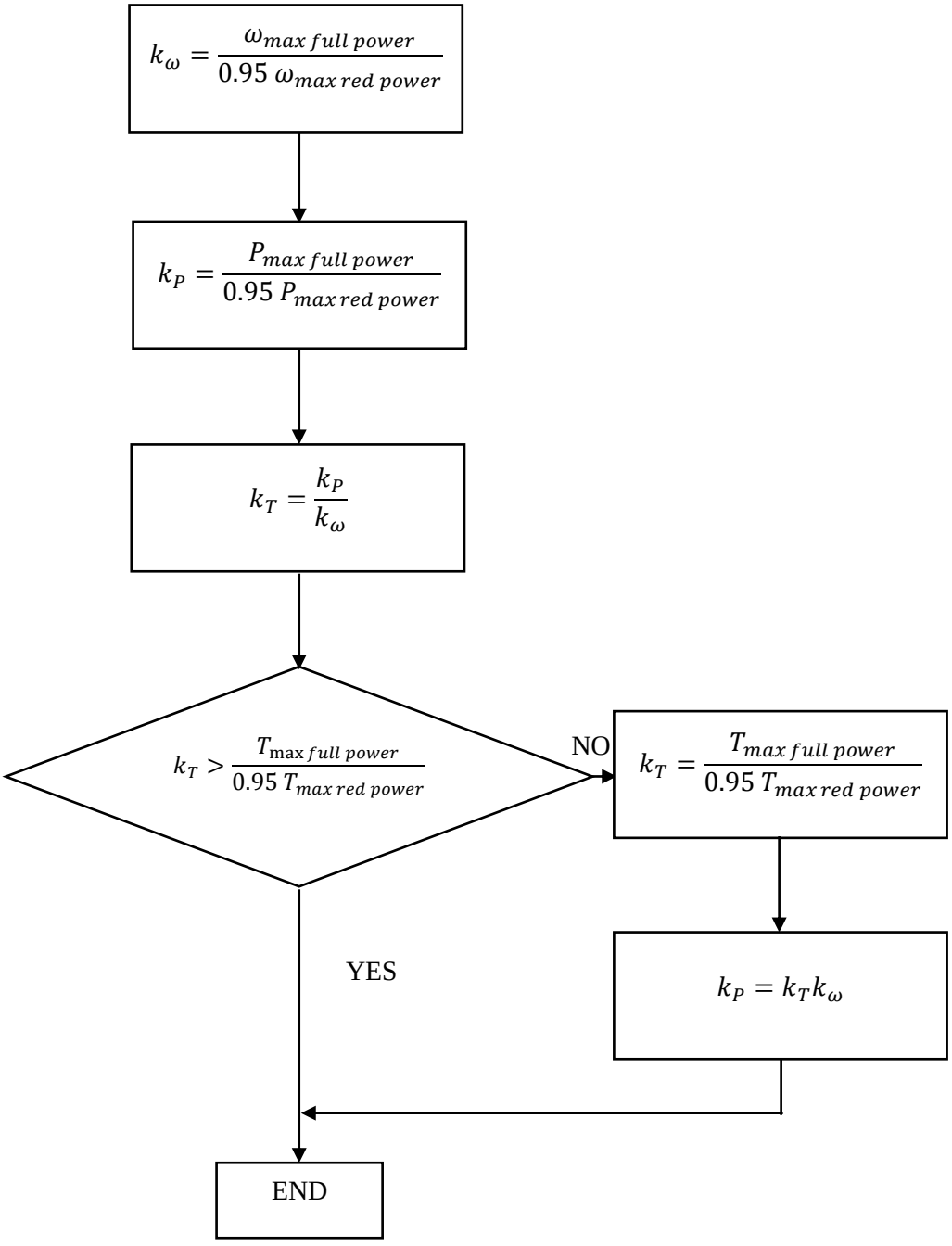

Figure 38, Flowchart for reduction factors evaluation

After that the reduction factors have been evaluated (Table 7), the complete EMR for reduced power HIL can be produced (Figure 39)[6].

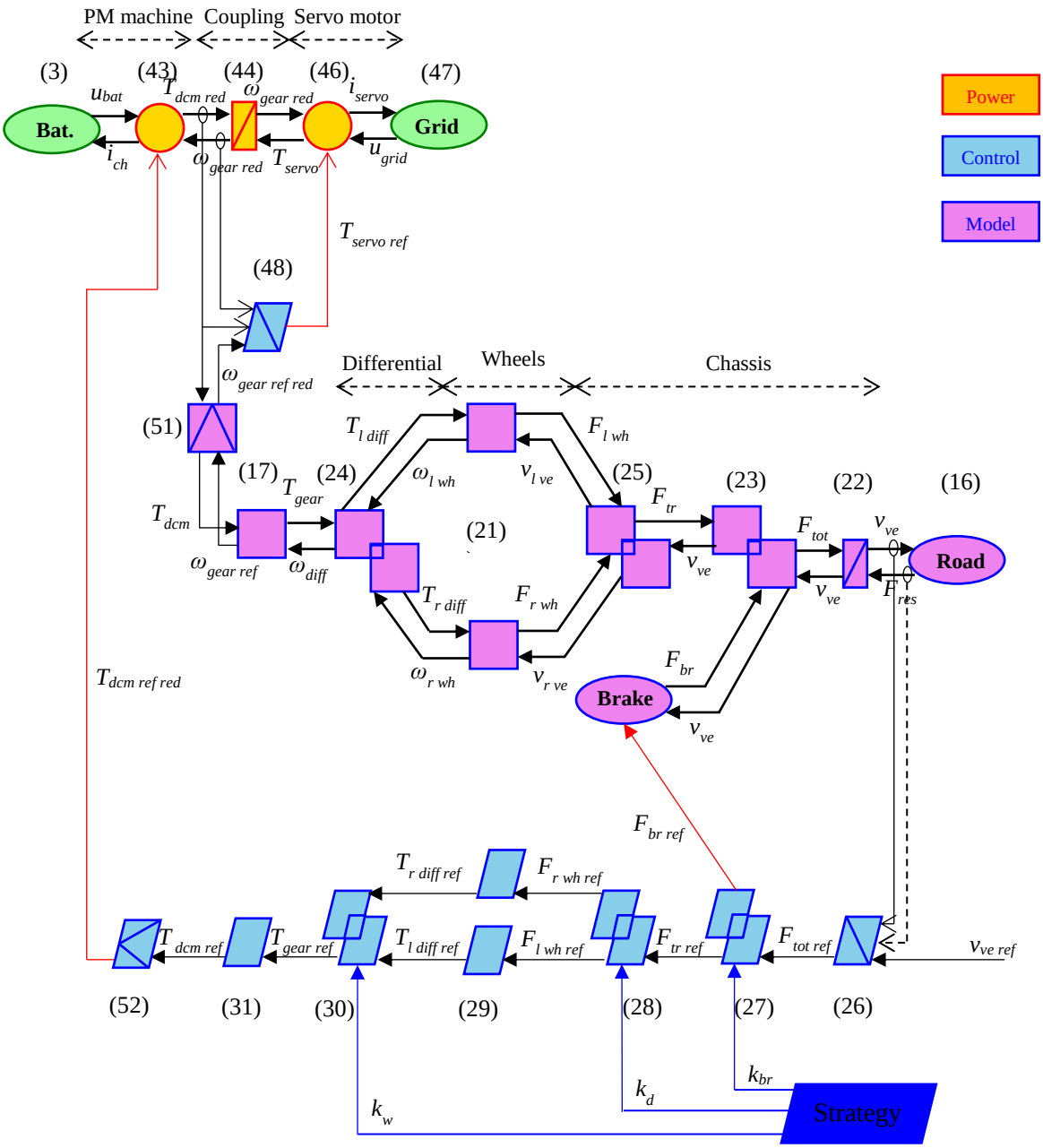

Figure 39, Complete EMR for Reduced Power HIL simulation

Table 7, Reduction factors for the studied application

$\mathbf{k_\omega}$	1.4035
$\mathbf{k_T}$	6.7397
$\mathbf{k_p}$	9.4591

[6] Please note that in this figure, in (17), ω_{gear} becomes $\omega_{gear\ ref}$.

5. Results and comparison between software and HIL simulation

5.1. EMR software simulation

5.1.1. Full Power software simulation

As already explained, the first simulation that has to be tested is the software simulation. To complete it, some further simplifications have been used, in order to reduce the complexity of the model.

The friction coefficient is not used in the final simulation, because is difficult to get from datasheet of the motors, and also because neglecting it, the final result is not affected in a significative way. For this reason, previous equations need to be redefined introducing some minor changes.

The chassis element ruled by (22) can be defined by this new equation:

$$(F_{tr} - F_{res}) = M_{eq3}\frac{dv_{ve}}{dt} \tag{58}$$

Controller parameters expressed by (36) have to be changed considering the new chassis transfer function:

$$G(s) = \frac{K_v}{\tau_v s} \tag{59}$$

With this, (38) can be substituted by the following set of equations:

$$\begin{cases} K_v = 1 \\ \\ \tau_v = \left(\dfrac{J_{eq2}}{R_{wh}^2} + M_{tot}\right) \end{cases} \tag{60}$$

that are used later on to evaluate k_i and k_p through (37).

After these last adjustments, simulation of the model in Figure 34 can be implemented using Matlab/Simulink©. To create this, EMR library is used [20]. In Figure 40 is presented the complete EMR as implemented in Matlab/Simulink©.

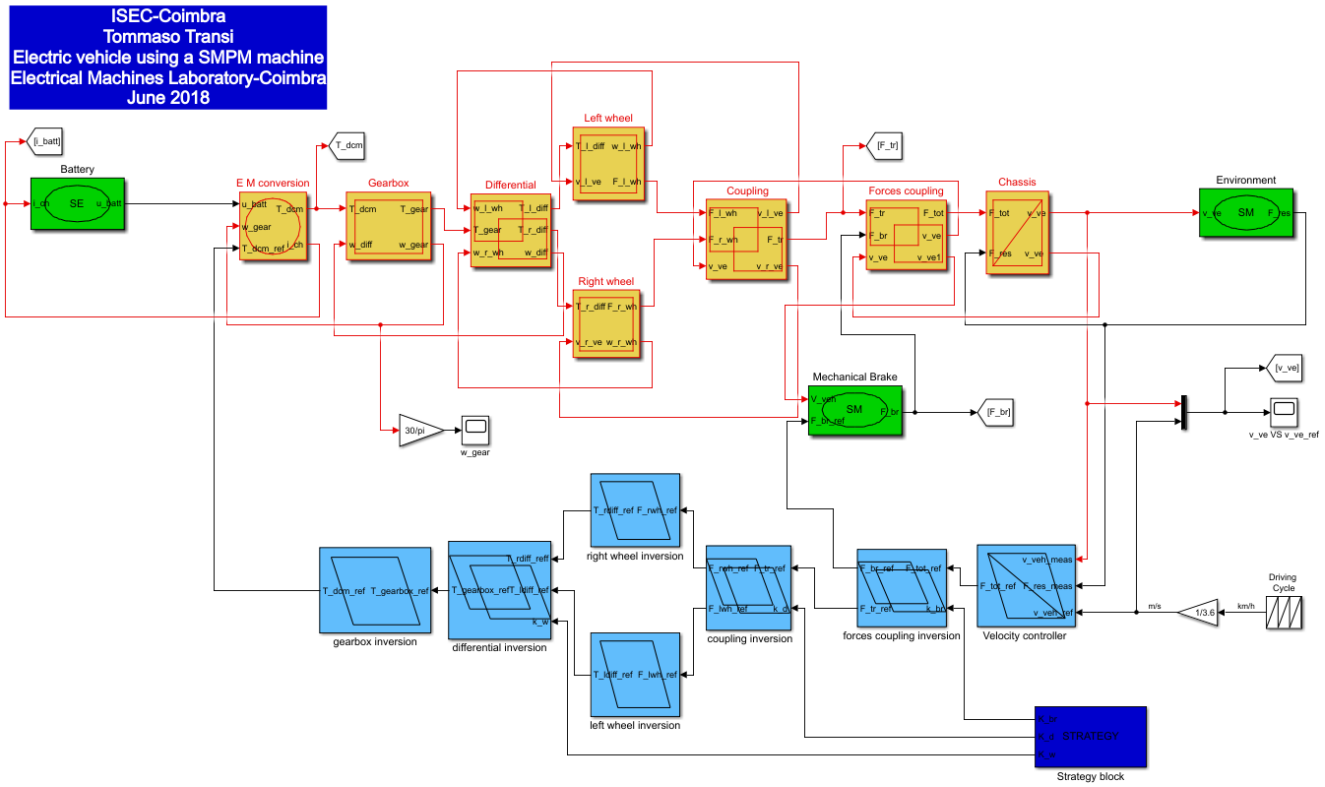

Figure 40, Matlab/Simulink©-based EMR and control scheme for quasi-static model

With this simulation, different configurations can be tested: the most interesting one, is to try different values for k_{br}. Indeed, changing this value, the ratio between mechanical braking and regenerative braking is varied; when k_{br} is equal to 0 all the braking force will be recovered by the electrical path, and when is equal to 1 all the braking force will come from mechanical braking. The values that are going to be analysed are 0.3, 0.6 and 1.

In Figure 41 k_{br} is equal to 0.3. As it was expected the mechanical braking force is lower than the regenerative braking force; another key aspect that highlights the presence of regenerative braking is the behaviour of the SoC value that when a braking condition occurs, tends to increase. The battery current follows the expected behaviour with some negative currents (from the mechanical side towards the battery pack-side) during decelerations. All the readings do not pass the limits already reported for this specific application (Appendix B-) such as maximum current in the battery pack (270 A that is equal to 3C for continuous discharge current, as indicated in datasheet) and maximum torque delivered by the two electrical machines (PMS 156L/air cooled, Appendix A-).

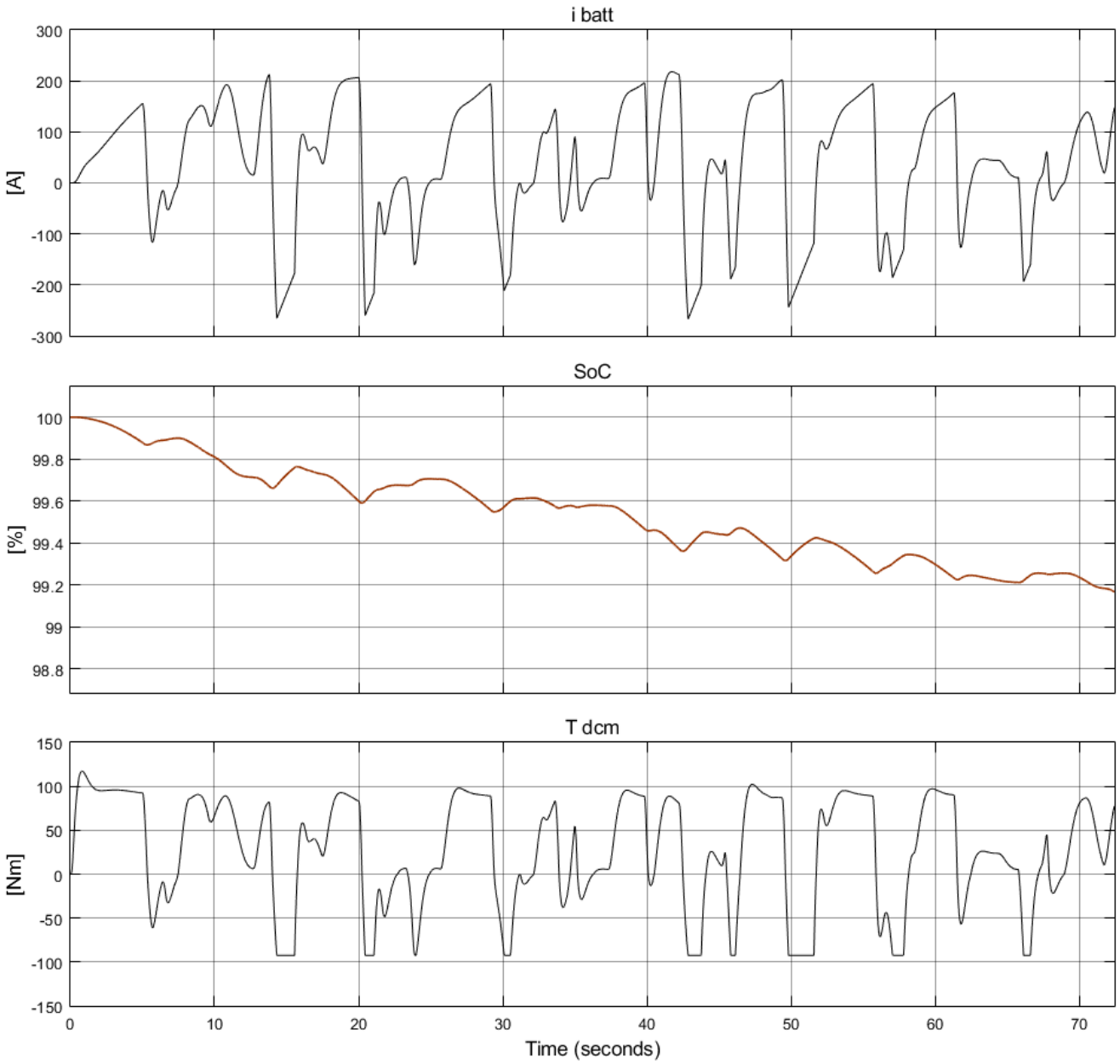

Figure 41, Results for k_{br}=0.3: i_{batt} (top), SoC (centre), T_{dcm} (bottom)

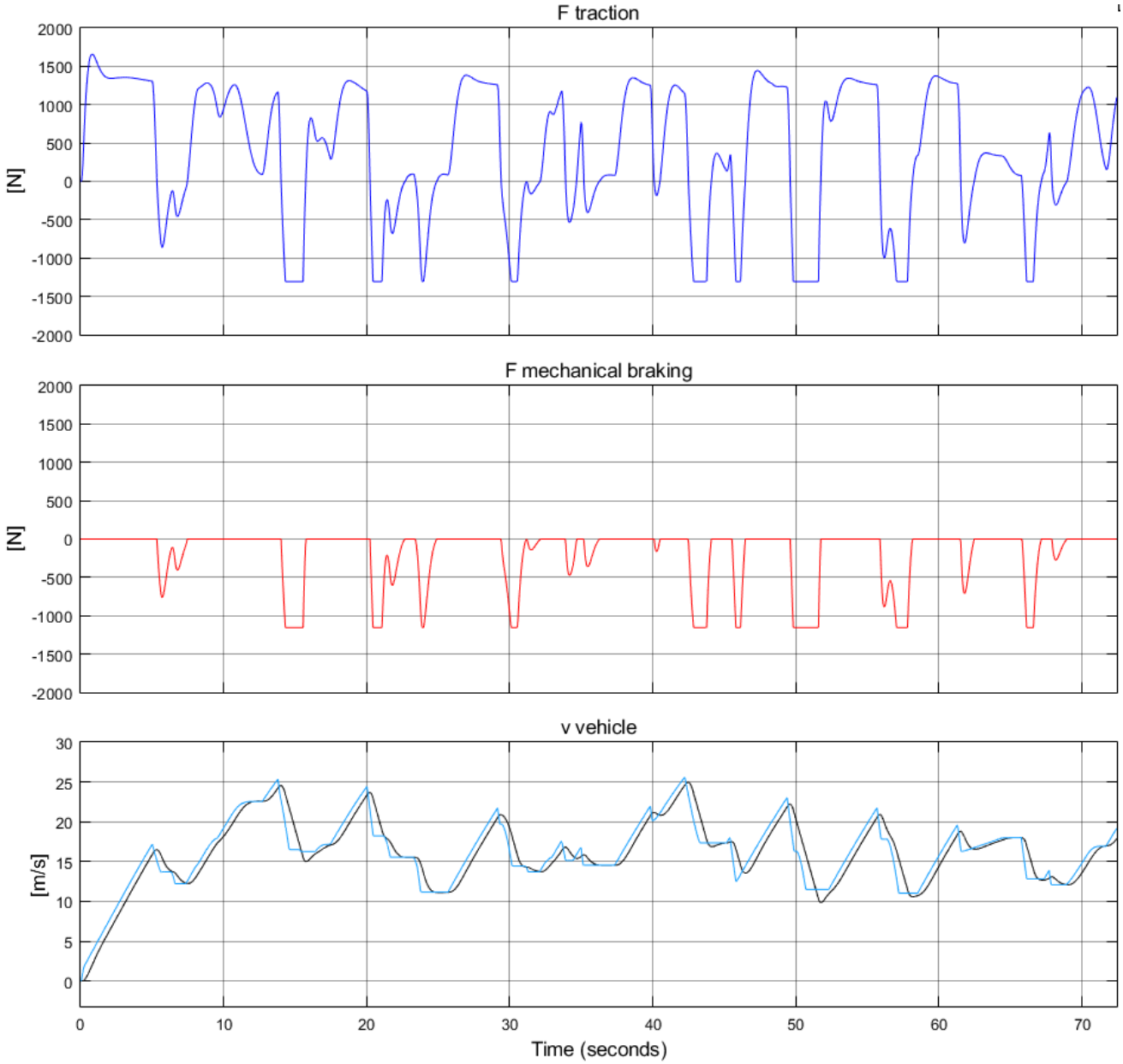

Figure 42, Results for k_{br}=0.3: F_{tr} (top), F_{br} (centre), v_{ve} (bottom)

Figure 43 and Figure 44 present k_{br} equal to 0.6 and what is expected is a lower stress for battery pack during regenerative braking (lower negative currents) and higher values for mechanical braking force. Is important to notice that here the final SoC value is lower than the previous simulation, as it is expected. Finally, the mechanical stress from the point of view of the motor (T_{dcm}) is lower.

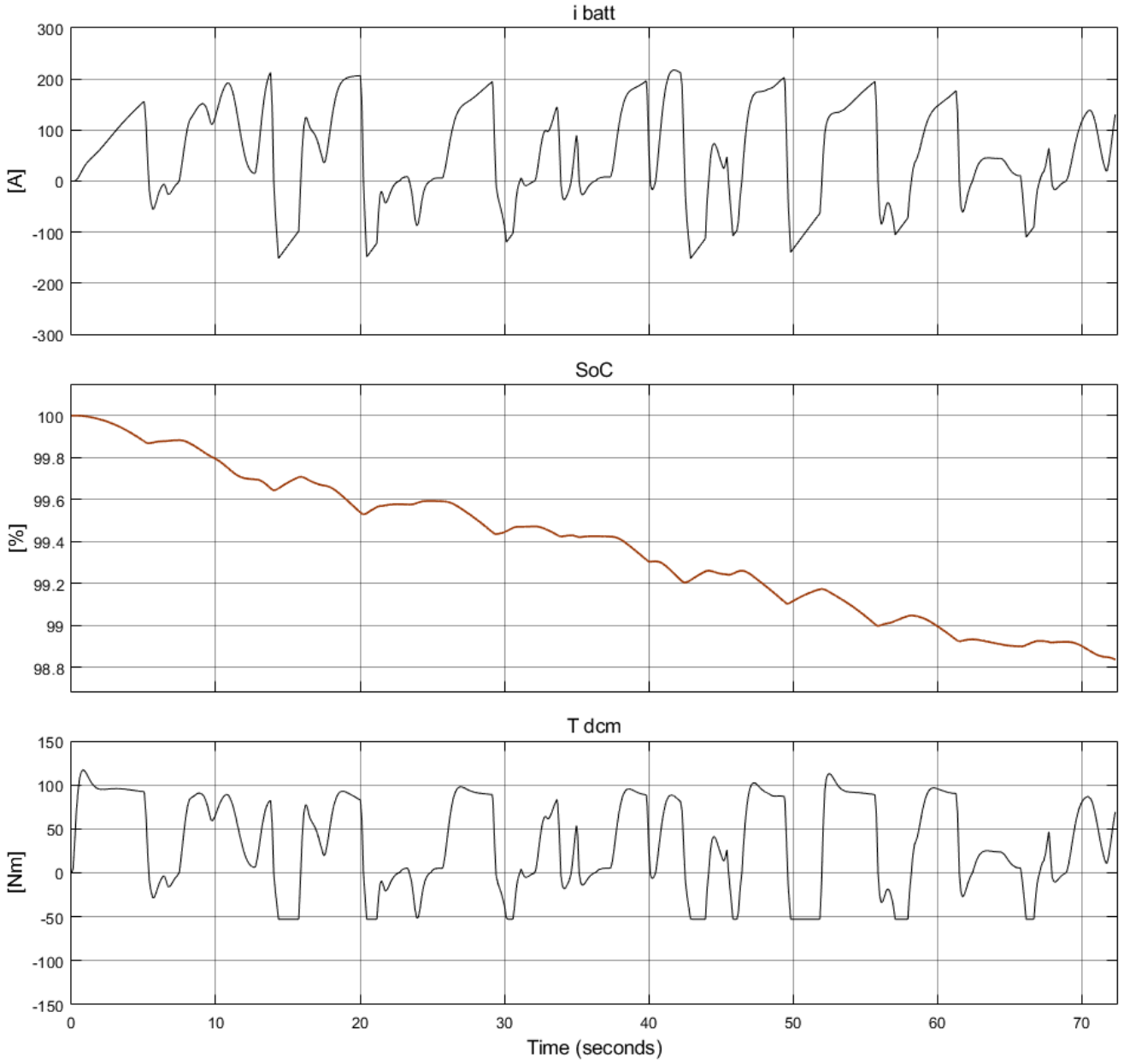

Figure 43, Results for k_{br}=0.6: i_{batt} (top), SoC (centre), T_{dcm} (bottom)

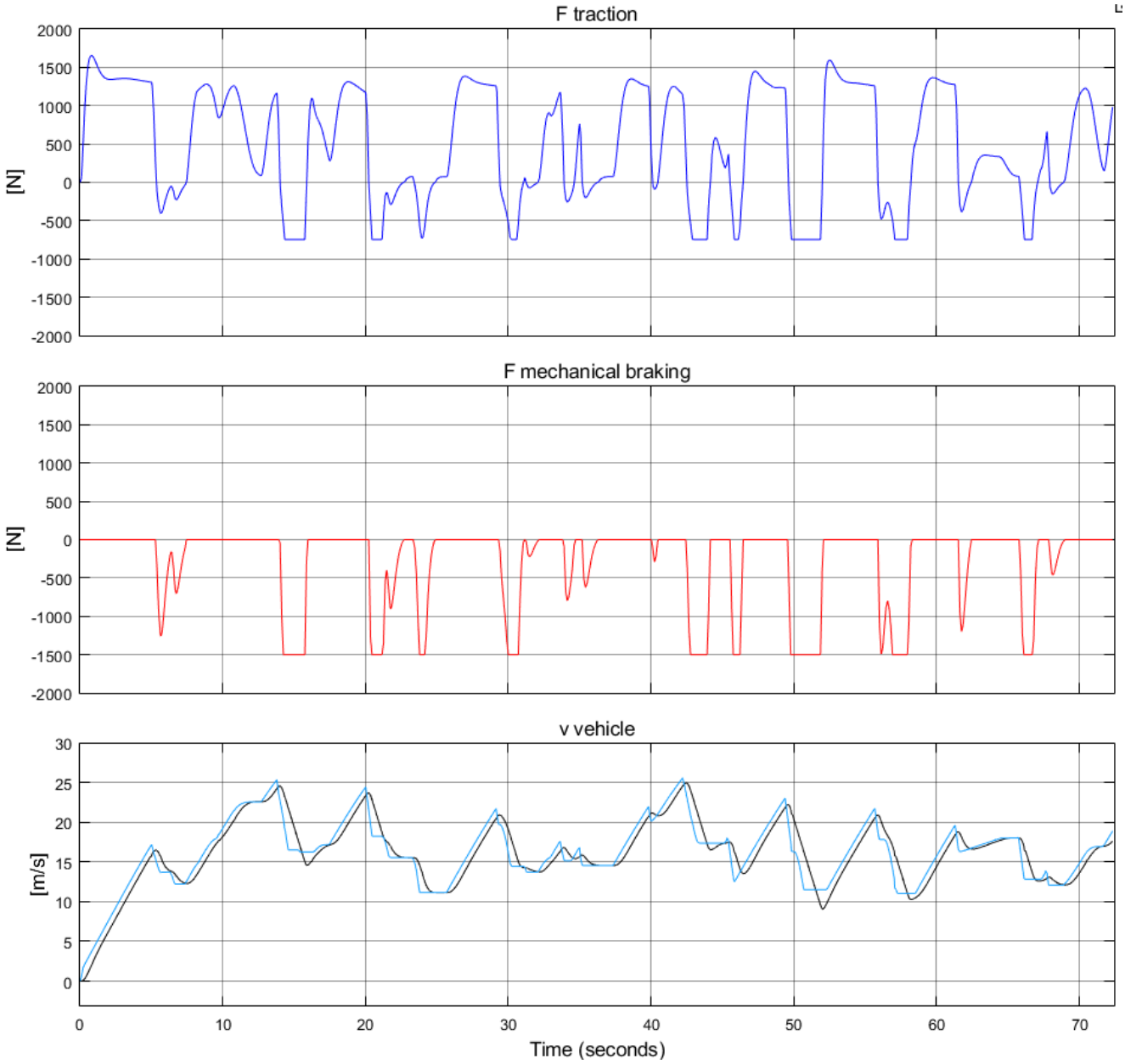

Figure 44, Results for k_{br}=0.6: F_{tr} (top), F_{br} (centre), v_{ve} (bottom)

In both previous cases the model behaves quite well, with the vehicle velocity that follows the reference with a certain delay that is acceptable. In conclusion, the model is well designed and it reacts well to the desired velocity reference.

When k_{br} value is set to 1 the system starts to not follow the reference for the velocity during hard braking conditions. Immediately after, controller tries to set the maximum achievable torque in order to reach the reference, but motors saturate and it is showed by the torque profile in Figure 45.There are three moments in which the torque value reaches the saturation value (between 17 *s* and 20 *s*, between 52 *s* and 57 *s* and finally between 61 *s* and 65 *s*). As far as the motors saturate, a mismatch between the measured vehicle velocity and the reference vehicle velocity occurs (Figure 46). It means that the controller is not able to impose enough braking force to the vehicle to follow the reference and consequently this is reflected also on the following acceleration part, as it is visible from the graph.

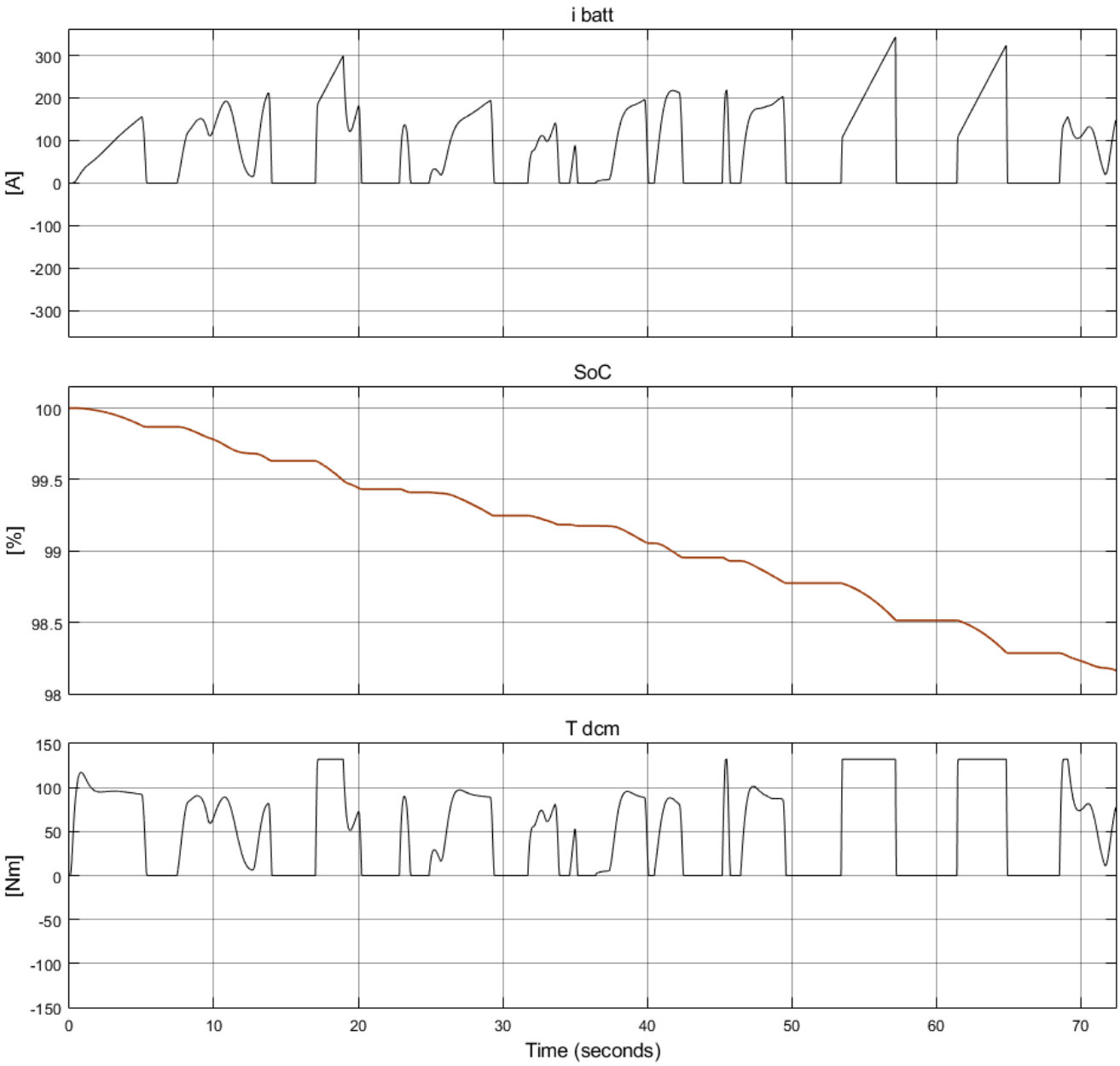

Figure 45, Results for k_{br}=1: i_{batt} (top), SoC (centre), T_{dcm} (bottom)

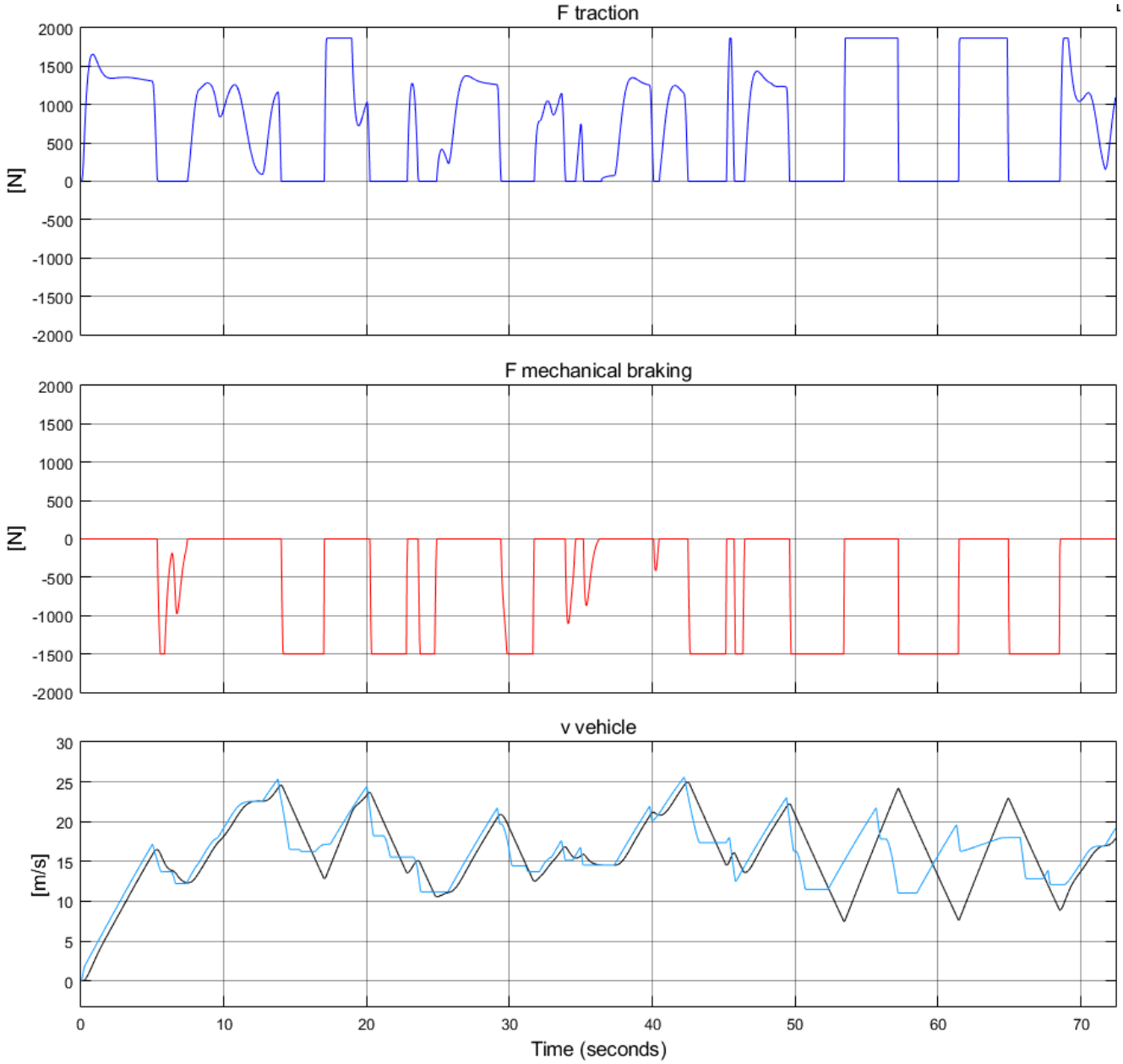

Figure 46, Results for k_{br}=1: F_{tr} (top), F_{br} (centre), v_{ve} (bottom)

5.1.2. Reduced Power software simulation

Once that the software simulation is completed, before passing to the HIL simulation, an additional simulation can be done. This is always a software-based simulation, in which the modelled system is not the actual one, but the one that includes the HIL-simulation devices (battery pack, traction motor and servo motor present in the laboratory). This simulation is used to evaluate which are the expected values from the HIL simulation, before than physically connect the devices.

In this simulation, as in the previous one, some minor changes are done in order to simplify the model; in addition to the changes already inserted in the complete EMR simulation, also the (44) has to be modified, to avoid the use of the friction coefficient:

$$T_{dcm} - T_{servo} = (J_{dcm} + J_{servo}) \frac{d\omega_{gear}}{dt} \tag{61}$$

This change leads to a new transfer function for the servo motor:

$$G(s) = \frac{K_s}{\tau_s s} \tag{62}$$

where (50) is substituted by:

$$\begin{cases} K_s = 1 \\ \\ \tau_s = (J_{dcm} + J_{servo}) \end{cases} \tag{63}$$

Through this, is possible to evaluate k_p and k_i using (49). In Figure 47 is reported the Matlab/Simulink© model layout, that follows exactly the structure already presented in Figure 39.

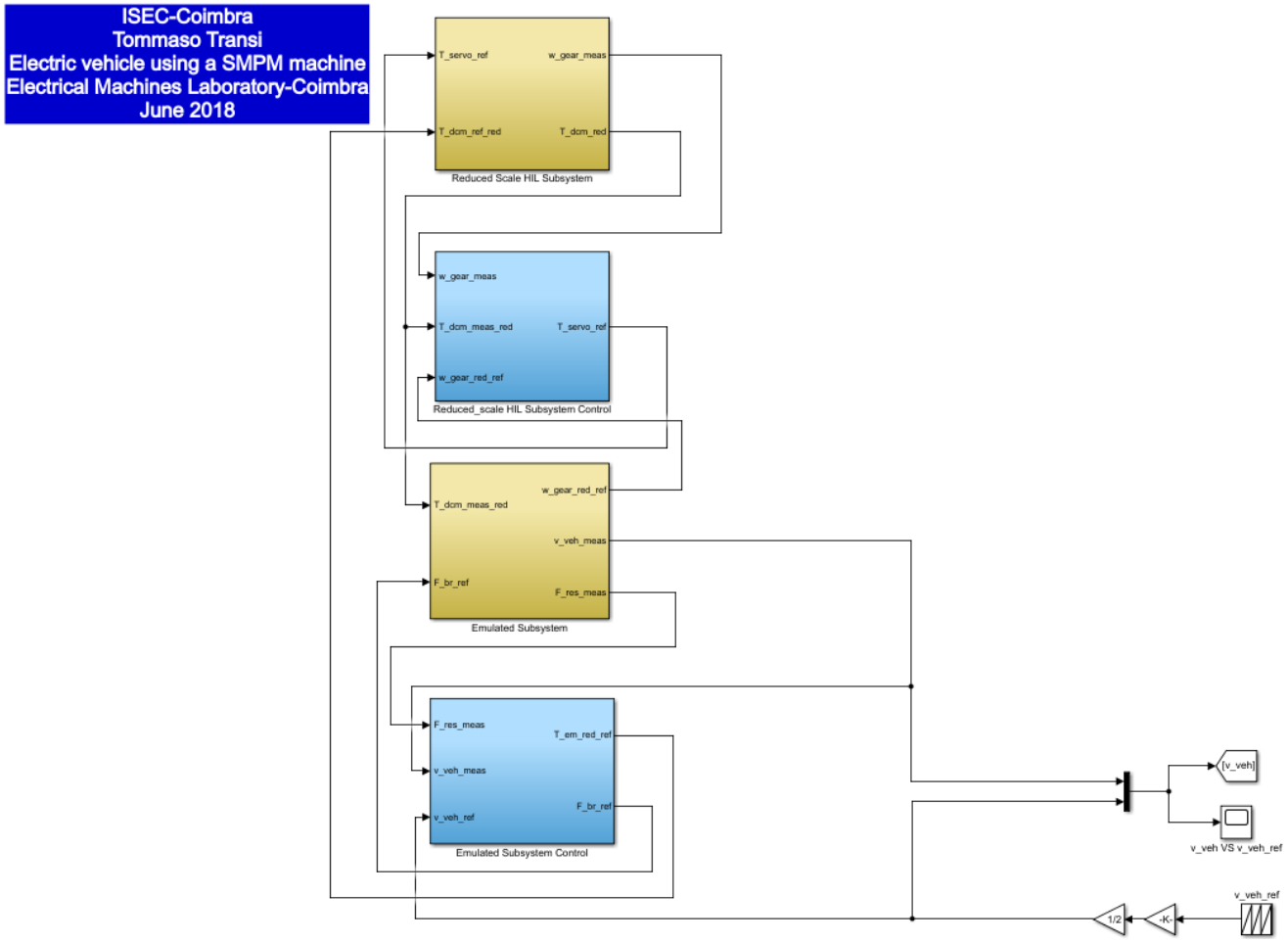

Figure 47, Matlab/Simulink© model for reduced power HIL software-based simulation

The structure of the “Reduced Scale HIL Subsystem” is reported in Figure 48 and the “Reduced Scale HIL Subsystem Control” contains the IP controller structure already presented in Figure 35. The two last subsystems from the bottom (“Emulated subsystem Control” and “Emulated Subsystem”) contain the elements already presented in Figure 40: the Emulated Subsystem contains the yellow and green blocks of the model and the Emulated subsystem control contains the control part (light blue blocks) of the model.

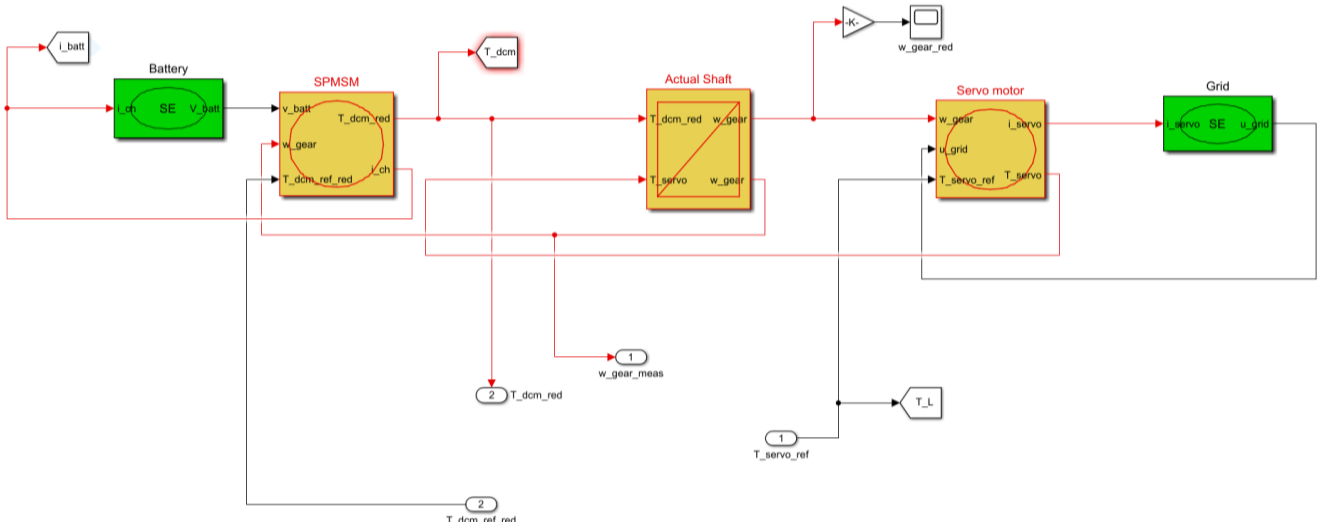

Figure 48, Reduced Scale HIL Subsystem

5.1.3. Test bench parameters for software and HIL simulation

The ISEC-IPC test bench is represented in Figure 49. The devices used are:

- $LiFePO_4$ batteries: SP-LFP40AHA
- Lithium Ion battery charger: GWL-Power-POW72V35A
- Battery Management System: BMS123
- SEVCON Synchronous traction motor drive: Gen4-72-80VDC
- Traction Permanent Magnet Synchronous Motor (PMSM): Heinzmann GmbH PMS120
- Variable Frequency Drive (VFD) servo: SEW-EURODRIVE MDX60a022050J-4-00
- Servo Permanent Magnet Synchronous Motor (PMSM): SEW-EURODRIVE Model: CMP80M/KY7RH1M/SM1
- dSPACE MicroAutoBox II 1401/1511-1512

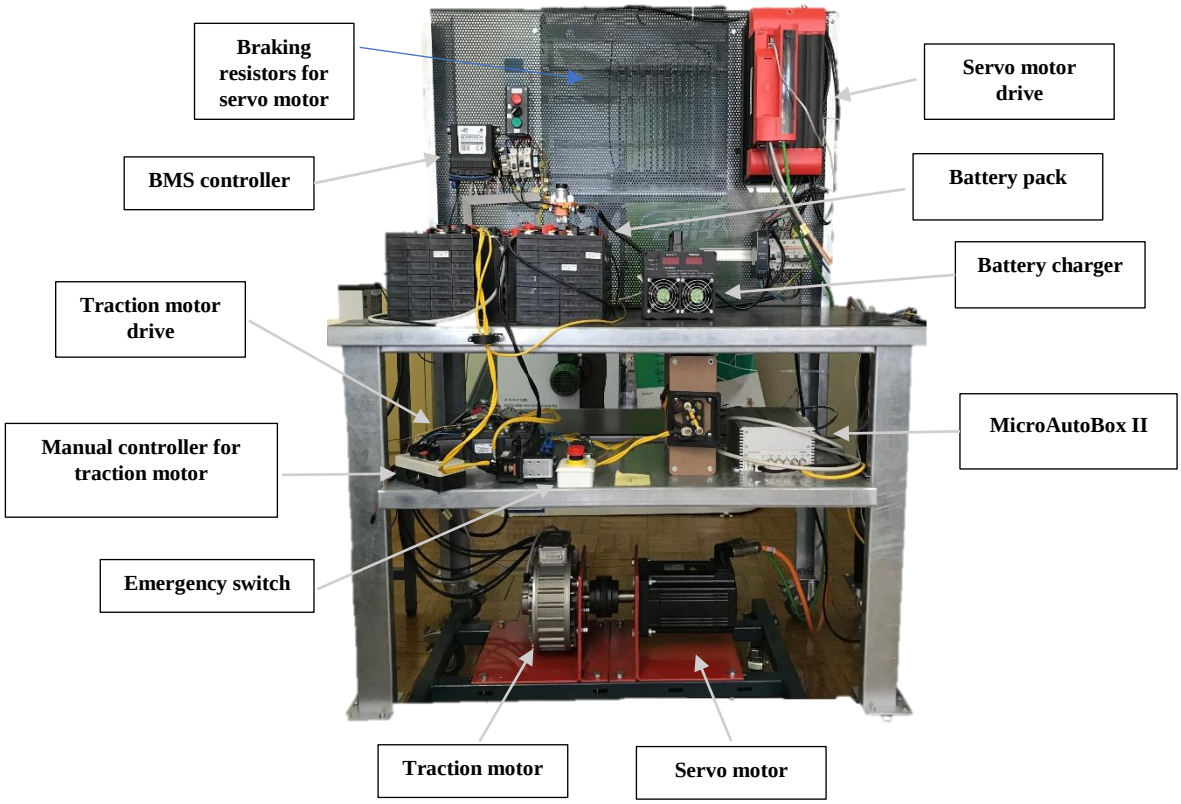

Figure 49, Test bench at ISEC-IPC

During the setting of the test bench, one main problem was encountered: the two drives for the motors do not accept negative reference values for the torque. This does not allow the implementation of the regenerative braking with the actual setup. To overcome this problem and conduce in any case an HIL simulation, k_{br} was set to 1 that means that the emulated braking force comes exclusively from the mechanical brake (no negative torque references). Results with this particular setting show another issue as already explained; due to the fast decelerations required to follow the reference, the controllers are not able to follow it without the help of the regenerative braking. That is the reason why in Figure 46 the measured vehicle velocity does not follow the reference in the last part of the simulation.

To overcome this other problem, the best solution is to reduce by one half the velocity reference profile, to avoid stressful situations for the controller. Results from the model already presented in Figure 47, are presented in Figure 50 and Figure 51.

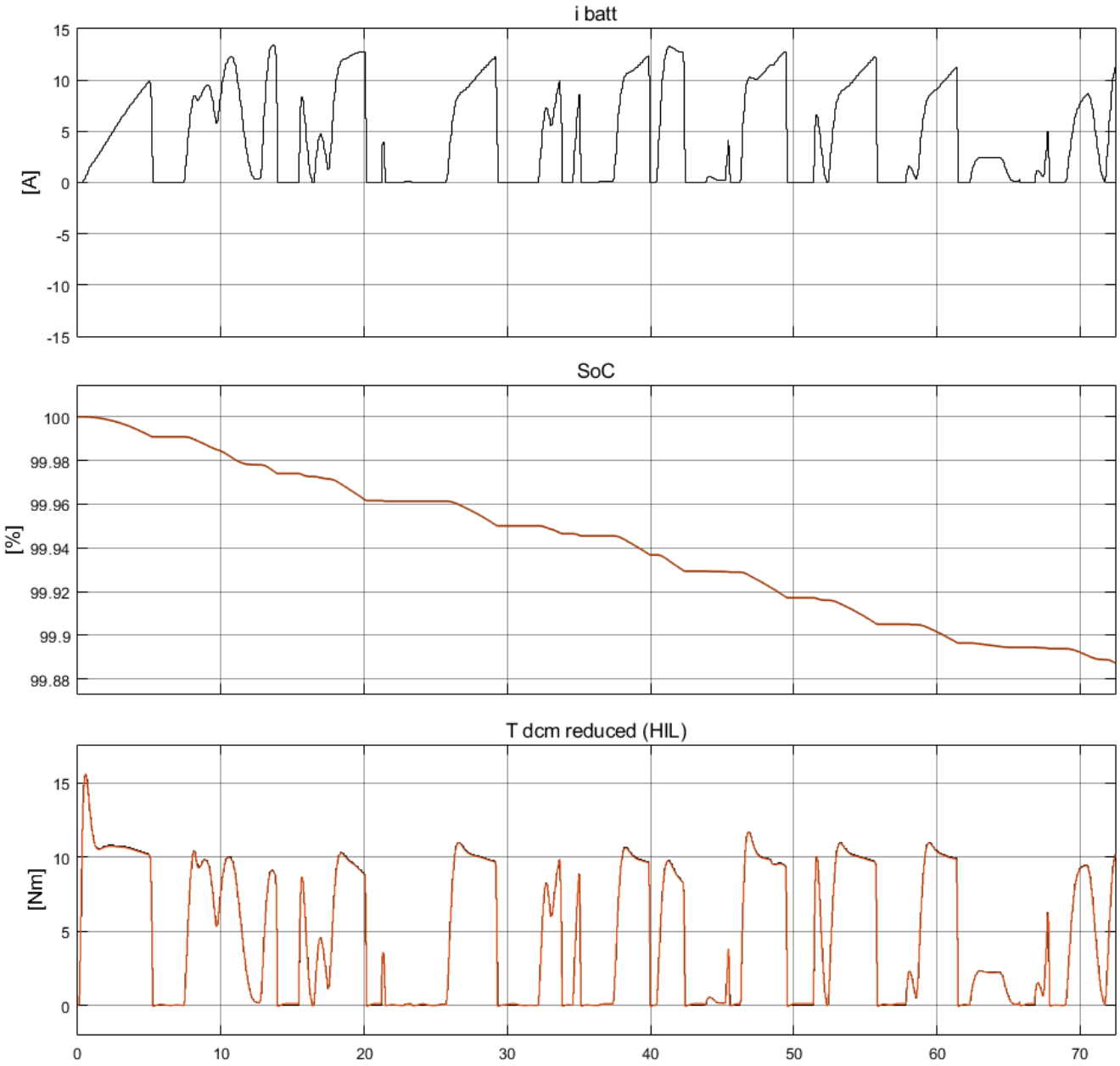

Figure 50, Results for k_{br}=1: i_{batt} (top), SoC (centre), $T_{dcm\ reduced}$ (bottom)

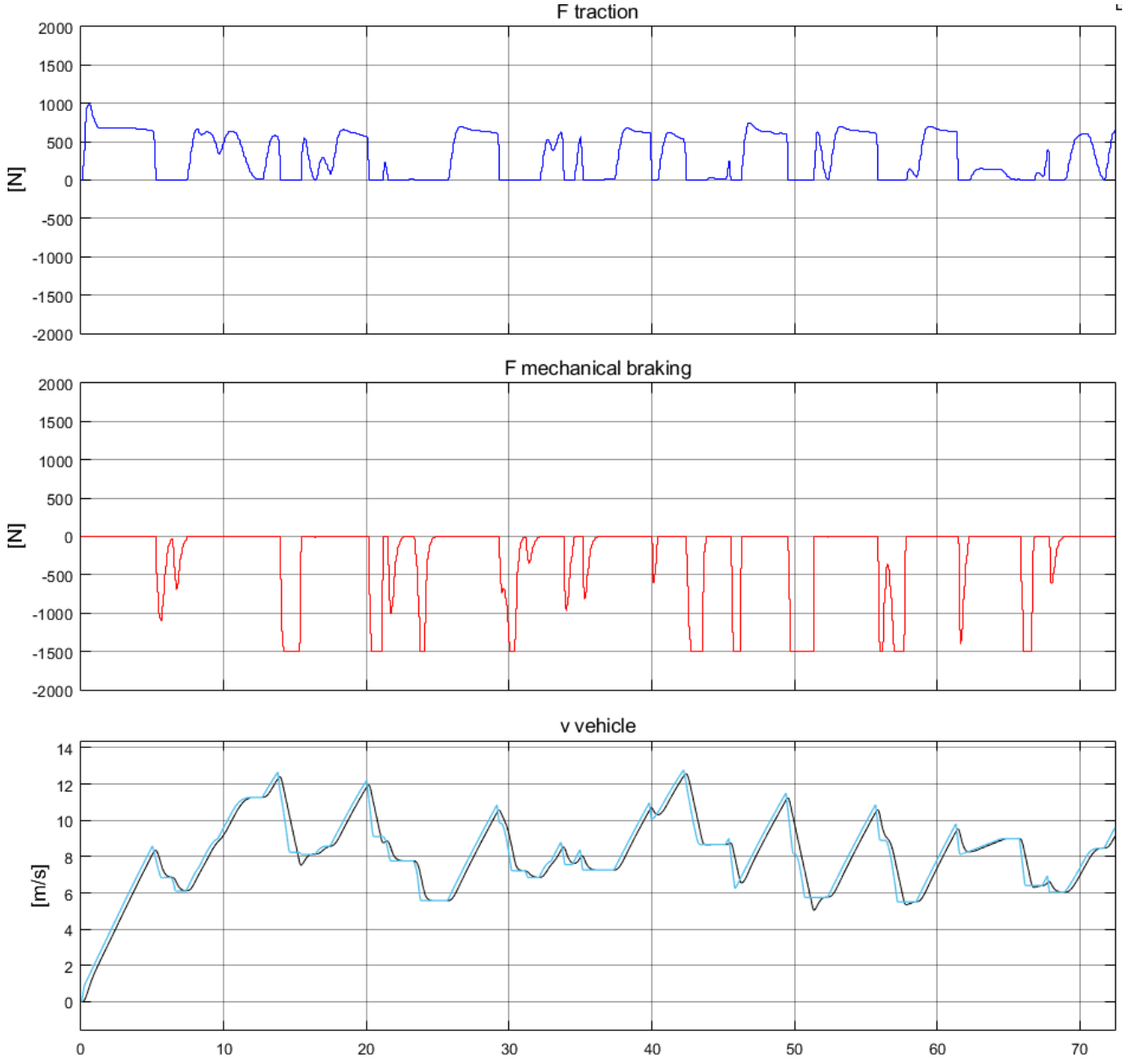

Figure 51, Results for k_{br}=1: F_{tr} (top), F_{br} (centre), v_{ve} (bottom)

With these further adjustments, results are good: the reduced torque at the traction motor respects the limits imposed by datasheets and battery currents are well below the limits. Now HIL can be safely implemented, with the available hardware.

5.2. HIL simulation and results

To implement HIL simulation the same structure used in the model presented in Figure 47 is used, with the only difference that "Reduced Scale HIL Subsystem" is replaced by the actual setup.

Some further blocks and regulations/gains are added in order to properly read and send signals to motor drives, through dSPACE MicroAutoBox II®. Connections between motor drives and dSPACE MicroAutoBox II®, and consequently between dSPACE MicroAutoBox II® and Matlab/Simulink© model are ensured by two types of signals: analog signals and digital signals. Analog signals are used to send from software part to hardware part

the reference signals, and digital signals are used to send measured values from hardware to software part. CANopen protocol is used to send digital signals. In Chapter 5.2 of [21] some tests were performed in order to verify dSPACE MicroAutoBox II® behaviour and how to control it using ControlDesk© software from dSPACE. All tests have been done again to be sure that the connections are still correct and the system is still operational.

Once that all the preparatory steps are done, the simulation can be run. To control the simulation from now on, ControlDesk© is used instead of Matlab/Simulink©; the experiment created in ControlDesk© used to perform the simulation, is based on the Matlab/Simulink© model reported in Figure 52 and also in Appendix D-

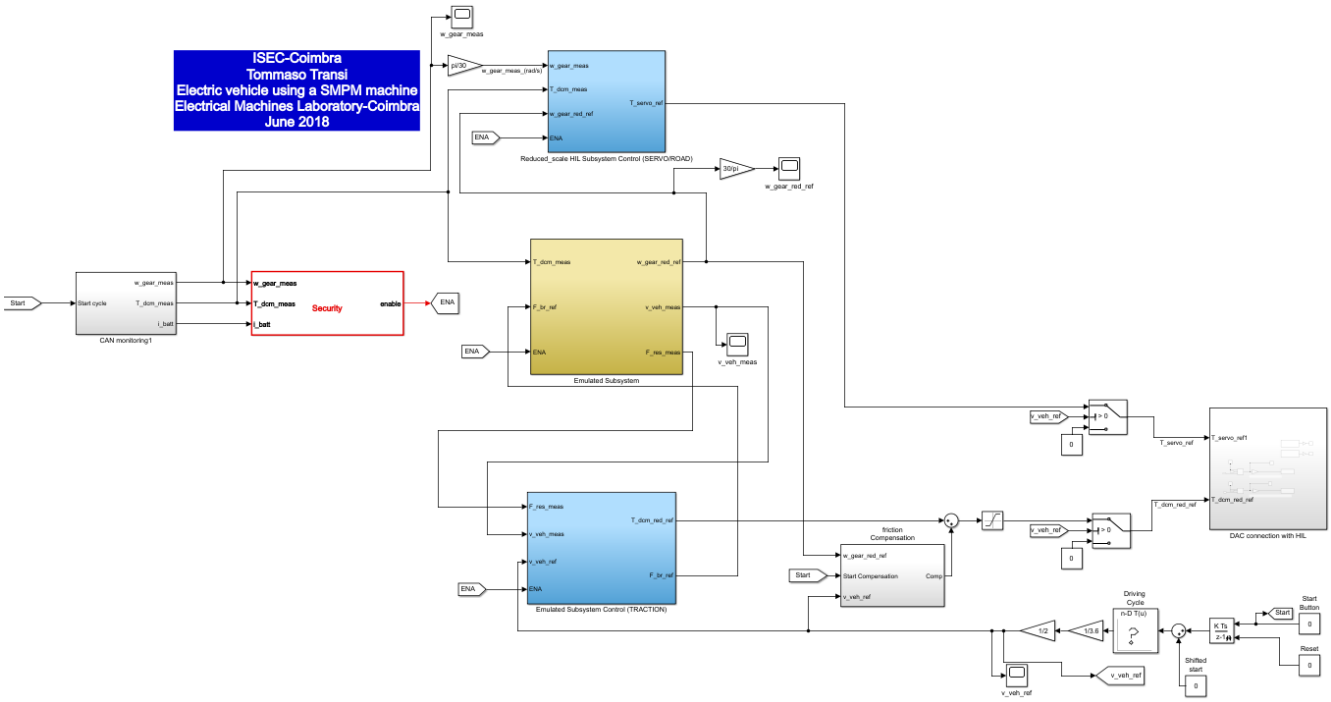

Figure 52, Matlab/Simulink© model for reduced power HIL, to be built in ControlDesk©

The security block present in Figure 52 is useful to stop the simulation in case of faults such as:

- Battery current value higher than the limit value
- Torque from the traction motor higher than the safety limit value
- Speed from the traction motor higher than the safety limit value

Is also visible in this model, the presence of some constants named “Start Button”, “Reset” and “Shifted Start”. These are initially set to 0, and can be changed directly from ControlDesk experiment once that the model is built; is important to note that these constants are mandatory to properly control the behaviour of the simulation. In Figure 53 is reported the ControlDesk experiment layout.

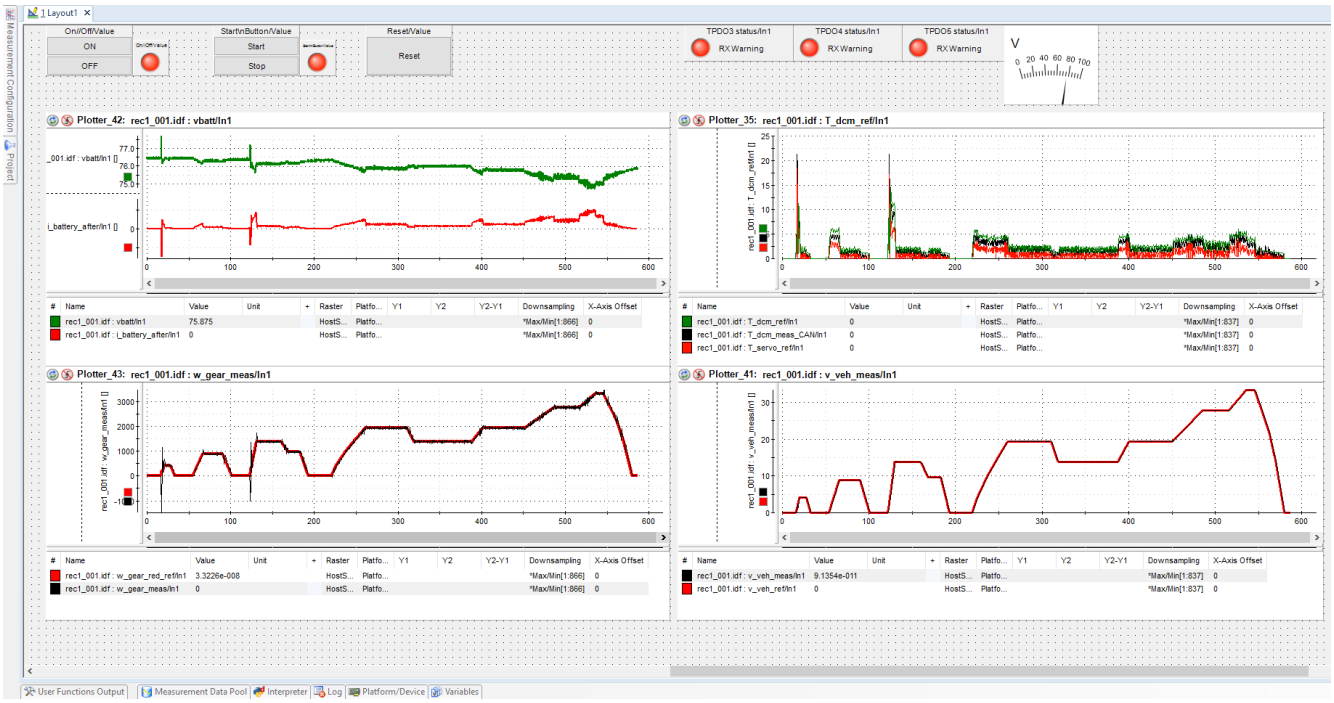

Figure 53, dSPACE ControlDesk® experiment layout for NEDC

First experiment uses as vehicle velocity reference, the NEDC that is a less stressing driving cycle compared with the one used for this application. As it can be noticed there are three sets of buttons on the top left-side of the workspace, with some LEDs that easily highlight the state of the driving cycle (Green=driving cycle started, Red= driving cycle stopped). Is present also a "Reset" button, that allows to reset the driving cycle and come back to the initial situation. On top right-side there are other three LEDs that indicate the status of the three used CANopen channels (Green= no errors, Red=some errors occurred during transmission). In the centre of the workspace there are four plotters in which the most important values are showed: from left to right and from top to bottom these are the values represented:

- Plotter 1: battery voltage in green and battery current in red
- Plotter 2: traction motor torque reference in green, traction motor torque measured through CANopen in black and servo motor torque reference in red
- Plotter 3: reference speed for traction motor in red and measured speed from traction motor in black
- Plotter 4: reference vehicle velocity in red and measured vehicle velocity in black.

This simulation shows that the model works perfectly, with only some overshoots for rotational speed at the beginning of the first and third slope; these spikes come from the faster time response of the servo motor controller compared to the traction motor controller (section 3.2).

After this initial trial, the actual driving cycle is used, and the experiment layout is the one showed in Figure 54.

Figure 54, dSPACE ControlDesk® experiment layout for actual driving cycle

In this simulation some bigger oscillations are visible in measured speed for traction motor, but this is due to the faster accelerations required from the reference for vehicle velocity; this creates transient situations in which the servo motor reacts faster than the traction one, causing oscillations. In any case, for the purpose of this work, the most important value is the vehicle velocity, that as it can be seen more precisely in Figure 55, is following with some not significant delay the reference.

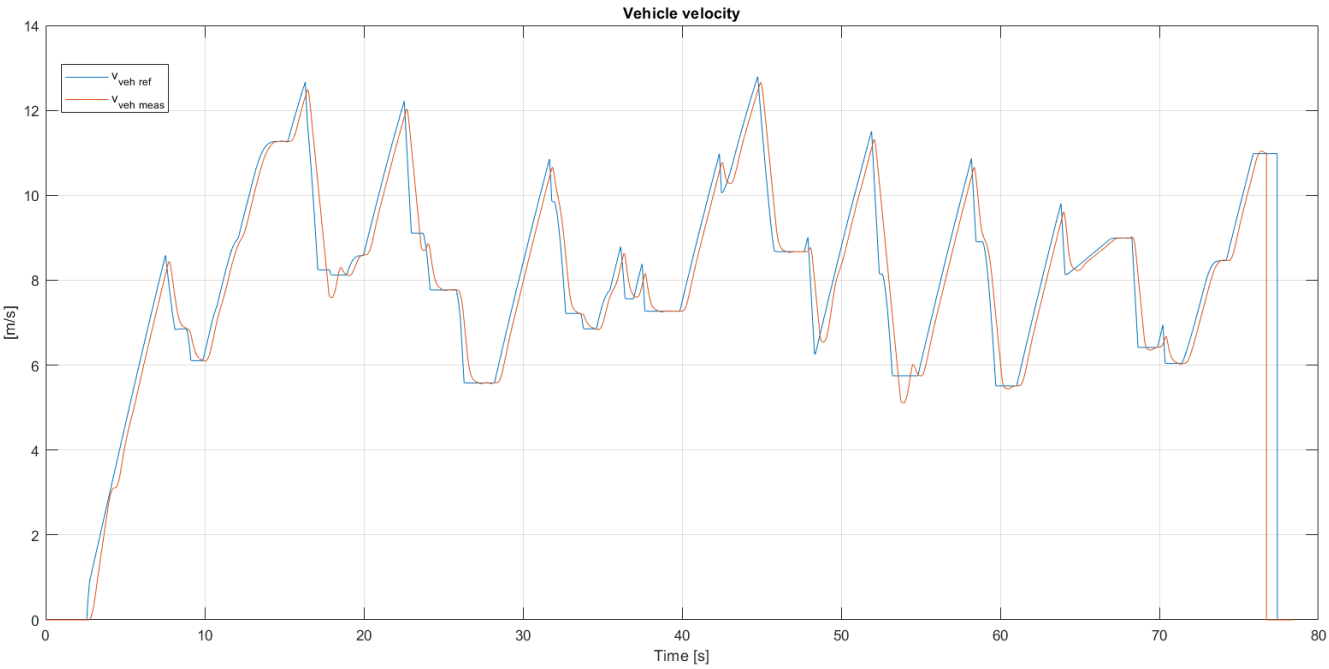

Figure 55, Vehicle velocity graph for actual driving cycle

Is also interesting to notice in Figure 56 the difference between the servo motor torque reference (orange line) and the traction motor torque reference (yellow line) with a difference between them of about 40% as it can be seen. This is due to the fact that the servo motor works as a load for the traction motor; the difference between the two reference values corresponds to the needed acceleration torque. It is not totally clear why the $T_{dcm\ meas}$ (blue line) differs around 2.5 Nm from the $T_{dcm\ ref}$ (yellow line). It should be noted that the "measured" torque is given by traction motor drive, very likely calculated from the currents and estimated flux, and not measured by an external mechanical independent torque meter. The difference can be due to torque calculation error from the drive or by inaccuracy of data transmission between software and hardware part. This difference can be the cause of the oscillations of the $T_{servo\ ref}$. To deeply understand the cause of this difference, more time and deeper investigations would be required.

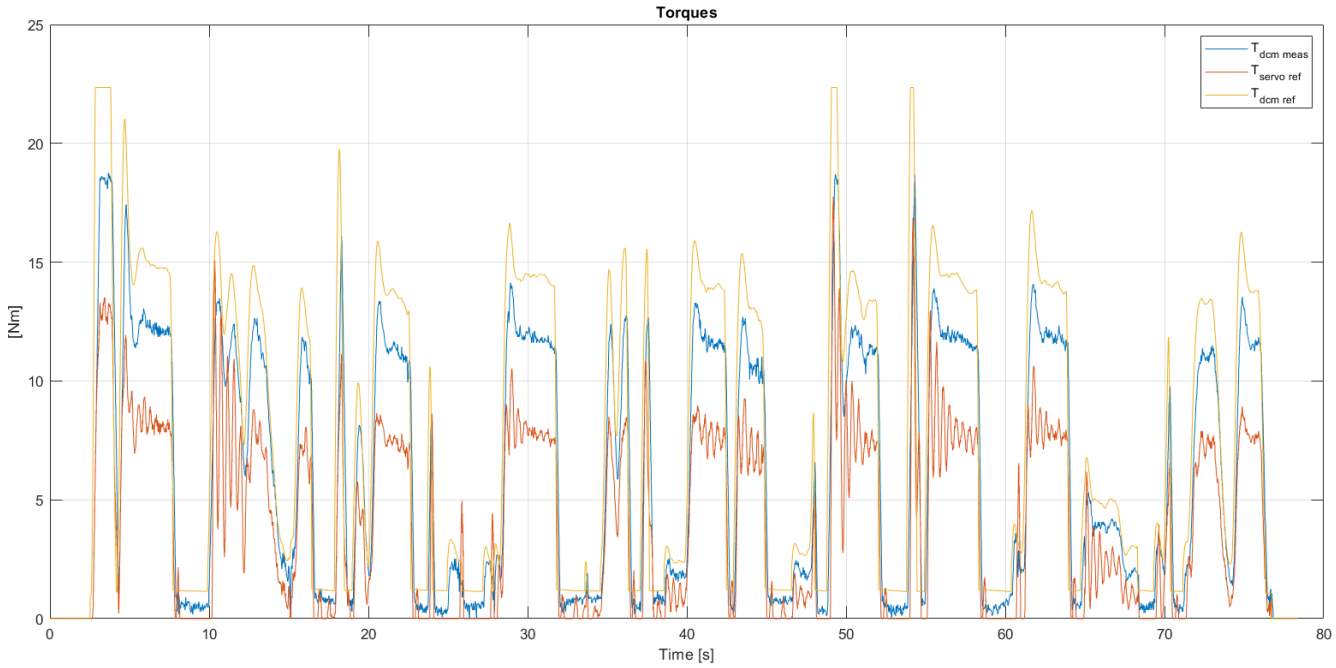

Figure 56, Torques graph for actual driving cycle

Battery current is always under the limits as it can be seen from Figure 57. The negative peak present around 3 *s* is due to the initial negative rotation of the two shafts due to the faster response of the servo motor, that starts rotating before than the traction one.

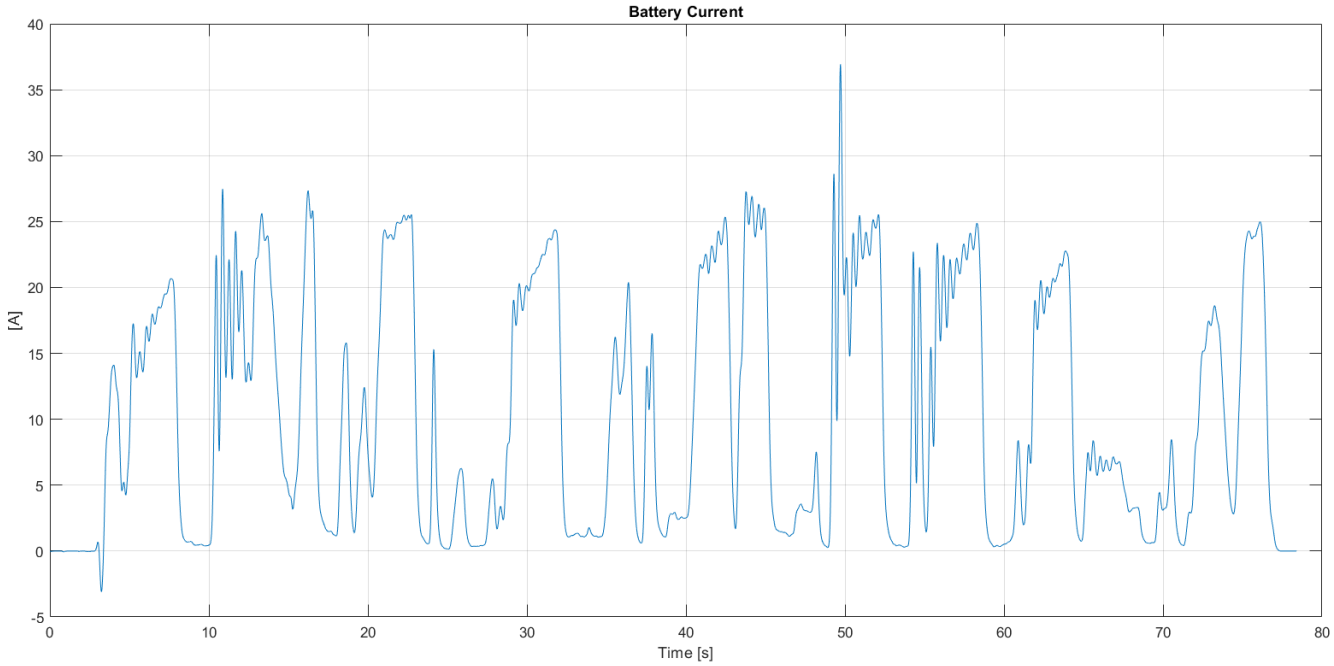

Figure 57, Battery current for actual driving cycle

Battery voltage behaves accordingly to the current, as it can be seen from Figure 58. Here, the initial voltage is around 77.7 *V* because the battery pack is not fully charged at the beginning of the simulation.

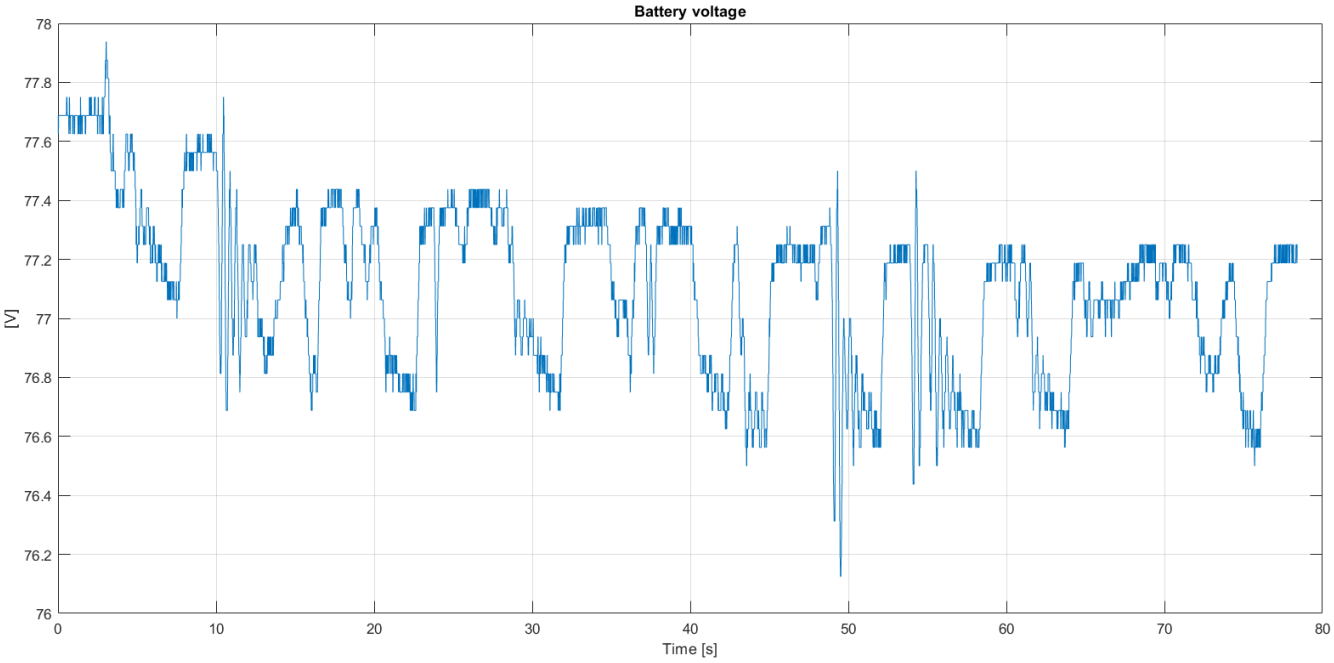

Figure 58, Battery voltage for actual driving cycle

5.3. Comparison between HIL and EMR

Results from HIL simulation represent the closest to reality-results: in this simulation external factors such as mechanical link between the two motor shafts, ageing of the battery cells, EMI issues and other unknown variables can heavily affect the final result. Is also true that one of the reasons why HIL simulation is used, is the possibility to include these external factors that would be impossible to be reproduced in an easy way through a software simulation.

As it can be noticed from the comparison between the vehicle velocity graph elaborated through software simulation (Figure 59) and the one from HIL simulation (Figure 60), results are almost equal, with some little differences. In Figure 60 there is an initial zero-velocity state that represent the elapsed time between the start of the measurements and the start of the driving cycle. In HIL the driving cycle is not automatically stopped, that is the reason why it is manually stopped and the measurement is stopped at 80 *s*.

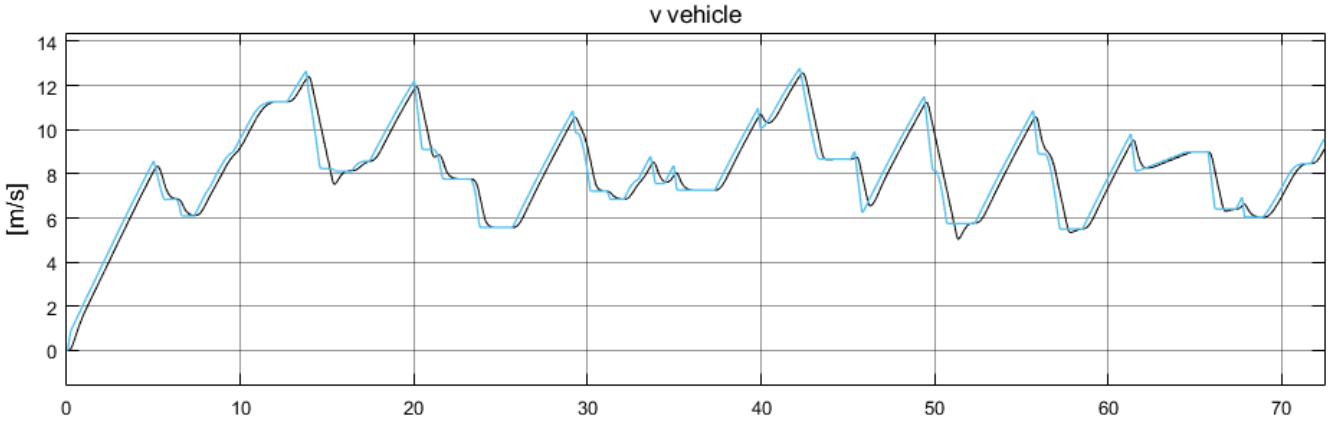

Figure 59, Vehicle velocity for software simulation

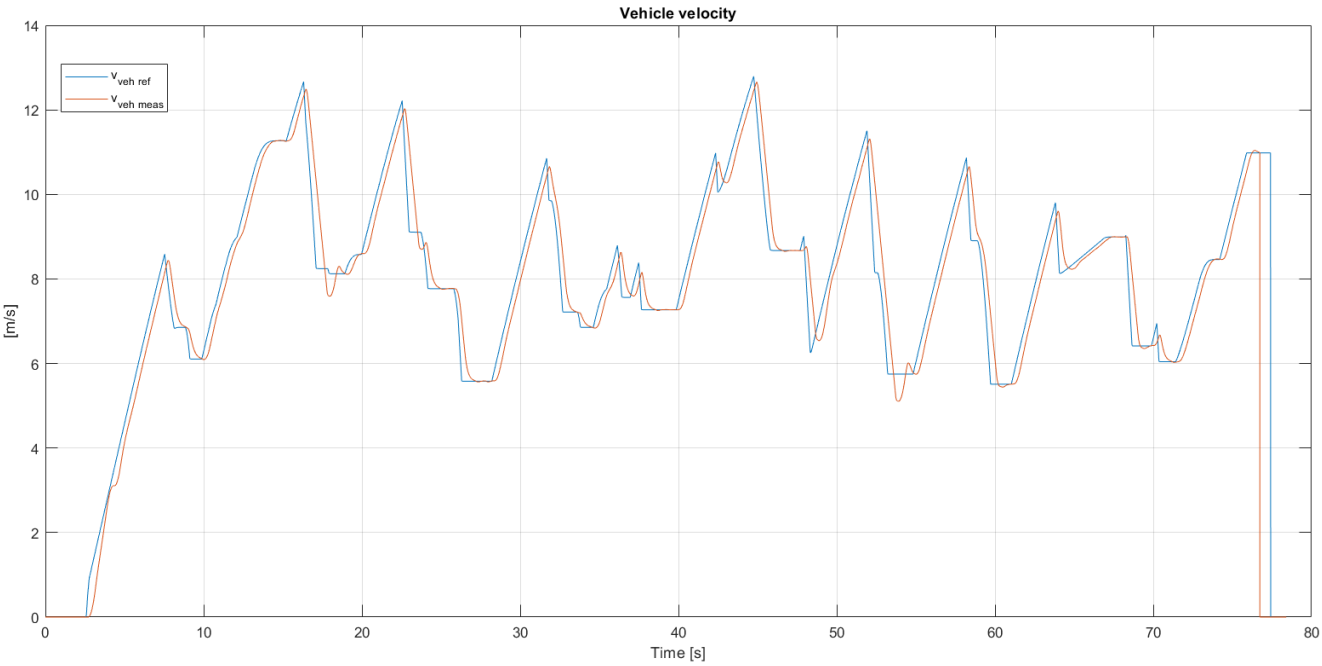

Figure 60, Vehicle velocity for HIL simulation

Battery current has more differences between software simulation and HIL simlation; oscillations in torque at the rotor shaft directly influence the battery voltage and consequently the battery voltage. Apart from oscillations and some peaks corresponding to overshoots in rotor speed, results from HIL simulation have the same shape than the software simulation. Values are higher in HIL simulation due in part to the initial SoC of the battery pack; in software simulation was 100%, and here is around 96% that implies higher current values to obtain the same amount of torque. Another factor that has led to an increase of battery current is the battery model used in software simulation that is quite simple and does not take into account ageing of the cells, temperature and other factors difficult to be modelled. This is a good example to demonstrate that software simulation can give only a rough idea of what will be the result in an actual environment with real devices, but sizing of components and devices has always to be done after an HIL simulation.

Figure 61, Battery current from software simulation

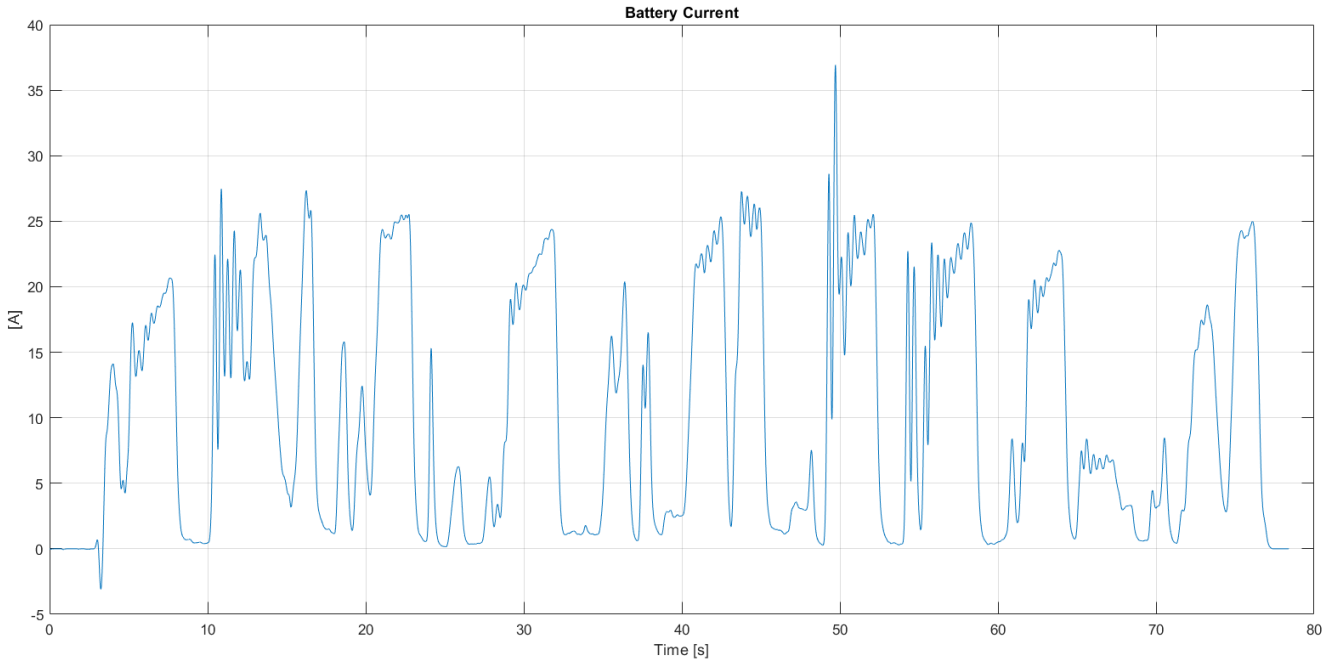

Figure 62, Battery current from HIL

Last consideration that has to be done is about the real positive influence of regenerative braking in such an application. As already explained, due to hardware constraints, this cannot be implemented in HIL simulation in the present status of the setup, but as it can be seen, for a rough estimation also the software simulation gives good results.

Using the Matlab/Simulink© model presented in 5.1.2, and changing k_{br} from 1 to 0.3, SoC value is considered:

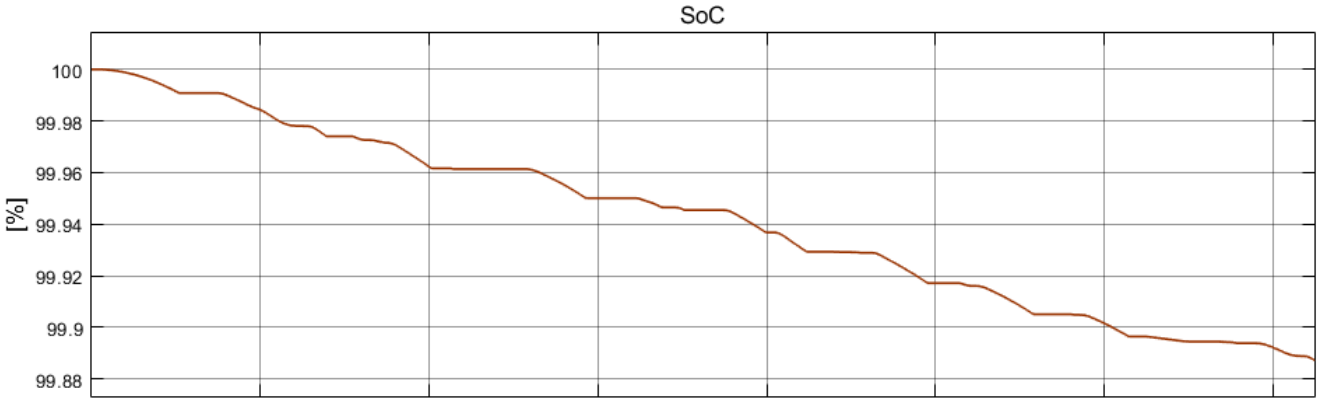

Figure 63, SoC for k_{br}=1 (No regenerative braking)

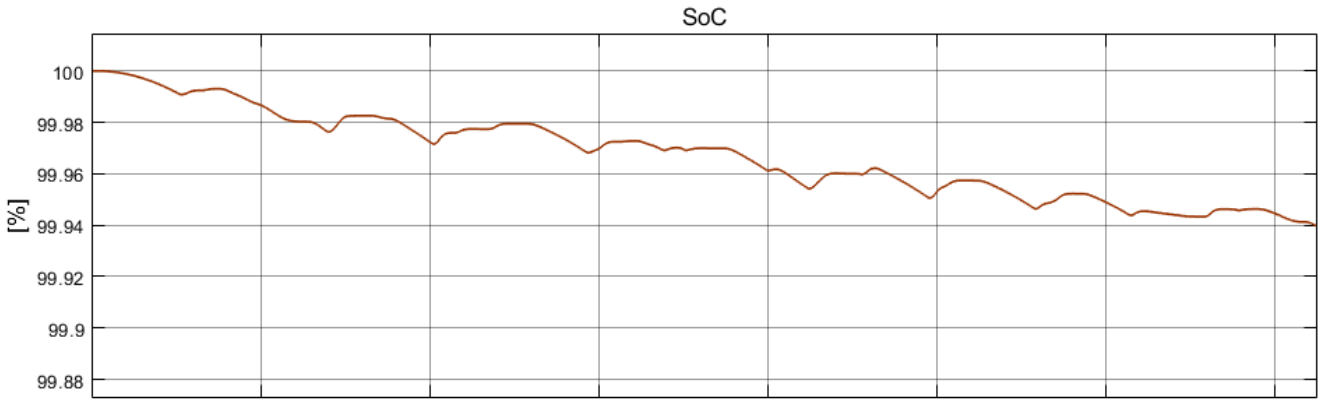

Figure 64, SoC for k_{br}=0.3 (with regenerative braking)

The comparison between Figure 63 and Figure 64 clearly demonstrate that the regenerative effect is beneficial, especially in such an application where many heavy decelerations are present, as this one.

6. Conclusions and future work

6.1. Conclusions

The objective of this work of thesis was to simulate an electric race car, starting from a software simulation and successively a reduced power HIL simulation, considering regenerative braking effect. Regenerative braking has been successfully implemented in software simulation, highlighting that in such an application as a race car, allows around 60% more range, as it can be stated looking at Figure 64 compared to Figure 63.

HIL simulation was conducted only for the case with no regenerative effect because of hardware constraints that do not allow to send negative torque reference. This allows to make comparisons between software simulation and HIL simulation, only for no regenerative braking conditions, that finally demonstrate the validity of the two simulations and the coherence between the two. There are some differences between results from the two simulations, but this is due to the presence of some frictional forces and other parasitic effects not considered in software simulation.

Is demonstrated that HIL simulation can be beneficial to increase results accuracy and to reduce development time, avoiding use of complicated models in simulation for devices such as battery pack. For this work of thesis, most of the time was invested into create a proper way to connect ControlDesk experiment and Matlab/Simulink© model. This part has to be done only once, and in this case Lotrakul's work [21] was beneficial to speed up the procedure. Once that this part is completed, is faster to set and run HIL simulation than software simulation, achieving also results closer to reality compared to the software simulation.

6.2. Future work

The most interesting thing about the test bench that was discovered during this work, is that the motor drives cannot receive negative signals and furthermore MicroAutoBox II in the actual configuration cannot send these (is mounted a DS1511 board, instead of DS1511b that allows sending also negative values [22]). This is crucial to include regenerative braking in simulation, so the first step to implement it also in HIL, is to solve this issue. One solution could be to change the hardware, but this would imply high costs, or to arrange the software simulation part to send the negative references in another way.

Due to the fact that the motors mounted on the simulated FSAE car and the traction motor of the test bench are from the same constructor and model with the only difference of the power range, HIL simulation is even closer to reality; the manufacturing for the two motors is equal and the type of magnets, temperature effects, mechanical responses, frictional coefficients and other parameters are exactly the same. Could be interesting try to change the type of traction motor and make some comparisons between different motor technologies such as Interior Permanent Magnets (IPM) motors or Switched Reluctance (SR) motors.

6.3. Quality report

This work of thesis was developed in ISEC-IPC with an intermediate stay of about one month at University of Lille in L2EP laboratories.

During the first month in Coimbra, first contact with the test bench and some of the experiments already done by Lotrakul to test the operativity of the system were performed. During this period, all the manuals and the thesis from Lotrakul [21] were deeply studied to understand all the functionalities of the system. Moreover, during this first approach some confidence with the hardware part was acquired, some improvements to connections were done, in order to reduce some EMI issues and also to better block pins and connections in SEVCON Gen4 DB-25 port. After that, an .XLS file was produced to clearly define all the connections; this document is added in Appendix E-.

Once that this first approach was finished, EMR study and development was started, moving to University of Lille. There, the concept of EMR was studied and applied to a general case of an electric vehicle; a master report was produced explaining all the procedure to complete this simulation [23].

After that, heading back to Coimbra, implementation of HIL simulation, with some adaptations from the original model developed in Lille, was completed. To obtain the driving cycle that the car should follow on the race track, OptimumLap© software was used: this software allows to simulate the behaviour of a specific car on a specific track, showing parameters such as maximum speed, elapsed time to complete the track, acceleration and deceleration values, etc. From these results, only the velocity of the car was used to create the velocity reference for the vehicle. This part was particularly hard, due to the very reduced available time to create models, run simulations, adjust some hardware settings that were need for the new model, properly tuning controllers for HIL simulation and produce this written work.

The overall experience was completely satisfactory and final results demonstrate that the initial target is fulfilled. The intermediate stay in Lille was useful to learn EMR technique and basics of HIL simulation. All the HIL implementation was done at ISEC-IPC.

7. References

[1] European Commission, “A European Strategy for Low-Emission Mobility,” Brussels, 2016.

[2] S. Morsy, C. Mckerracher, N. Kou, L. Goldie-Scot, O. A. and D. Doherty, “Bloomerg New Energy Finance-Electric Vehicle Outlook 2018,” 2018. [Online]. Available: https://about.bnef.com/electric-vehicle-outlook/#toc-download. [Accessed June 2018].

[3] P. G. Pereirinha, M. Gonzalez, I. Carrillero, D. Ansean, J. Alonso and J. C. Viera, “Main Trends and Challenges in Road Transportation Electrification,” Gijòn (Spain), 2018.

[4] M. Toll, “Regenerative braking: how it works and is it worth it in small EVs?,” 24 April 2018. [Online]. Available: https://electrek.co/2018/04/24/regenerative-braking-how-it-works/. [Accessed 04 June 2018].

[5] Formula-SAE, “Formula SAE events,” [Online]. Available: https://www.sae.org/attend/student-events/. [Accessed June 2018].

[6] A. Bouscayrol, “Hardware In the Loop Simulation,” in *Industrial Electronics Handbook*, 2nd ed., vol. Control and Mechatronics, Chicago, CRC Press, Taylor & Francis group, 2011.

[7] D. Maclay, “Simulation gets into the loop,” *IEEE Review*, pp. 109-112, May 1997.

[8] Markets and Markets, “marketsandmarkets,” November 2015. [Online]. Available: https://www.marketsandmarkets.com/Market-Reports/hardware-loop-market-11343527.html. [Accessed 02 July 2018].

[9] A. Bouscayrol, J. P. Hautier and B. Lemaire Semail, “Graphic Formalisms for the Control of Multi-Physical Energetic Systems: COG and EMR,” in *Systemic Design Methodologies for Electrical Energy*, 1st ed., vol. I, ISTE Willey editions, 2012.

[10] A. L. Allegre, A. Bouscayrol, J. N. Verhille, P. Delarue, E. Chattot and E. S. Fassi, “Reduced-scale power Hardware-In-the-Loop simulation of an innovative subway.,” *IEEE Transaction on Industial Electronics*, vol. 57, pp. 1175-1185, April 2010.

[11] M. A. Martins Pessoa, “Controlo de motores sìncronos de ìmanes permanentes para veìculo eléctrico de elevado desempenho,” Relatório de Projecto , Coimbra, 2011.

[12] P. G. Pereirinha, “VPPC 2014 Interview for TVI,” 2014. [Online]. Available: https://youtu.be/SCPiF3psN6s?t=1s. [Accessed July 2018].

[13] “VPPC2014 Website,” 27-30 October 2014. [Online]. Available: http://www.vppc2014.org/home.html. [Accessed July 2018].

[14] J. P. Silva Ribeiro, J. P. Oliveira Lopes and P. R. Aquino Ferreira, “Body Phisec 3.0-Estudo Aerodinamico,” Relatório da Unidade Curricular de Projeto, Coimbra, 2014.

[15] R. German, S. Shili, A. Sari, P. Venet and A. Bouscayrol, “Characterization Method for Electrothermal Model of Li-Ion Large Cells,” in *IEEE Vehicle Power and Propulsion Conference (VPPC)*, Belfort, France, 2017.

[16] P. Delarue, A. Bouscayrol and E. Semail, “Generic control method of multi-leg voltage-source-converters for fast practical implementation,” *IEEE Transaction on Power Electronics,* vol. 18, no. 2, pp. 517-526, March 2003.

[17] S. Temel, S. Yagly and S. Goren, “P, PD, PI, PID CONTROLLERS- Recitation 4 Report. Discrete time Control Systems,” 2013. [Online]. Available: https://www.scribd.com/document/209613239/EE402Recitation. [Accessed 04 06 2018].

[18] F. Briz, *"Power Sytems in HEV and EV (PSHEV)" Course for EMMC-STEPS- "Hybrid Electric Vehicles" Lecture Slides,* Gijòn, 2017.

[19] T. Letrouvé, A. Bouscayrol, W. Lhomme, N. Dollinger and F. M. Calvairac, “Different models of a traction drive for an electric vehicle simulation,” in *IEEE-VPPC'10,* Lille (France), 2010.

[20] L2EP-Lille, “EMR Website- EMR Library,” [Online]. Available: http://www.emrwebsite.org/library.html.

[21] P. Lotrakul, “Power HIL Simulation of an Electric Minibus Powertrain,” Universidad de Oviedo, Gijòn (Spain), 2017.

[22] dSPACE GmbH, *MicroAutoBox II Hardware installation and Configuration manual,* 2014.

[23] T. Transi, “EMR of an Electric Vehicle with Mechanical Differential,” Report from stay in Lille, Lille, 2018.

APPENDICES

Appendix A- Electrical Machines Datasheets

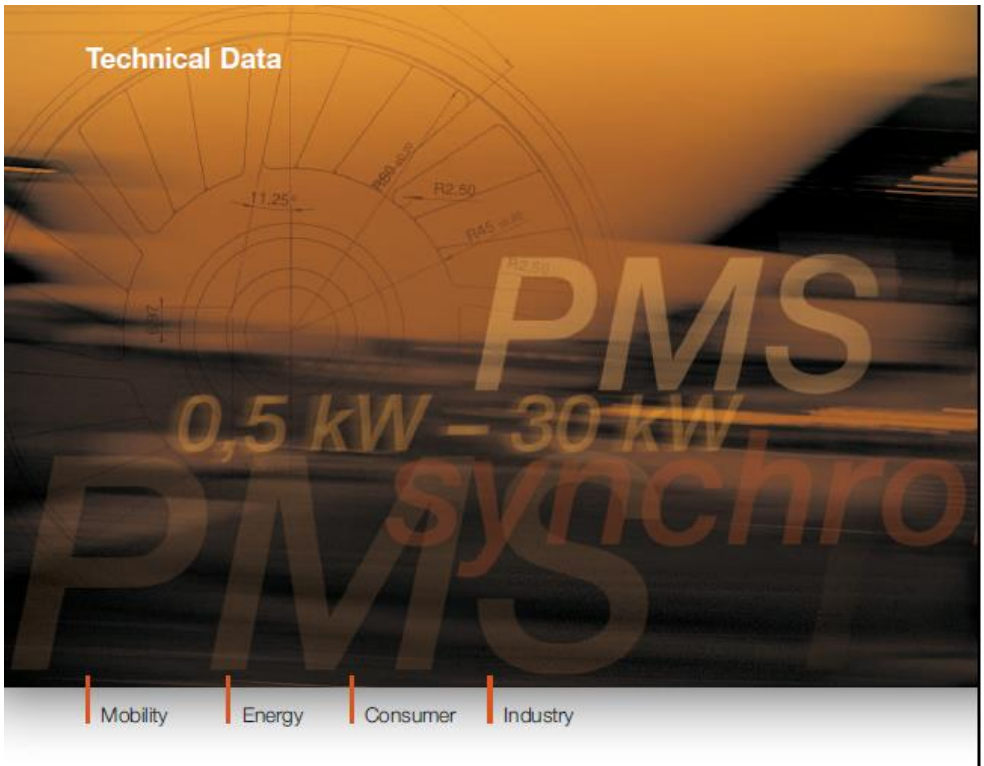

MOTORS

High efficient, brushless AC-Synchronus Disc-Motors with
Patented Rotor Technology

PERM MOTOR
Member of the HEINZMANN Group

High efficient, brushless AC-Synchronus Disc-Motors with Patented Rotor Technology

Our motors are used in all applications, where low weight, compact construction, high efficiency and high dynamic features are requested. For example in electric Vehicles, NEV's, turf applications, commuters, floorcare machinery, boats, and in a wide rage of industrial applications. The motors are available in a sensorless version, and several other sensor system solutions.

- Power-range from 0.5 kW up to 30 kW air- or watercooled
- For battery Voltage 24 V – 96 V or line powered 110 V – 400 V
- Complete drive trains with gear boxes and brakes are available on request
- Controllers on request

Advantages:

- High power-density due to double-stators
- High efficiency
- Low inertia due to special plastic rotor
- Integrated solutions as a built in motor possible
- Flat construction
- Completely closed, system of protection IP 54

PMS-Motor air-cooled

PMS-Motor water-cooled

Typical efficiency as a function of the speed for the PMS Motor Series

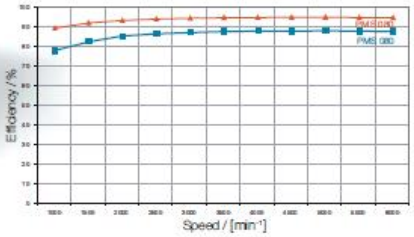

Technical data

Type series 080		Rated Power: 0.4 - 1.4 kW / Depending on rpm
Motor Peak Torque	10 Nm	Permitted peak torque during pulsed operation up to ~ 30 % of rated rpm
Pulsed-operation	ca. 13 Nm	Permitted pulsed-operation for 0.5 sec. with speed > 50 rpm
Moment of Inertia	3.8 kgcm²	Based on standard shaft-Version
Weight	ca. 3.2 kg	With sin/cos Encoder, without brake

PMS 080

	24 V DC		48 V DC		72 V DC		from 320 V DC	
Speed [min⁻¹]	Torque [Nm]	Power [kW]	Torque [Nm]	Power [kW]	Torque [Nm]	Power [kW]	Torque [Nm]	Power [kW]
1500	2.7	0.4	2.9	0.5	–		–	
3000	3.2	1.0	3.2	1.0	3.2	1.1	3.2	1.0
4500	2.3	1.1	2.8	1.3	2.8	1.3	2.8	1.3
6000	1.9	1.2	2.2	1.3	2.2	1.4	2.2	1.3

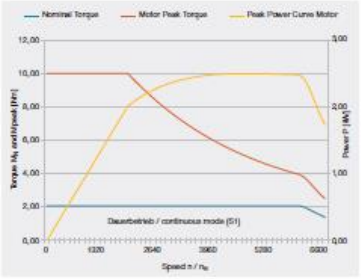

Type series 100		Rated Power: 1.2 - 3.0 kW / Depending on rpm
Motor Peak Torque	20 Nm	Permitted peak torque during pulsed operation up to – 30 % of rated rpm
Pulsed-operation	ca. 24 Nm	Permitted pulsed-operation for 0.5 sec. with speed > 50 rpm
Moment of Inertia	9.6 kgcm²	Based on standard shaft-Version
Weight	ca. 5.8 kg	With sin/cos Encoder, without brake

PMS 100

	24 V DC		48 V DC		72 V DC		from 320 V DC	
Speed [min⁻¹]	Torque [Nm]	Power [kW]	Torque [Nm]	Power [kW]	Torque [Nm]	Power [kW]	Torque [Nm]	Power [kW]
1500	7.6	1.2	7.0	1.1	7.6	1.2	7.0	1.1
3000	4.8	1.5	7.6	2.4	7.0	2.2	6.7	2.1
4500	–		5.3	2.5	5.3	2.5	5.1	2.4
6000	–		4.3	2.7	4.3	2.7	4.8	3.0

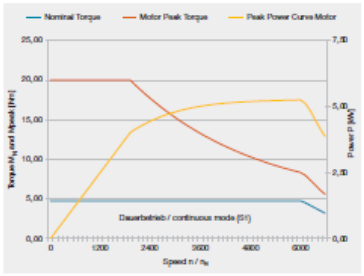

Type series 120		Rated Power: 3.2 - 7.0 kW / Depending on rpm
Motor Peak Torque	40 Nm	Permitted peak torque during pulsed operation up to – 30 % of rated rpm
Pulsed-operation	ca. 50 Nm	Permitted pulsed-operation for 0.5 sec. with speed > 50 rpm
Moment of Inertia	26.3 kgcm²	Based on standard shaft-Version
Weight	ca. 12.3 kg – 15.1 kg	With sin/cos Encoder, without brake

PMS 120 L / air-cooled

	48 V DC		72 V DC		96 V DC		from 320 V DC	
Speed [min⁻¹]	Torque [Nm]	Power [kW]	Torque [Nm]	Power [kW]	Torque [Nm]	Power [Nm]	Torque [Nm]	Power [kW]
1500	20.4	3.2	20.4	3.2	20.4	3.2	20.4	3.2
3000	18.5	5.8	19.1	6.0	19.1	6.0	19.1	6.0
4500	13.8	6.5	13.8	6.5	13.8	6.5	13.8	6.5
6000	10.4	6.5	11.1	7.0	11.1	7.0	11.1	7.0

PMS 120 W / water-cooled

	48 V DC		72 V DC		96 V DC		from 320 V DC	
1500	20.4	3.2	24.2	3.8	24.2	3.8	24.2	3.8
3000	19.1	6.0	23.9	7.5	22.9	7.2	23.9	7.5
4500	–		21.2	10.0	23.3	11.0	23.3	11.0
6000	–		–		19.9	12.5	19.9	12.5

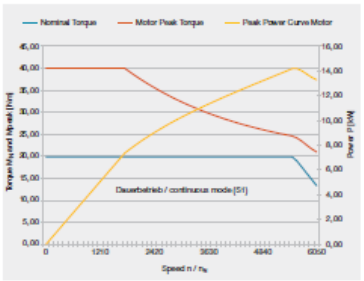

Type series 150/156		Rated Power: 6.5 - 30 kW / Depending on rpm
Motor Peak Torque	80 Nm	Permitted peak torque during pulsed operation up to ~ 30 % of rated rpm
Pulsed-operation	ca. 95 Nm	Permitted pulsed-operation for 0.5 sec. with speed > 50 rpm
Moment of Inertia	58.6 kg cm²	Based on standard shaft-Version
Weight	ca. 22.3 kg – 29.8 kg	With sin/cos Encoder, without brake

	48 V DC		72 V DC		96 V DC		from 320 V DC	
Speed [min⁻¹]	Torque [Nm]	Power [kW]	Torque [Nm]	Power [kW]	Torque [Nm]	Power [kW]	Torque [Nm]	Power [kW]
PMS 150 L / air-cooled								
1500	41.4	6.5	41.4	6.5	41.4	6.5	41.4	6.5
3000	27.4	8.6	36.6	11.5	36.6	11.5	36.6	11.5
4500	–		27.6	13.0	27.6	13.0	28.6	13.5
6000	–		21.5	13.5	21.5	13.5	23.8	15.0
PMS 150 W / water-cooled								
1500	47.7	7.5	50.1	8.0	50.1	8.0	50.1	8.0
3000	27.4	8.6	39.8	12.5	44.5	14.0	47.8	15.0
4500	–		28.7	13.5	33.9	16.0	38.2	18.0
6000	–		21.5	13.5	27.1	17.0	31.8	20.0
PMS 156 L / air-cooled								
1500	47.7	7.5	47.7	7.5	47.7	7.5	47.8	7.5
3000	35.0	11.0	44.5	14.0	44.5	14.0	38.2	12.0
4500	–		29.7	14.0	29.7	14.0	29.7	14.0
6000	–		–		27.1	17.0	27.1	17.0
PMS 156 W / water-cooled								
1500	–		–		–		63.6	11.0
3000	–		41.3	13.0	54.1	17.0	57.3	18.0
4500	–		34.0	16.0	42.5	20	48.8	23.0
6000	–		25.5	16.0	36.6	23.0	48.7	30.0

Other speed versions for your special application, on request.

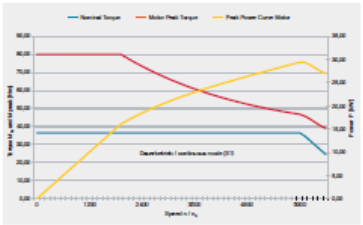

General technical specs for the PMS Motor series

Motortype:	Permanentmagnet AC-Synchronous Disc-Motor	Electrical strength:	Related to DIN EN 60034
Cooling:	• Aircooling with a min airstream of 5 m/s • Watercooling with max. 60 °C Max. operating pressure 3.0 bar Coolant quantity min. 6 l / min	Type of construction:	Flange type according IM B14
		Electrical connections:	Standard version with wire length ~ 1 m (connector version as an option, mating connector not included)
Operation mode:	S1 (continous)	Protection class:	IP 54
Polpairs:	4	Environmental temperature:	-10 °C to + 40 °C
Magnet material:	Neodynium-Iron-Bor	Demagnetization temperature:	KTY84 - 130 or PTC (NAT = 120° C)
Insulation Class:	Class F according VDE 0530	Shaft:	Standard shaft with key groove, other design on request

PM_DS_PMS_1_03-09_E

Perm Motor GmbH
Brand 24/1
79677 Schönau · Germany
Telefon +49 (0)7673/82087-00
Telefax +49 (0)7673/82087-99
info@perm-motor.de
www.perm-motor.de

PERM MOTOR
Member of the HEINZMANN Group

Appendix B- Battery cells Datasheet

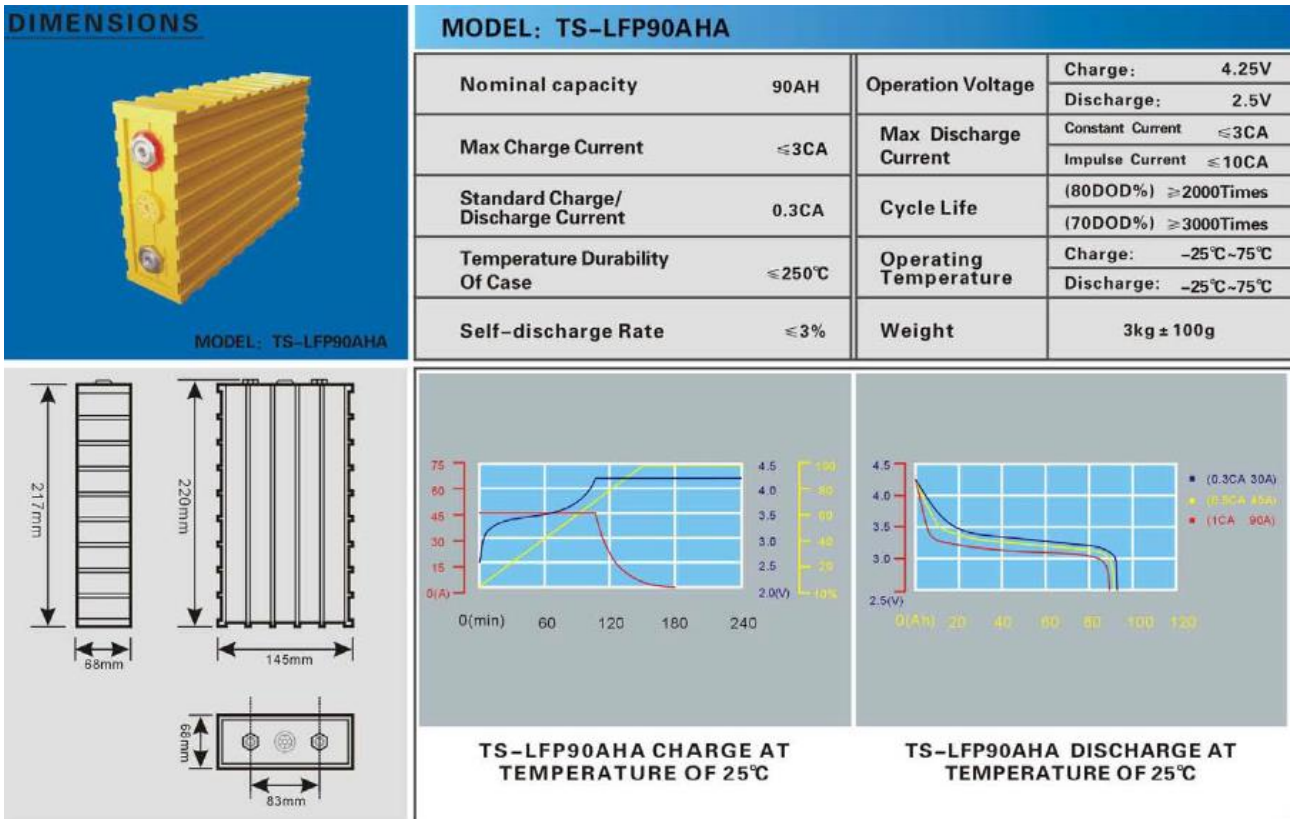

Appendix C- OptimumLap© Report

ISEC FSAE Electric

18 July 2018

Vehicle Configuration

Parameter	Value
Total Mass	375 kg
Drag Coefficient	0.29
Downforce Coefficient	1.2
Front Area	0.84 m^2
Tire Radius	0.24 m
Max Torque	95.4 N.m @ 1 rpm
Engine Efficiency	90 %
Type of Fuel	Lithiumion
Type of Transmission	Sequential Gearbox
Final Drive Ratio	3.57
Max Power	34.05 kW @ 6000 rpm
Power Mass Ratio	0.09 kW/kg

Performance Metrics

Metric	Value
Top Speed	155.23 km/h
Time for 0 to 100 km/h	13.91 s
Time for 100 to 0 km/h	2.03 s
Lateral Acceleration - Skidpad 50 m	16.79 m/s^2

Charts Summary

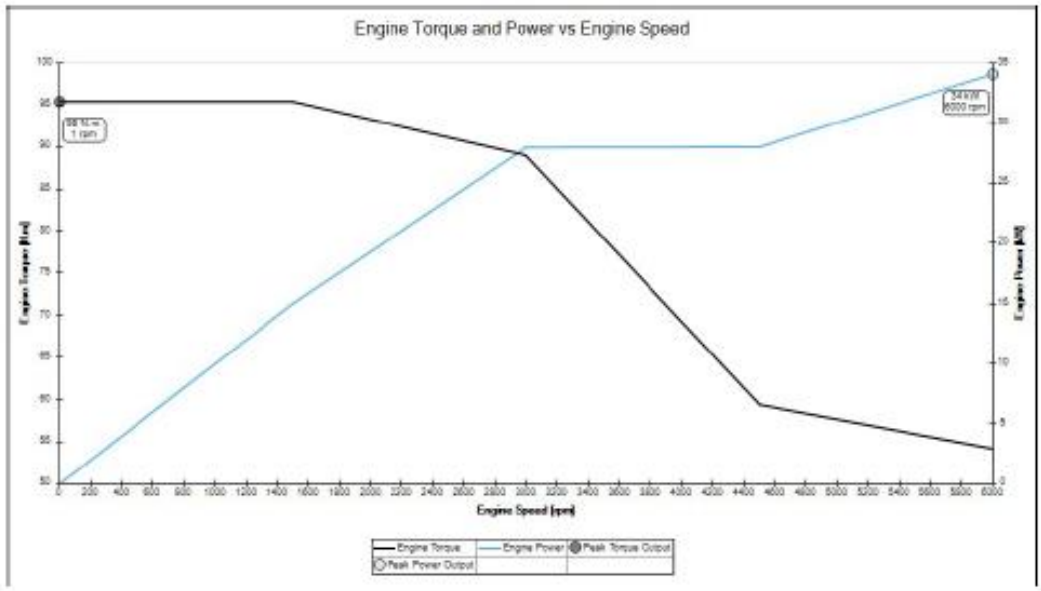
Engine Torque and Power vs Engine Speed
Engine Speed [rpm]
Engine Torque
Engine Power
Peak Torque Output
Peak Power Output

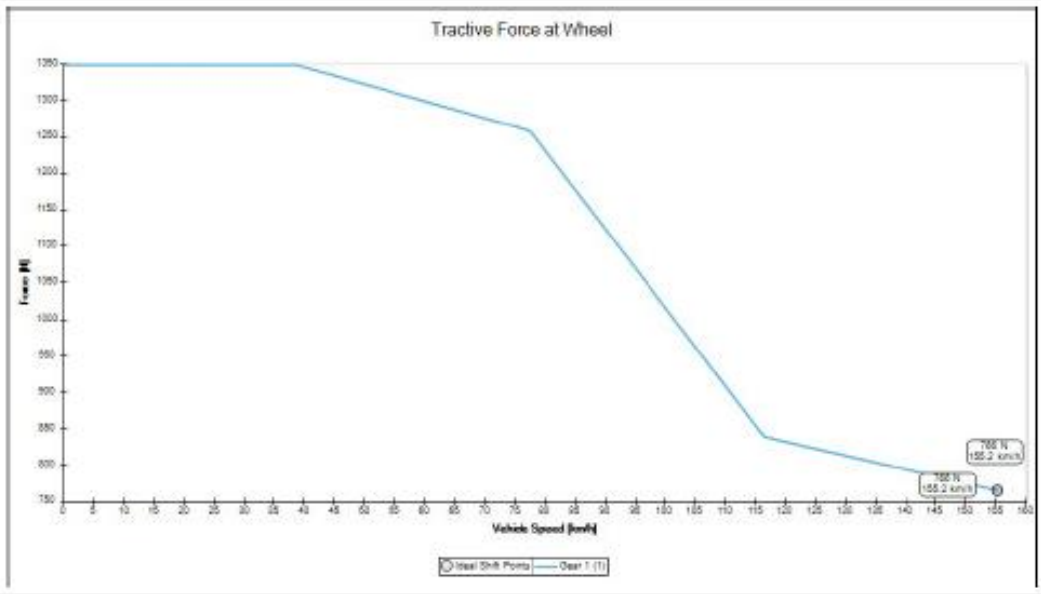
Tractive Force at Wheel
Vehicle Speed [km/h]
Ideal Shift Points
Gear 1 (1)

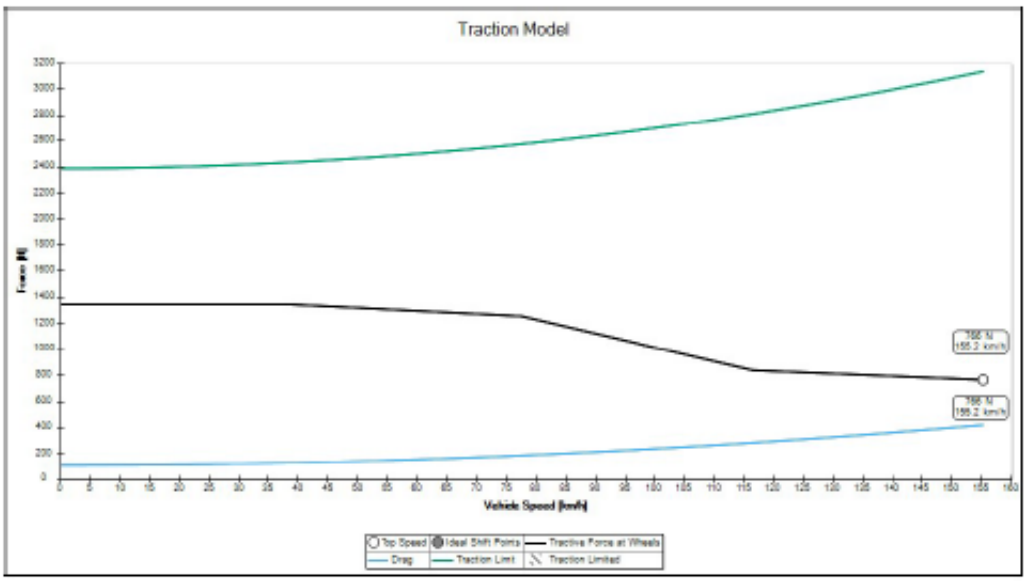
Traction Model
Vehicle Speed [km/h]
Top Speed
Ideal Shift Points
Tractive Force at Wheels
Drag
Traction Limit
Traction Limited

Appendix D- Matlab/Simulink© model for reduced power HIL, to be built in ControlDesk

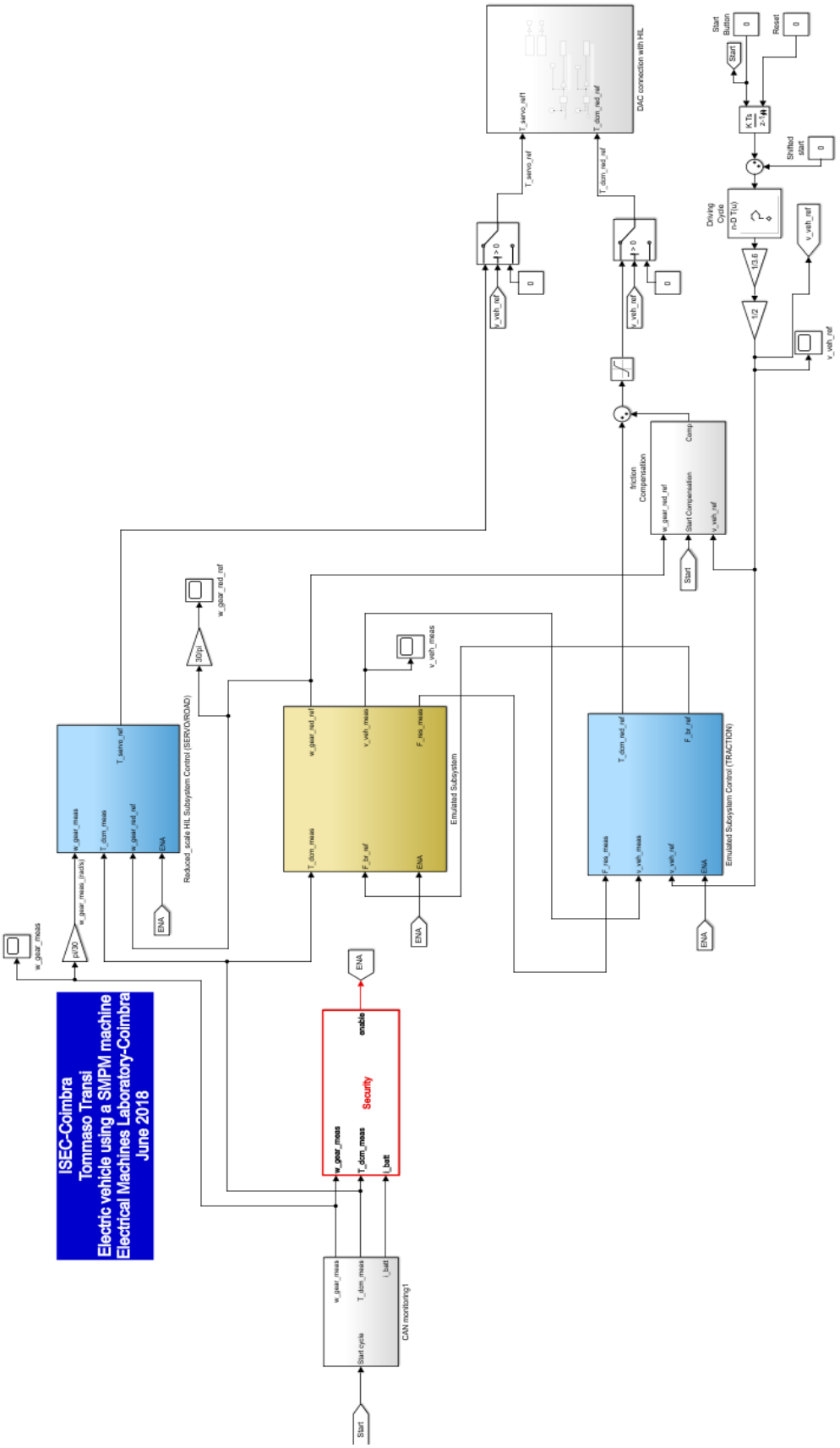

Appendix E- All connections Legenda

# Pin	Function	Cable	Color	Notes
1	Key switch	Green Cable From F3	*BLUE*	
2	CAN Termination	SHUNT	*WHITE*	Shunt with #24 because CAN 2 is not present
3	Contactor 1	CONTACTOR	*BLUE*	
4	Contactor 1 Vss	CONTACTOR	*BLUE*	
5	Hall U/2	#	#	EMPTY
6	Key switch	Green Cable From F3	*RED*	
7	Contactor 2	#	#	EMPTY
8	Contactor 2 Vss	#	#	EMPTY
9	Driveability 1	#	#	EMPTY
10	Key switch (?)	Green Cable From F3	*RED*	
11	Contactor 3	#	#	EMPTY
12	Contactor 3 Vss	#	#	EMPTY
13	CAN High 2	#	#	EMPTY
14	Encoder A	#	#	EMPTY
15	0 V Sensor	MOTOR SENSOR	*YELLOW*	
16	CAN High 1	CAN TO USB/ CAN 1	*BROWN & ORANGE (2 CABLES)*	Here I insert also the CAN High from CAN 1 Cable (dSPACE)
17	Hall V/3	#	#	EMPTY
18	Foot Switch	MANUAL CONTROL	*YELLOW-GREEN*	
19	Reverse Switch			EMPTY
20	Handbrake	#	#	EMPTY
21	Sin Input	MOTOR SENSOR	*PINK*	
22	Throttle	ANALOG 1	*BROWN & BLUE (2 CABLES)*	There are two cables here: one is to send analog signal and the other one is used as redundancy to verify that the sent signal corresponds to the one that has arrived.
23	Analog Brake	#	#	EMPTY
24	CAN Low 2	SHUNT	*WHITE*	Shunt with #2 because CAN 2 is not present
25	Encoder B	#	#	EMPTY
26	Vss 5/10 V	MOTOR SENSOR	*GREEN*	
27	CAN Low 1	CAN TO USB/ CAN 1	*WHITE-BROWN & WHITE-GREEN (2 CABLES)*	Here I insert also the CAN Low from CAN 1 Cable (dSPACE)
28	CAN Vss 2	#	#	EMPTY
29	Hall W/1	#	#	EMPTY
30	Forward Switch	MANUAL CONTROL	*BLUE*	
31	Seat Switch	#	#	EMPTY
32	Driveability 2	#	#	EMPTY
33	KTY +	MOTOR SENSOR	*WHITE*	
34	Supply Potientometer	STAND ALONE	*YELLOW*	
35	Cos Input	MOTOR SENSOR	*BROWN*	

CABLES

ANALOG 1 (dSPACE)

Color	Function	Notes
BROWN	Analog Output	
BLUE	Analog Input	
WHITE-BROWN	Ground	Connected to B- (SEVCON)

CAN 1 (dSPACE-SEVCON)

Color	Function	Notes
ORANGE	CAN High	
WHITE-ORANGE	Ground	
WHITE-GREEN	CAN Low	

CAN TO USB

Color	Function	Notes
BROWN	CAN High	
GREEN	Ground	
WHITE-BROWN	CAN Low	

Pin Scheme

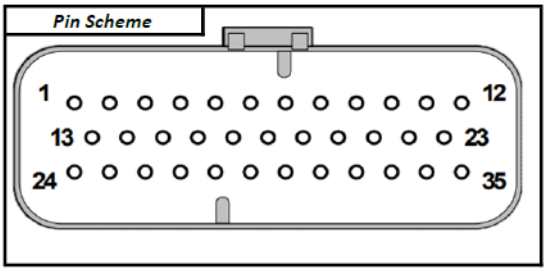

ANALOG 2 (dSPACE)

Color	Function	Notes
BROWN	Analog Output	Connected to X11-#2 (SEW)
BLUE	Analog Input	Connected to X11-#2 (SEW)
WHITE-GREEN	Ground	Connected to X11 -#4 (SEW)

CAN 2 (dSPACE-SEW)

Color	Function	Notes
ORANGE	CAN High	Connected to X12-#2 (SEW)
GREEN & WHITE-GREEN	CAN Low	Connected to X12-#3 (SEW)
WHITE-ORANGE	Ground	Connected to X12 -#1 (SEW)
BROWN	Inhibits the Controller (??)	Connected to X13-#1&8 (SEW)
WHITE-BROWN	Ground	Connected to X13-#7&9 (SEW)

MANUAL CONTROLLER

Color	Function	Notes
BLUE	Forward Switch	
YELLOW-GREEN	Foot Switch	
RED	Throttle by Pot.	Stand-Alone
BLUE	Ground (Conn. To B-)	Stand-Alone
YELLOW	Potentiometer Supply	Stand-Alone